UCP2 inhibition induces ROS/Akt/mTOR axis: Role of GAPDH nuclear translocation in genipin/everolimus anticancer synergism

Elsevier Editorial System(tm) for Free Radical Biology and Medicine
Manuscript Draft

Manuscript Number:

Title: UCP2 inhibition induces ROS/Akt/mTOR axis: role of GAPDH nuclear translocation in genipin/everolimus anticancer synergism

Article Type: Original article

Keywords: pancreas cancer; uncoupling proteins; UCP2; mTOR; everolimus; GAPDH; cell death.

Corresponding Author: Dr. Massimo Donadelli, Ph.D.

Corresponding Author's Institution: University of Verona

First Author: Ilaria Dando, Ph.D.

Order of Authors: Ilaria Dando, Ph.D.; Raffaella Pacchiana; Elisa Dalla Pozza; Ivana Cataldo; Stefano Bruno; Paola Conti; Marco Cordani; Anna Grimaldi; Giovanna Butera; Michele Caraglia; Aldo Scarpa; Marta Palmieri; Massimo Donadelli, Ph.D.

Abstract: Several studies indicate that mitochondrial uncoupling protein 2 (UCP2) plays a pivotal role in cancer development by decreasing reactive oxygen species (ROS) produced by mitochondrial metabolism and by sustaining chemoresistance to a plethora of anticancer drugs. Here, we demonstrate that inhibition of UCP2 triggers Akt/mTOR pathway in a ROS-dependent mechanism in pancreatic adenocarcinoma cells. This event reduces the antiproliferative outcome of UCP2 inhibition by genipin, creating the conditions for the synergistic counteraction of cancer cell growth with the mTOR inhibitor everolimus. Inhibition of pancreatic adenocarcinoma cell growth and induction of apoptosis by genipin and everolimus treatment are functionally related to nuclear translocation of the cytosolic glycolytic enzyme glyceraldehyde 3-phosphate dehydrogenase (GAPDH). The synthetic compound (S)-benzyl-2-amino-2-(S)-3-bromo-4,5-dihydroisoxazol-5-yl-acetate (AXP3009), which binds GAPDH at its redox-sensitive Cys152, restores cell viability affected by the combined treatment with genipin and everolimus, suggesting a role for ROS production in the nuclear translocation of GAPDH. Caspase-mediated apoptosis by genipin and everolimus is further potentiated by the autophagy inhibitor 3-methyladenine revealing a protective role for Beclin1-mediated autophagy induced by the treatment. Mice xenograft of pancreatic adenocarcinoma further confirmed the antiproliferative outcome of drug combination without toxic effects for animals. Tumor masses from mice injected with UCP2 and mTOR inhibitors revealed a strong reduction in tumor volume and number of mitosis associated with a marked GAPDH nuclear positivity. Altogether, these results reveal novel mechanisms through which UCP2 promotes cancer cell proliferation and support the combined inhibition of UCP2 and of Akt/mTOR pathway as a novel therapeutic strategy in the treatment of pancreatic adenocarcinoma.

Suggested Reviewers: Francesca Zazzeroni
Professor, Department of Biotechnological and Applied Clinical Sciences,, University of L'Aquila, Italy

francesca.zazzeroni@univaq.it

Jordi Oliver
Professor, Department of Fundamental Biology and Health Sciences,,
University of the Balearic Islands, Spain
jordi.oliver@uib.es

Chiara Riganti
Professor, University of Turin, Italy
chiara.riganti@unito.it

Carlo Leonetti
Regina Elena Cancer Institute, Rome
carlo.leonetti@ifo.gov.it

Tarik Regad
University of Nottingham UK
tarik.regad@ntu.ac.uk

Evzen Amler
Charles University of Prague
evzen.amler@lfmotol.cuni.cz

Antonio Giordano
Temple University of Philadelphia PA
giordano@temple.edu

UNIVERSITÀ di VERONA
Dipartimento di NEUROSCIENZE, BIOMEDICINA E MOVIMENTO

Free Radical Biology & Medicine Verona, July 28th 2017

Editorial Office

Dear Professor Vina,

we wish to thank you for your efforts in handling our manuscript (FRBM-D-17-00405) entitled "*UCP2 inhibition induces ROS/Akt/mTOR axis: role of GAPDH nuclear translocation in genipin/everolimus anticancer synergism"* and for giving us the opportunity to revise and improve it. We greatly appreciated your thoughts and those from the Reviewers. We revised the manuscript accordingly. As you proposed in your Editorial decision letter on June 25th 2017 reported below, we kindly ask you to use the same Referees to assure consistency in the review process of our manuscript.

Dear Dr. Donadelli,
Thank you for resubmitting the above-mentioned article to Free Radical Biology & Medicine.
We have completed the review of your manuscript and a summary is enclosed below. Although some merit was found in your manuscript (see below), the stated priority for publication (to the Editor) was quite low. Free Radical Biology & Medicine can now accept about 30% of submitted manuscripts. Therefore, as is the case with your manuscript, the decision reflects the relative priority assigned by the reviewer as much as the assessment of scientific merit.

It appears from the enclosed comments that some portions of the study were considered interesting but not sufficiently well documented. Those comments suggest that an entirely rewritten manuscript addressing each of the issues raised may receive a more positive response from these reviewers. That manuscript may have to delete some parts and include new experiments. Such a substantially altered manuscript would then be considered as a new submission. This, of course, does not guarantee acceptance of the new submission, which would still undergo a rigorous review. If you desire to follow this path, please refer to this letter and manuscript number, as well as provide responses to the reviewer comments, and I will use these same referees to assure consistency in the review process.

Yours sincerely,
Jose Vina
Associate Editor
Free Radical Biology & Medicine

As required by Reviewers, we have revised the manuscript in order to highlight the novelty of the study and to help the readers to keep the overall aim of the study. As required by Reviewers, we

have also deleted some parts of the manuscript and performed additional experiments, which straighten the conclusions of the manuscript. The new results have been inserted in the main figures and properly discussed in the text. Overall, we have point-by-point answered to all the criticisms of the Reviewers and we hope our manuscript might be suitable for publication in your journal.

Yours sincerely,

Ilaria Dando and Massimo Donadelli

University of Verona, Italy

UNIVERSITÀ di VERONA
Dipartimento di NEUROSCIENZE, BIOMEDICINA E MOVIMENTO

Free Radical Biology & Medicine Verona, July 28th 2017
Editorial Office

Dear Professor Vina,
please find below the detailed, itemized list of our responses to the Reviewers' suggestions/comments and the changes we have made in the resubmitted Manuscript No.: FRBM-D-17-00405. Title: *UCP2 inhibition induces ROS/Akt/mTOR axis: role of GAPDH nuclear translocation in genipin/everolimus anticancer synergism.*

Reviewers' comments:

Reviewer #1:
The goal of the authors is to demonstrate that the combined inhibition of UCP2 and of Akt/mTOR pathway is a novel therapeutic strategy in the treatment of PDAC. The paper is well carried out and examines with a lot of suitable methods each step of experimental protocol, but there are some contradictions. Therefore, I have these remarks for the authors:

Introduction
Pag 5, lines 89-92. The authors previously demonstrated that UCP2 inhibition triggers PDAC cell death by ROS-dependent nuclear translocation of the glycolytic enzyme glyceraldehyde 3-phosphate dehydrogenase (GAPDH) and stimulation of autophagy in PDAC cells [19]. In the present study, they showed that UCP2 inhibition triggers the oncogenic Akt/mTOR pathway, which has an established role in cancer proliferation. Therefore the authors must also give to the PDAC cells an inhibitor of this pathway.

Therefore, UCP2 inhibition has two conflicting effects. What is the explanation for these conflicting effects? Inhibition of UCP2 causes death of PDAC cells or induces cell proliferation?
Response: As reported by the Reviewer, our previous studies have shown that ROS stimulation after UCP2 inhibition with specific siRNA or genipin results in cell death of PDAC cells caused by oxidative stress that promotes GAPDH nuclear translocation (Dando et al., BBA 2013), gemcitabine chemotherapy sensitivity (Dalla Pozza et al., BBA 2012), and cellular energy metabolism alterations (Brandi et al., FRBM 2016). As shown in our previous studies, cell death of chemoresistant PDAC cells is strictly dependent on the production of ROS since the addition of the NAC scavenger allows the recovery of cell death induced by UCP2 inhibition. In the same context of cancer cell death by oxidative stress (also demonstrated by other researchers in other types of cancer), we here demonstrate that ROS produced by UCP2 inhibition also stimulate the Akt/mTOR oncogenic pathway in vitro and in vivo. This event may be interpreted as an extreme attempt of the tumor cells to survive in the hostile and cytotoxic condition, such as that generated by UCP2 inhibition. This behavior is not surprising because many pro-survival molecular mechanisms are known to be adopted by tumor cells in critical conditions. The consequence of our discovery implies that an Akt/mTOR pathway inhibitor, such as everolimus, which is a molecule of high clinical interest in oncology, has to be associated to UCP2 inhibition and oxidative stress in order to induce a full cell death of PDAC cells. In this study, we show for the first time that the association of genipin and everolimus can determine a synergistic cell death effect on PDAC cells both in vitro and in a murine model. We have modified the Introduction of the manuscript to better highlight this crucial issue.

Is the reduction of cell growth by genepin due to another mechanism different from UCP2 inhibition?

Response: The possibility that cell growth reduction by genipin could be due to another mechanism different from UCP2 inhibition is very unlikely. Indeed, we have previously demonstrated and published that the knockdown by siRNA of the specific target of genipin, i.e. UCP2, significantly reduces cell death by genipin in PDAC cells (Brandi et al., FRBM 2016).

Results

Pag 18, line 402: "drug combination strongly enhances ROS production as compared with single drugs (Fig. 2B) and the ROS-mediated antiproliferative effect in PDAC cells (Fig. 2C)." Previously the authors affirm that ROS trigger Akt/mTOR pathway (Figure 1D shows that Akt and P70S6K phosphorylation induced by genipin is at least partially rescued by NAC demonstrating the involvement of ROS production in this signaling regulation driven by UCP2 blockage). It needs to explain this.

Response: We thank the Reviewer for this suggestion because this crucial consideration might need further explanations for clarity to the readers. As the Reviewer reports, we show that inhibition of UCP2 causes the stimulation of the Akt/mTOR oncogenic pathway in a ROS-dependent manner (Figure 1). Then, we show that combined genipin and everolimus treatment results in a strong increase in ROS (Figure 2B) and cell death (Figure 2C). This apparent contradiction can be explained by the observation that in the combined treatment the Akt/mTOR pathway is blocked by the pharmacological effect of everolimus even in the presence of high ROS levels (Figure 2A). In addition, the strong ROS stimulation and the concomitant Akt/mTOR inhibition observed after the combined treatment are mechanisms known to lead to GAPDH nuclear positivity, which we observe both in vitro and in vivo (Figure 3). Therefore, the GAPDH nuclear translocation is likely due to its oxidation and its failure to be phosphorylated by Akt/mTOR. These observations explain why the combined treatment results in a strong cell death effect despite ROS increase may potentially strongly stimulate the oncogenic Akt/mTOR pathway. An explanation of the above mentioned issue has been added in the appropriate Results section indicated by the Reviewer.

Reviewer #2:

1. Sedlak et al reported that the GAPDH mediates a novel cell death cascade (JAMA. 2006;295 (1):81-9.). Cytotoxic stimuli, via nitric oxide generation, lead to the binding of GAPDH to the protein Siah1, translocation of GAPDH-Siah1 to the nucleus, and ultimately cell death. Xing et al. Identified GAPDH as a protein target of the saframycin antiproliferative agents (Proc Natl Acad Sci USA. 2004;101(16):5862-6.). Drugs targeting on GAPDH hence plays important role for their action on cancer cells.

Your previous reports disclosed that UCP2 inhibition triggers ROS-dependent nuclear translocation of GAPDH and autophagic cell death in pancreatic adenocarcinoma cells (REF-18,19). Rapamycin and genipin enhanced antitumor activity in lung cancer (Su et al., Journal of Clinical Oncology. 2015;33 (15, Suppl.):e13595.).

Fiorini et al. (Onconase induces autophagy sensitizing pancreatic cancer cells to gemcitabine and activates Akt/mTOR pathway in a ROS-dependent manner. Biochim Biophys Acta. 2015;1853(3):549-60.) studied the precise mechanisms determining cytotoxicity in pancreatic cancer cells of onconase (ONC). ONC inhibited the expression of UCP2 and of MnSOD triggering

mitochondrial superoxide ion production. ONC-induced reactive oxygen species (ROS) were responsible for Akt/mTOR pathway stimulation determining the sensitivity of cancer cells to mTOR inhibitors and lessening autophagic stimulation. The conclusion made in this manuscript is not extended far from that of previous studies, thus reveals limited novelty for this manuscript.

Response: The Reviewer mentions some studies that constitute the scientific bases and, thus, the prerequisites of the present manuscript. Indeed, in the Discussion section, we have described our results referring to those previous studies mentioned by the Reviewer. For the Reviewer point of view, the present study reveals limited novelty. However, it should be stressed that we demonstrate here for the first time the strong synergistic antiproliferative effect on PDAC cells after UCP2 and mTOR inhibition. The Reviewer mentions the study "Rapamycin and genipin enhanced antitumor activity in lung cancer (Su et al., Journal of Clinical Oncology. 2015;33 (15, Suppl.):e13595.)". However, this is an abstract meeting and, to our best knowledge, no peer-reviewed articles related to this statement have yet been published.

In addition, we demonstrate that GAPDH nuclear translocation observed in vitro and in vivo is not a side effect in our system, but it is functionally involved in growth inhibition and apoptosis as shown by using the AXP3009 compound. Indeed, the addition of AXP3009 significantly counteracts GAPDH nuclear translocation (Fig. 4D) and cell growth inhibition (Fig. 4E) and apoptosis (Fig. 5B) induced by combined treatment.

Furthermore, in the present study, we demonstrate for the first time that UCP2 can regulate the critical pathway Akt/mTOR in a ROS-dependent way in vitro and in vivo. Since UCP2 is a mitochondrial antioxidant protein also involved in some key regulations of the energetic metabolism, the aberrant alteration of Akt/mTOR by UCP2 can be considered a relevant crossroad of the two distinct aspects in cancer, regulation of oxidative stress and energetic metabolism. Although several years of studies have highlighted the critical role of the antioxidant mitochondrial uncoupling protein UCP2 in driving tumor progression, the downstream effects and the mechanisms by which UCP2 intersects and alters the activity of other signaling pathways remains largely unknown. Our manuscript provides novel mechanistic insights into the oncogenic signaling regulation by UCP2 and unveils the combined inhibition of the antioxidant UCP2 and mTOR as a strategic therapeutic approach for cancer. Moreover, beyond cancer UCP2 is involved in a plethora of physiologic and pathologic events, including regulation of atherosclerotic plaque formation, immune response, food intake, and metabolic and oxidant diseases (Donadelli et al. Cell. Mol. Life Sci. 2014, 71:1171–1190). Thus, we believe that the consequences of our findings might be very relevant not only for cancer research.

The Reviewer mentions our previous study by Fiorini et al. describing the effect of onconase in PDAC cells. Although the involvement of some antioxidant proteins/enzymes as UCP2 and MnSOD has been described and the Akt/mTOR pathway has been demonstrated to be regulated in a ROS-mediated manner, the overall context is completely different because onconase is a ribonuclease enzyme secreted in oocytes and early embryos of *Rana pipiens*. Onconase may determine a plethora of unknown events into the cells altering the overall conclusions, thus confining the results of that article to the specific experimental conditions used. Instead, in the present manuscript, we used specific target drugs, everolimus and genipin, to specifically study the regulation of UCP2 and Akt/mTOR signaling and their therapeutic potential in mice xenograft.

2. Everolimus is a currently approved drug for the treatment of pancreatic tumours. However, genipin has not been developed for clinical used yet. Genipin and everolimus combination for pancreatic tumor therapy seems not feasible in clinical application.
Response: We agree with the Reviewer about the clinical relevance of everolimus. Concerning genipin, we are fully aware that this compound has not been developed for clinical use, however, in our opinion, it remains a valuable tool for the preclinical investigation of UCP2 roles and for the study of the potential clinical usage of new generation UCP2 inhibitors for therapy. We have modified the Discussion section by adding these observations.

3. There are several main themes in this manuscript that authors may need to figure out which is the major one. 1. UCP2 inhibition induces ROS/Akt/mTOR axis. 2. Role of GAPDH nuclear translocation. 3. Combination of UCP2 inhibitior genipin and mTOR inhibitor everolimus for pancreatic adenocarcinoma cell treatment. If the genipin/everolimus combination for anticancer synergism is the main themes of this manuscript, more experimental designs should address on the synergistic effects. UCP2 inhibition induces ROS/Akt/mTOR axis and the GAPDH nuclear translocation could merely the markers for the effect evaluation.
Response: As the Reviewer underlines, the synergistic antiproliferative effect on pancreatic cancer cells of the combined treatment genipin+everolimus is a crucial finding of our manuscript. We have now extended the analysis of synergism on five PDAC cells lines having different origins (primary tumor or metastasis); different mutational status; different resistance/sensitivity to the standard chemotherapy (i.e. gemcitabine). The curves of PDAC cell growth after increasing concentrations of single drugs and their combinations are reported in the new Figure 3A. The analysis of synergism obtained by using the dedicated software CalcuSyn is reported in the new Figure 3B. To further describe the level of synergism observed, we report in the new Table 1 the relative parameters of synergism obtained with CalcuSyn, i. e. CI_{50}, CI_{75}, the percentage of synergism, and the DRI_{50} values for each drug (genipin and everolimus) and for all five PDAC cell lines tested. Further, we report in the new Supplementary Figure 3 the isobolograms of IC_{50} values for all cell lines tested. Material and Methods, Results, Figures, and Discussion Section have been modified accordingly. Overall, these new data strongly reinforce our statement that genipin and everolimus can synergistically inhibit growth of PDAC cells.

4. In the Fig.4, AXP3009 counteracts cell growth inhibition by genipin/everolimus treatment. The G alone, G + AXP3009, E alone, E + AXP3009 should be included in the experimental design.
Response: We agree with the Reviewer's comment and we have now performed new experiments. Data are reported in the new Figure 5E of the resubmitted manuscript. Intriguingly, concerning single drug treatments, AXP3009 is able to counteract cell growth inhibition by genipin in accordance with our previous article that demonstrated that UCP2 inhibition triggers ROS-dependent nuclear translocation of GAPDH and PDAC cell death (Dando et al. BBA-Molecular Cell Research 2013). On the contrary, AXP3009 is not able to counteract cell growth inhibition by everolimus in accordance with the observation that everolimus alone fails to regulate GAPDH nuclear translocation (Figure 4B). We thank the Reviewer for this suggestion, which gave us the opportunity to improve our manuscript.

5. The synergistic effect of genipin/everolimus combination in cancer therapy should be based on effect of genipin/everolimus >> sum of (genipin alone + everolimus alone)。Additive effect is different to synergistic effect。
Response: In the present manuscript, we refer to synergistic effects (and not additive) on the basis of the computational elaboration of our data reporting inhibition of cell growth of PDAC cells

treated with increasing concentrations of the two drugs in both single and combined settings with a fixed molar ratio. CalcuSyn software is specifically dedicated to the analysis of synergism by calculating the Combination Index (CI) values with the Chou-Talalay equation, which takes into account both the potency (IC_{50}) and the shape of the dose-effect curves. All synergism parameters, i.e. CI, DRI, percentage of synergism, isobolograms, are provided for all the five PDAC cell lines tested.

6. The 1st paragraph in the Discussion displays only introductory information that lacks specific discussing issue. You may omit it or combine with the 2nd paragraph.
Response: We agree with the Reviewer. The mentioned paragraph has been removed.

UCP2 inhibition induces ROS/Akt/mTOR axis: role of GAPDH nuclear translocation in genipin/everolimus anticancer synergism

Ilaria Dando[1#], Raffaella Pacchiana[1], Elisa Dalla Pozza[1], Ivana Cataldo[2], Stefano Bruno[3], Paola Conti[4], Marco Cordani[5], Anna Grimaldi[6], Giovanna Butera[1], Michele Caraglia[6], Aldo Scarpa[2], Marta Palmieri[1], Massimo Donadelli[1#].

[1]*Department of Neuroscience, Biomedicine and Movement, Biochemistry Section, University of Verona, Verona, Italy;*
[2]*Applied Research on Cancer Centre (ARC-Net) and Department of Diagnostics and Public Health, University of Verona, Verona, Italy;*
[3]*Food and Dug Department, University of Parma, Parma, Italy;*
[4]*Department of Pharmaceutical Sciences, University of Milan, Milan, Italy;*
[5]*Biochemistry Department; Universidad Autónoma de Madrid (UAM), Instituto de Investigaciones Biomédicas "Alberto Sols" (CSIC-UAM), IdiPAZ, Madrid, Spain;*
[6]*Department of Biochemistry, Biophysics and General Pathology, University of Campania "L. Vanvitelli", Naples, Italy.*

[#]Corresponding authors:

Massimo Donadelli, PhD. University of Verona, Strada Le Grazie 8, 37134 Verona, Italy. Phone: +39 045 8027281; fax: +39 045 8027170; e-mail: massimo.donadelli@univr.it;

Ilaria Dando, PhD. University of Verona, Strada Le Grazie 8, 37134 Verona, Italy. Phone: +39 045 8027174; fax: +39 045 8027170; e-mail: ilaria.dando@univr.it

Running title: Everolimus and genipin induce anticancer synergism

Keywords: pancreas cancer, uncoupling proteins, UCP2, mTOR, everolimus, GAPDH, cell death.

Abstract

Several studies indicate that mitochondrial uncoupling protein 2 (UCP2) plays a pivotal role in cancer development by decreasing reactive oxygen species (ROS) produced by mitochondrial metabolism and by sustaining chemoresistance to a plethora of anticancer drugs. Here, we demonstrate that inhibition of UCP2 triggers Akt/mTOR pathway in a ROS-dependent mechanism in pancreatic adenocarcinoma cells. This event reduces the antiproliferative outcome of UCP2 inhibition by genipin, creating the conditions for the synergistic counteraction of cancer cell growth with the mTOR inhibitor everolimus. Inhibition of pancreatic adenocarcinoma cell growth and induction of apoptosis by genipin and everolimus treatment are functionally related to nuclear translocation of the cytosolic glycolytic enzyme glyceraldehyde 3-phosphate dehydrogenase (GAPDH). The synthetic compound (S)-benzyl-2-amino-2-(S)-3-bromo-4,5-dihydroisoxazol-5-yl-acetate (AXP3009), which binds GAPDH at its redox-sensitive Cys152, restores cell viability affected by the combined treatment with genipin and everolimus, suggesting a role for ROS production in the nuclear translocation of GAPDH. Caspase-mediated apoptosis by genipin and everolimus is further potentiated by the autophagy inhibitor 3-methyladenine revealing a protective role for Beclin1-mediated autophagy induced by the treatment. Mice xenograft of pancreatic adenocarcinoma further confirmed the antiproliferative outcome of drug combination without toxic effects for animals. Tumor masses from mice injected with UCP2 and mTOR inhibitors revealed a strong reduction in tumor volume and number of mitosis associated with a marked GAPDH nuclear positivity. Altogether, these results reveal novel mechanisms through which UCP2 promotes cancer cell proliferation and support the combined inhibition of UCP2 and of Akt/mTOR pathway as a novel therapeutic strategy in the treatment of pancreatic adenocarcinoma.

1. Introduction

Pancreatic ductal adenocarcinoma (PDAC) is a devastating disease that remains the fourth leading cause of cancer-associated deaths [1, 2]. Despite advances in multimodal therapy [3, 4], PDAC remains extraordinarily lethal, with a 5-year overall survival rate of approximately 5% [1, 5]. Delayed diagnosis, early metastasis, and resistance to almost all the classes of cytotoxic drugs are considered the main reasons for the extremely poor prognosis of pancreas cancer patients [6]. For these reasons, research is now focused on the identification of more efficient therapeutic targets as well as new prognostic and diagnostic biomarkers in order to improve the clinical management of PDAC.

Everolimus, a well-tolerated analogue of rapamycin with improved pharmacokinetic properties and reduced immunosuppressive effects [7], has been approved by the Food and Drug Administration (FDA) in 2012 for the treatment of advanced/metastatic renal cell carcinoma, subependymal giant cell astrocytoma and progressive neuroendocrine tumors of pancreatic origin [8]. Recently, Peng *et al.* demonstrated that everolimus, by inhibiting mTOR complex, can overcome the resistance to gemcitabine-based treatment of PDAC cell lines inducing caspase-dependent apoptosis and cell cycle arrest in the G2 phase [9].

The uncoupling proteins (UCPs) belong to the superfamily of mitochondrial carrier proteins located in the mitochondrial inner membrane [10]. Among them, UCP2 has been found overexpressed in several tumor types triggering both tumorigenesis and cancer progression [11]. An extensive study on Oncomine data sets revealed that UCP2 gene is overexpressed in most of the cancer types examined, i.e. ovarian, bladder, esophageal, testicular, kidney, colorectal, lung, breast, leukemia, prostate, as well as pancreas cancers [12]. Concerning PDAC, some studies have shown that also the protein level of UCP2 is significantly higher in cancer samples than in the adjacent normal tissues, suggesting that UCP2 may sustain pancreatic tumor growth [13]. Along this line of evidence, our research group previously demonstrated that UCP2 is involved in PDAC

chemoresistance to gemcitabine treatment and that this treatment further induces the expression of UCP2 gene [14]. Furthermore, we recently demonstrated that UCP2 promotes the metabolic shift from mitochondrial oxidative phosphorylation (mtOXPHOS) to the glycolytic pathway sustaining the Warburg effect and PDAC cell proliferation [15]. All these properties are mainly ascribable to the diminution of mitochondrial reactive oxygen species (ROS) driven by UCP2, whose antioxidant property is due to the transport of protons from the intermembrane space to the mitochondrial matrix bypassing ATP synthase. This results in a decrease of several consequential events, including mitochondrial inner membrane potential, electron leakage from respiratory electron transport chain and superoxide ion generation into the mitochondrial matrix [16]. Therefore, mild uncoupling of mtOXPHOS may be considered the first line of defense against oxidative stress in cancer cells [17]. Overall, UCP2 overexpression may be considered a strategy adopted by cancer cells to protect themselves from excessive ROS production but can also be a potential target for therapy for different cancers particularly resistant to standard chemotherapies, such as PDAC [18]. We previously demonstrated that UCP2 inhibition triggers PDAC cell death by ROS-dependent nuclear translocation of the glycolytic enzyme glyceraldehyde 3-phosphate dehydrogenase (GAPDH) and stimulation of autophagy in PDAC cells [19]. In the present study, we show for the first time that although UCP2 inhibition determines PDAC cell growth inhibition, it can also stimulate the oncogenic Akt/mTOR pathway in a ROS-dependent manner, *in vitro* and *in vivo*. This is likely due to an extreme attempt of cancer cells to survive in these stressful conditions and provides the rationale for a combined therapeutic setting with the mTOR inhibitor everolimus in PDAC.

2. Material and Methods

2.1 Drugs and chemicals

Genipin (methyl-2-hydroxy-9-hydroxymethyl-3-oxabicyclonona-4,8-diene-5-carboxylate), everolimus (RAD001), *N*-acetyl-l-cysteine (NAC), and 3-methyladenine (3-MA) were obtained from Sigma-Aldrich. Genipin and everolimus were solubilized in DMSO, NAC was solubilized in bi-distilled sterile water, and 3-MA was freshly prepared and solubilized in cell culture medium. The GAPDH inhibitor (S)-benzyl-2-amino-2-(S)-3-bromo-4,5-dihydroisoxazol-5-yl-acetate (AXP3009) has been designed and synthetized in the laboratory of Dr. Paola Conti at the Department of Pharmaceutical Sciences (University of Milan, Italy) and solubilized in methanol. The chemical structure and the synthesis of the AXP3009 compound have been previously described in Bruno and colleagues [20]. All chemicals were stored at -80°C.

2.2 Cell culture

Pancreatic adenocarcinoma PaCa44, PaCa3, Panc1, MiaPaCa2, and T3M4 cell lines were grown in RPMI 1640 medium (Gibco, Thermo Fisher), supplemented with 2 mM glutamine, 10% FBS, and 50 µg/ml gentamicin sulfate (BioWhittaker, Lonza), and incubated at 37°C with 5% CO_2.

2.3 Immunoblot analysis

Whole cell lysates. Cells were harvested, washed in PBS, and re-suspended in lysis buffer in the presence of phosphatase and protease inhibitors (50 mM Tris–HCl pH 8, 150 mM NaCl, 1% Igepal CA-630, 0.5% Na-Doc, 0.1% SDS, 1 mM Na_3VO_4, 1 mM NaF, 2.5 mM EDTA, 1 mM PMSF, and 1× protease inhibitor cocktail). After incubation on ice for 30 min, the lysates were centrifuged at 5,000 × g for 10 min at 4 °C and the supernatant fractions were used for Western blot analysis.

Cytoplasmic and nuclear lysates. Cells were harvested, washed in PBS, and re-suspended in lysis buffer A (10 mM Hepes, 0.1% Igepal CA-630, 1.5 mM $MgCl_2$, 10 mM KCl) in the presence of

phosphatase and protease inhibitors (1 mM Na_3VO_4, 1 mM NaF, 0.5 mM DTT, 1 mM PMSF, and 1× protease inhibitor cocktail). After incubation on ice for 10 min, the lysates were centrifuged at 3,000 × g for 10 min at 4 °C and the supernatant fractions, containing cytoplasmic proteins, were used for Western blot analysis, whereas the pellets, containing nuclei, were re-suspended in lysis buffer C (20 mM Hepes, 25% glycerol, 420 mM NaCl, 1.5 mM $MgCl_2$, 0.2 mM EDTA) in the presence of phosphatase and protease inhibitors. After incubation on ice for 15 min, the lysates were centrifuged at 15,000 × g for 10 min at 4 °C and the supernatant fractions were used for Western blot analysis.

Protein concentration was measured by Bradford reagent (Pierce) using bovine serum albumin as a standard. Protein extracts (50 μg/lane for whole cell lysate immunoblots and 6 μg/lane for cytoplasmic and nuclear cell lysate immunoblots) were resolved on a 12% SDS-polyacrylamide gel and electro-blotted onto PVDF membranes (Millipore). Membranes were blocked in 5% low-fat milk in TBST (50 mM Tris pH 7.5, 0.9% NaCl, 0.1% Tween 20) for 1 h at room temperature (RT) and probed overnight at 4 °C with anti-phospho(Ser473)-Akt (1:2,000; Cell Signalling #4060), anti-Akt (1:1,000; Cell Signalling #9272), anti-α-tubulin (1:2,500; Oncogene #CP06-100UG), anti-phospho(Thr389)-P70S6K (1:1,000; Cell Signalling #9206), anti-P70S6K (1:1,000; Cell Signalling #2708), anti-glyceraldehyde 3-phosphate dehydrogenase (GAPDH) (1:1,000; Cell Signaling, #5174S), anti-Lamin B1 (1:1,000; Millipore #05-1531), anti-α-tubulin (1:2,500; Oncogene #CP06-100UG), anti-Bcl2 (1:1,000; Cell Signalling #2872), anti-caspase 3 full length (1:1,000; Cell Signalling #9662), anti-caspase 9 full length (1:1,000; Enzo Life Sciences #ALX-210-815-C100), anti-Beclin1 (1:1,000; Cell Signalling Technology #4122), anti-Hsp90 (1:1,000; Cell Signalling #4874) antibodies. Horseradish peroxidase conjugated anti-mouse (1:10,000; KPL #074-1806) or anti-rabbit IgGs (1:2,000; Cell Signalling #7074) were used as secondary antibodies. The immunocomplexes were visualized by chemiluminescence using the ChemidocMP imaging system (Bio-Rad Laboratories) and the intensity of the chemiluminescence response was measured by

149 processing the image with NIH Image J software (http://rsb.info.nih.gov/nih-image/). Amido Black
150 staining was used to confirm equal cytoplasmic and nuclear protein loading in different lanes.
151
152 *2.4 Transient transfection assays*
153 Exponentially growing cells were seeded at $5x10^3$ cells/well in 96-well plates for
154 monodansylcadaverine (MDC) assay and at $2.5x10^5$ cells/plate in 60 mm cell culture plates for
155 protein extractions. UCP2 and Beclin-1 silencing experiments were carried out with specific small
156 interfering RNA (siRNA): siRNA UCP2 (5′-GCUAAAGUCCGGUUACAGATT-3′), siRNA
157 Beclin-1 (5'-ACAGUGAAUUUAAACGACAGCAGCU-3'), siRNA GAPDH (Ambion,
158 #4390850), and a non-targeting siRNA (5'-CAGUCGCGUUUGCGACUGG-3') used as negative
159 control were purchased by Ambion, Thermo Fisher. Cells were transfected with siRNA at a final
160 concentration of 50 nM Lipofectamine 3000 transfection reagent (Thermo Fisher), according to the
161 manufacturer's instructions. Transfection efficiency of cells was about 40% as previously assessed
162 by cytofluorimetric analysis using a pGFP plasmid vector [14].
163
164 *2.5 Analysis of reactive oxygen species (ROS) and mitochondrial superoxide ion production*
165 *ROS production*. The non-fluorescent diacetylated 2′,7′-dichlorofluorescein (DCF-DA)
166 probe (Sigma-Aldrich), which becomes highly fluorescent upon oxidation, was used to evaluate
167 intracellular ROS production. Briefly, cells were plated in 96-well plates ($5x10^3$ cells/well) and, the
168 day after, were treated with the various compounds at the indicated concentrations for 24 h. At the
169 end of the various treatments, the cells were incubated in culture medium with 10 μM DCF-DA for
170 15 min at 37 °C. The cells were washed with Hanks' buffer (20 mM Hepes, pH 7.2, 10 mM
171 glucose, 118 mM NaCl, 4.6 mM KCl, and 1 mM $CaCl_2$) and the DCF fluorescence was measured
172 by using a multimode plate reader ($Ex_{485\ nm}$ and $Em_{535\ nm}$) (GENios Pro, Tecan). The values were
173 normalized on cell proliferation by crystal violet assay.

Mitochondrial superoxide ion production. The nonfluorescent MitoSOX red probe (Molecular Probes) was used to evaluate mitochondrial O_2•− production. The probe is live-cell permeative and is rapidly and selectively targeted to the mitochondria where it becomes fluorescent after oxidation by O_2•−, but not by other ROS or reactive nitrogen species. Briefly, cells were plated in 96-well plates ($5x10^3$ cells/well) and, the day after, were treated with the various compounds at the indicated concentrations for 24 h. At the end of the various treatments, cells were incubated in culture medium with 0.5 μM MitoSOX at 37 °C for 15 min. The cells were then washed with Hanks' buffer and fluorescence was measured by using a multimode plate reader ($Ex_{535\ nm}$ and $Em_{590\ nm}$) (GENios Pro, Tecan). The values were normalized on cell proliferation by crystal violet assay. Three independent experiments were performed for each assay condition.

2.6 Cell proliferation assay

Cells were seeded in 96-well plates ($5x10^3$ cells/well) and the day after were incubated with various compounds at the indicated conditions (see figure legends). At the end of the treatments, cell growth was evaluated by Crystal Violet (Sigma-Aldrich) staining. The dye was solubilized in 1% SDS in PBS and measured photometrically ($A_{595\ nm}$) to determine cell viability (GENios Pro, Tecan). Three independent experiments were performed for each assay condition.

2.7 Drug combination studies

The compounds were added for 48 h at the following concentration ranges: 500 nM–200 μM for genipin and 25 nM–10 μM for everolimus, maintaining the ratio genipin:everolimus 20:1. The CI was calculated by the Chou-Talalay equation, which takes into account both the potency (IC_{50}) and the shape of the dose-effect curve [21] by using the CalcuSyn software. The general equation for the classic isobologram is given by CI=(D)1/(Dx)1+(D)2/(Dx)2+[(D)1*(D)2]/[(Dx)1*(Dx)2], where (Dx)1 and (Dx)2 in the denominators are the doses (or concentrations) for D1 (drug 1) and D2 (drug 2) alone that give x% growth inhibition, whereas (D)1 and (D)2 in the numerators are the

doses of drug 1 and drug 2 in combination that also inhibited x% cell viability (i.e., isoeffective). CI<1 indicates synergism, whereas CI=1 and CI>1 indicates additive effect and antagonism, respectively. CI/effect curve represents the CI versus the fraction (0–1) of cells killed by drug combination. The synergism percentage was obtained analyzing CI/effect curve and measuring the CI values at each 0.05 fraction, that is, 5% growth inhibition, of the antiproliferative effect. Dose reduction index (DRI) represents the measure of how much the dose of each drug in a synergistic combination may be reduced at a given effect level compared with the doses of each drug alone.

2.8 Immunofluorescence analysis of GAPDH nuclear translocation

PaCa44 cells treated or untreated with genipin and everolimus were fixed in 4% paraformaldehyde for 15 min and, after 4 changes (10 min each) of PBS, were permeabilized in 0.1% Triton X–100 for 5 min in PBS. To saturate unspecific binding sites, the cells were incubated for 45 min at RT with a blocking solution containing 5% BSA and 0.05% Triton X-100 in PBS. Samples were then incubated overnight at 4 °C with anti-GAPDH (1:100; Cell Signalling #5174S) primary antibody diluted in blocking solution. After 3 washes with PBS (10 min each), cells were incubated for 1 h at RT in the dark with specific secondary antibodies (1 μg/mL) conjugated with Alexa Fluor-488 (Molecular Probes). The incubation with secondary antibody was followed by 10 min incubation at RT with Hoechst dye (10 μg/ml). Samples were mounted in anti-bleaching medium (Dako Fluorescent Mounting Medium). The negative control procedure omitted the primary antibody. Slices were examined by fluorescence microscope (DM6000B, Leica Microsystem).

2.9 Structural characterization of AXP3009-bound recombinant GAPDH

His-tagged human GAPDH was recombinantly expressed in *E. coli*. Circular dichroism spectra of GAPDH at 10 μM concentration were collected at 25°C with a JASCO J-715 spectropolarimeter in a buffered solution containing 10 mM sodium phosphate at pH 7.6.

Measurements were made either in the 250-345 nm range, using a path length of 1 cm, or in the 190-250 nm range, using a path length of 0.1 cm, in both cases with a 0.5 nm data pitch, a 50 nm/min scanning speed and with 3-5 accumulations per spectrum. GAPDH spectra were collected in the absence of AXP3009 and upon overnight incubation with 30-100 μM AXP3009, to allow for the completion of the time-dependent binding [20]. The thermal stability of AXP3009-bound and unbound GAPDH was monitored with the spectropolarimeter set at 222 nm using a temperature ramp in the 30-80°C range, generated with a JASCO PTC-348 WI temperature controller. Each spectral observation and each denaturation kinetics was confirmed by at least two independent experiments. The elution times of AXP3009-bound and unbound GAPDH were measured on a superdex 200 increase 3.2/300 column (GE Healthcare) mounted on a Prominence HPLC system (Shimadzu) with the detector set at 280 nm. The column was pre-equilibrated and then developed with a solution containing 10 mM sodium phosphate, 50 mM sodium chloride pH 7.6. The flow rate was 0.15 mL/min. The column was calibrated with commercially available gel-filtration standards (Sigma-Aldrich), including carbonic anhydrase (29 kDa), conalbumin (75 kDa), ferritin (440 kDa) and blue dextrane (2000 kDa).

2.10 Apoptosis assay

Cells were seeded in 96-well plates ($5x10^3$ cells/well) and, the day after, treated with the various compounds at the indicated conditions (see figure legends). At the end of the treatment, cells were fixed with 2% paraformaldehyde in PBS at RT for 30 min, then washed twice with PBS and stained with annexinV/FITC (Bender MedSystem) in binding buffer (10 mM HEPES/NaOH pH 7.4, 140 mM NaCl and 2.5 mM $CaCl_2$) for 10 min at RT in the dark. Finally, cells were washed with binding buffer solution and fluorescence was measured by using a multimode plate reader ($Ex_{485\ nm}$ and $Em_{535\ nm}$) (GENios Pro, Tecan). The values were normalized on cell proliferation by Crystal Violet assay. Three independent experiments were performed for each assay condition.

252 *2.11 RNA extraction and qPCR*

253 Total RNA was extracted from 10^6 cells using TRIzol Reagent (Thermo Fisher) and 1 µg of
254 RNA was reverse transcribed using first-strand cDNA synthesis. Real-time quantification was
255 performed in triplicate samples by SYBR Green detection chemistry with Power SYBR Green PCR
256 Master Mix (Applied Biosystems) on a 7900 HT Fast Real-Time PCR System (Thermo Fisher).
257 Normalization was performed analysing the ribosomal protein large P0 (RPLP0) mRNA expression
258 level. The primers used were: CHOP For, 5'-GCAGCCCATGAAGGAGAAAG-3'; CHOP Rev, 5'-
259 CGGTCGATTTCCTGCTTGAG-3'; UCP2 For, 5'-CTCCTGAAAGCCAACCTCAT-3'; UCP2
260 Rev, 5'-CCCAAAGGCAGAAGTGAAGT-3'; GAPDH For, 5'-ATCAGCAATGCCTCCTGCAC-
261 3'; GAPDH Rev, 5'-TGGTCATGAGTCCTTCCACG-3'; Beclin1 For, 5'-
262 GTAGACCGGACTTGGGTGAC-3'; Beclin1 Rev, 5'-CTGCATGGTGCTGTTGTTG-3'; RPLP0
263 For, 5'-ACATGTTGCTGGCCAATAAGGT-3' and RPLP0 Rev, 5'-
264 CCTAAAGCCTGGAAAAAGGAGG-3'. The thermal cycle reaction was performed as follows: 95
265 °C for 10 minutes followed by 40 cycles at 95 °C for 15 seconds and 60°C for 1 minute. The
266 average of cycle threshold of each triplicate was analyzed according to the $2^{(-\Delta\Delta Ct)}$ method. Three
267 independent experiments were performed for each assay condition.

268

269 *2.12 Autophagosome formation assay*

270 To quantify the induction of autophagy, cells were treated with the various compounds (see
271 figure legends) and then were incubated with the fluorescent probe monodansylcadaverine (MDC;
272 Sigma-Aldrich). MDC is a selective marker for acidic vesicular organelles, such as autophagic
273 vacuoles and especially autolysosomes.

274 *Flow cytometry*: briefly, following the treatments, cells were incubated with 50 µM MDC in
275 PBS at 37 °C for 15 min. After incubation, cells were washed with PBS, trypsinized, and
276 immediately analyzed by flow cytometry. All fluorescences were analyzed with a FACScalibur
277 flow cytometer (Becton Dickinson). The fluorescent emissions were collected through a 530 nm

band pass filter (FL-1 channel). At least 10,000 events were acquired in log mode. For the quantitative evaluation of MDC, CellQuest software (Becton Dickinson) was used to calculate mean fluorescence intensities (MFIs) by the formula MFI-treated/MFI-control, where MFI-treated is the fluorescence intensity of cells treated with the various compounds and MFI-control is the fluorescence intensity of cells untreated. Figures show the means of fluorescence intensity ± SD from three independent experiments.

Multimode plate reader: briefly, cells were seeded in 96-well plates ($5x10^3$ cells/well) and treated with the various compounds at the indicated conditions (see figure legends). At the end of the treatments, cells were incubated in culture medium with 50 μM MDC at 37 °C for 15 min. After incubation, cells were washed with Hanks' buffer and fluorescence was measured by using a multimode plate reader ($Ex_{340\ nm}$ and $Em_{535\ nm}$) (GENios Pro, Tecan). The values were normalized on cell proliferation by Crystal Violet assay. Three independent experiments were performed for each assay condition.

2.13 Detection of acidic vesicular organelles with acridine orange

In acridine orange (AO) stained cells, the cytoplasm and nucleus are bright green and dim red, whereas acidic compartments are bright red. The intensity of the red fluorescence is proportional to the degree of acidity. Following the treatments (see figure legend), cells were incubated with AO solution (1 μg/ml) at 37 °C for 15 min, then were washed with PBS, and observed with a fluorescence microscope (Nikon Eclipse TE300 Inverted microscope - Nikon Instruments).

2.14 Immunoprecipitation assay

Following the treatments (see figure legend), cells were washed twice with ice-cold PBS/BSA, and lysed for 30 min at 4 °C in lysis buffer (50 mM Tris, pH 7.4, 150 mM sodium chloride, 1% Nonidet P-40, 1 mM EDTA, 1 mM sodium orthovanate, 1 mM sodium fluoride, 1

304 µg/ml leupeptin, 1 µg/ml aprotinin, 1 µg/ml pepstatin A, 1 mM PMSF). Lysates were centrifuged at
305 10,000 x g for 10 min and supernatants were collected. Protein concentration was determined by
306 Lowry method using bovine serum albumin for the standard curve. Protein lysates (120 µg) were
307 incubated with anti-Beclin1 (Cell Signalling Technology #4122) and anti-Hsp90 (Cell Signalling
308 #4874) primary antibodies overnight at 4°C. Immune complexes were collected with 50 µl of
309 protein A-agarose and incubated for 16 h at 4°C. The protein A-agarose/ immune complex was
310 washed twice with cold PBS, resuspended in 20 µl of SDS-loading buffer, heated to 95°C for 5 min
311 and used for protein gel blotting analysis. Proteins were separated by 12.5% polyacrylamide gel
312 SDS-PAGE (Mini-PROTEAN® TGX Stain-Free™ Precast Gels, BIORAD). After electrophoretic
313 separation the proteins were transferred on nitrocellulose filter (Trans-Blot Turbo Mini, BIORAD)
314 by Western Blotting, using Trans-Blot Turbo®Transfer System (BIORAD) and the filter was
315 reacted using either anti-Beclin1 or anti-Hsp90 antibodies. After incubation with secondary
316 antibodies, the signal was detected using enhanced chemiluminescence detection reagents Clarity™
317 Western ECL Blotting Substrate (BIORAD). The bands derived from western blotting were
318 analyzed and quantified by Image Lab 5.2.1 software obtained by ChemiDocTMXRS^{+} (BIORAD)
319 and the expression of total protein was used for normalization. The error bars shown in the
320 histograms represent the standard deviation from the mean of different densitometric scanning in at
321 least 3 different experiments.
322
323 *2.15 In vivo studies*
324 All procedures involving mice were performed in compliance with our institutional animal
325 care guidelines and following national and international directives (D.L. 4 March 2014, no. 26;
326 directive 2010/63/EU of the European parliament and of the council). PaCa44 cells ($1x10^6$
327 cells/mice) were s.c. injected into the dorsal flank of six nude female mice for each condition (5
328 weeks of age; Charles River Laboratories, Inc.). For the control groups, mice received 200 µl
329 injections of 1X PBS. One week after cell inoculation, experimental group received 30 mg/kg

genipin based on previous published data [22], or/and 4.5 mg/m^2 everolimus based on its clinical use following US Food and Drug Administration directives, and vehicle solution (PBS) for control group, by intraperitoneal injection biweekly for 4 weeks. Body mass was recorded weekly for each animal. Tumor size was monitored weekly in two perpendicular dimensions parallel to the surface of the mouse using a caliper. Tumor volume was calculated using the formula of V = π/6 x [(w x L)^(3/2)]. Animals were sacrificed at the volume of 2 cm^3. After euthanizing the mice, the neoplasms along with the visceral organs (heart, kidney, liver, lung, and pancreas) were retrieved for each mouse. All the samples were formalin fixed [in 10% (v/v) neutral-buffered formalin for 24-48 h] and paraffin embedded for further evaluations. Serial histological sections (4-6 μm thick) were obtained from each paraffin block and stained for histology assessment.

Hematoxylin and eosin (H&E) stain: One 4μm H&E slide was obtained for each sample (neoplasm and normal tissue) for each mouse to perform histopathological evaluation, including mitotic rate, grade of tumour necrosis and presence of lympho-granulocytic infiltrate in parenchyma of visceral organs and skin as sign of potential drug-related cytotoxicity. Mitotic count was assessed as absolute number of mitosis on 10 consecutive HPFs (high power field, 400X magnification) for each neoplastic sample.

Immunohistochemistry: 4 μm slides were obtained for each sample for immunohistochemical evaluation for anti-GAPDH (clone D16H11; 1:900; Cell Signalling) and phospho-Akt (clone EP2109Y; 1:100; Abcam). Human breast carcinoma was considered as positive control for GAPDH, while prostatic carcinoma for p-Akt. All the samples were analysed by a pathologist, blind for the treatment and control groups distribution. GAPDH-positivity was defined by the identification of a more intense nuclear stain compared to cytoplasmic and/or background stain. A count of viable GAPDH-positive neoplastic cells was assessed on 20 consecutive HPFs, away from necrotic area, in order to avoid potential artefacts due to necrosis. The apoptotic cells were excluded from the count because it was not always possible to discriminate between nuclear and cytoplasmic positivity due to the alterations occurring in the late apoptotic phases (nuclear

shrinkage and blebbing). Qualitative and quantitative p-Akt cytoplasmic and membranous expression was evaluated on neoplastic viable cells on 20 consecutive HPFs, away from necrotic area, in all the samples analysed. The quantitative analysis was performed through an evaluation of the percentage of p-Akt positive cells on each slide.

2.16 Statistical analysis

ANOVA (post hoc Bonferroni) analysis was performed by GraphPad Prism 5 (GraphPad Software, Inc., La Jolla, CA, USA). P-values < 0.05, 0.01, or 0.001 were indicated as *, **, or ***, respectively.

3. Results

3.1 UCP2 inhibition stimulates Akt/mTOR signaling pathway in a ROS-dependent manner

Previously, we demonstrated that ROS production by UCP2 inhibition triggers PDAC cell death [19]. Here, we show that this production concurrently induces the oncogenic Akt/mTOR pathway. **Figure 1A** shows that the activated form of Akt (phospho-Ser473Akt) is significantly increased after treatment with the UCP2 inhibitor genipin both in tumor masses derived from PDAC xenografts and in PDAC PaCa44 cells. Following the knockdown of UCP2 expression, the observed increase of the Thr389-phosphorylated level of P70S6K, a direct target of mTOR kinase complex, indicates that the Akt/mTOR pathway is functionally stimulated by UCP2 inhibition and also provides a valuable control of UCP2 inhibition (**Fig. 1B**). Accordingly, **Supplementary Figure 1** demonstrates the effective knockdown of UCP2 gene expression by siRNA-UCP2 as compared with a scramble siRNA used as negative control. In addition, the increase of Thr389-phosphorylation of P70S6K is revealed in three PDAC cell lines treated with genipin, thus indicating that Akt/mTOR induction is a common event in PDAC cells after UCP2 blockage (**Suppl. Fig. 2**). **Figure 1C** shows that genipin strongly induces ROS production and the radical scavenger *N*-acetyl-L-cysteine (NAC) counteracts this event. To investigate whether Akt/mTOR pathway regulation is functionally related to the antioxidant effect of UCP2, we analyzed Akt and

382 P70S6K phosphorylation levels in genipin-treated PDAC cells after NAC pre-treatment. **Figure 1D**
383 shows that Akt and P70S6K phosphorylation induced by genipin is at least partially rescued by
384 NAC demonstrating the involvement of ROS production in this signaling regulation driven by
385 UCP2 blockage.
386
387 *3.2 Genipin and everolimus synergistically inhibit PDAC cell proliferation through GAPDH*
388 *nuclear translocation*
389 Since stimulation of Akt/mTOR pathway has an established role in cancer proliferation and
390 everolimus, an oral anticancer mTOR inhibitor used in clinics, has shown particularly promising
391 results in cancer patients by inhibiting tumour growth and displaying anti-angiogenic effects also in
392 combined therapies [23], we investigated whether genipin and everolimus combination might
393 determine an enhanced antiproliferative effect in PDAC cells. First, we demonstrated that the
394 addition of everolimus counteracts both Akt and P70S6K phosphorylation induced by genipin (**Fig.**
395 **2A**), establishing the rational basis for the combined therapeutic strategy. In addition, drug
396 combination strongly enhances ROS production as compared with single drugs (**Fig. 2B**) and the
397 ROS-mediated antiproliferative effect in PDAC cells (**Fig. 2C)**. By a therapeutic point of view, the
398 addition of everolimus in the combined setting can assure the blockage of the Akt/mTOR pathway,
399 avoiding a further ROS-mediated Akt/mTOR signaling stimulation even in the presence of
400 enhanced ROS production.
401 In order to evaluate whether the antiproliferative effect of genipin+everolimus treatment was
402 synergistic, we analyzed cell growth inhibition curves by using the dedicated software CalcuSyn
403 (see Material and Methods). Dose-dependent analyses performed with increasing concentrations of
404 genipin and/or everolimus showed that the combined setting induces a strong antiproliferative
405 synergism in all five PDAC cell lines tested, as revealed by the curve of the combination index (CI)
406 values ± sd *versus* the fraction (0 → 1) of cells killed by drug combination (**Fig. 3A**). CI values
407 lying below 1 are widely distributed in the x axis, indicating a synergistic effect occurring at both

low and high drug concentrations in all PDAC cell lines tested (**Fig. 3B**). In particular, CI_{50} values of all PDAC cell lines are markedly below 1 indicating a strong synergism, and the reduction folds (dose reduction index; DRI) of drug concentration to obtain 50% cell growth inhibition in combination setting as compared to each drug administered alone (DRI_{50}) are reported in **Table 1**. Moreover, isobolograms at the IC_{50} of each drug for each PDAC cell line are reported in **Supplementary Figure 3**, further supporting the synergistic effect observed in these conditions. Taken together, these data demonstrate that the addition of everolimus to genipin treatment produces a synergistic PDAC cell growth inhibition which is likely due to both enhanced ROS production in combined setting and to the counteraction of genipin-induced Akt/mTOR oncogenic signaling by everolimus. DRI_{50} values obtained *in vitro* suggest that this synergism might allow decreasing the concentrations of the two compounds reducing eventual side effects.

Since we previously demonstrated that UCP2 inhibition determines a ROS-dependent nuclear translocation of GAPDH [19] and since GAPDH nuclear translocation is counteracted by Akt/mTOR pathway through direct phosphorylation of the enzyme [24], we explored if nuclear GAPDH positivity is further enhanced by the drug combination treatment. Importantly, we proved that tumor masses derived from mice treated with the combined therapy show a considerable increase in the number of GAPDH-positive nuclei (**Fig. 4A**). Also *in vitro*, we observed that the combined treatment strongly increases the amount of GAPDH positive nuclei, as compared to genipin-treated PDAC cells (**Fig. 4B**). Representative images of nuclear GAPDH positivity after PDAC cell treatment with the drug combination are reported in **Figure 4C**. The total amount of GAPDH mRNA remains unchanged after treatments (**Fig. 4D**), indicating that genipin and everolimus regulate the subcellular distribution of the enzyme rather than its expression level. To investigate the functional role of GAPDH nuclear translocation in cell growth inhibition by drug combination, we used the 3-bromo-isoxazoline derivative (S)-benzyl-2-amino-2-(S)-3-bromo-4,5-dihydroisoxazol-5-yl-acetate (AXP3009) (see Material and Methods), previously reported to alkylate the catalytic cysteine residue of tetrameric *Plasmodium falciparum* GAPDH (*Pf*GAPDH)

without affecting other solvent-exposed cysteine residues [20]. In consideration of the negative cooperativity of NAD^+ binding [25] and structural observations [26], it was concluded that the alkylation of one subunit of the GAPDH tetramer produces a conformational rearrangement that severely limits the accessibility of the remaining active sites [20]. Since 3-bromo-isoxazoline derivatives were also shown to bind to the redox sensitive catalytic cysteine of *human* GAPDH (*h*GAPDH) [27], we hypothesized that AXP3009 can alter *h*GAPDH conformation, prevent intracellular GAPDH oxidation by ROS produced after cell treatment with genipin and everolimus, and counteract GAPDH nuclear translocation. To test this hypothesis, we first investigated AXP3009-induced conformational rearrangements of recombinant *h*GAPDH. Circular dichroism spectra of *h*GAPDH pre-incubated with AXP3009 show significant differences in the 250-345 nm range, suggesting significant tertiary alterations in comparison to the control sample (**Figure 5A**). The melting temperature, as determined by the fitting of the thermic denaturation kinetics, is 2.2°C lower when *h*GAPDH is pre-incubated with AXP3009 (61.4±0.1 *versus* 63.6±0.1), suggesting a difference in stability of the two forms (**Figure 5B)**. Finally, gel filtration experiments of AXP3009-bound and unbound *h*GAPDH show a small but significant difference in the apparent molecular weight (**Figure 5C)**. Both forms fall within the range of the tetramer (expected weight 148000 Da), but with a 12% difference that might reflect a difference in shape or a different stability of the quaternary structure. Furthermore, we tested the specificity of AXP3009 on GAPDH interaction by knocking-down intracellular GAPDH expression with siRNA-GAPDH (**Suppl. Fig. 4A**), revealing that after target deprivation the compound loses its cytotoxic effect on PDAC cells (**Suppl. Fig. 4B**). Importantly, **Figure 5D** shows that AXP3009 stabilizes the cytosolic localization of the GAPDH enzyme by diminishing its nuclear transport, thus providing a valuable tool to investigate the role of nuclear GAPDH in cell death induced by genipin and everolimus treatment. According to the cell death-related role assumed by nuclear GAPDH translocation [28], we observed that AXP3009 is able to completely restore PDAC cell proliferation affected by genipin alone or by genipin and everolimus combined treatment (**Fig. 5E**).

460

461 *3.3 Genipin and everolimus strongly induce apoptosis in PDAC cells*

462 We further investigated whether apoptosis is involved in PDAC cell growth inhibition by
463 drug combination. As shown in **Figure 6A**, annexin V assay revealed that PDAC cells treated with
464 the drug combination expose a strongly higher amount of phosphatidylserine as compared to single
465 treatments or untreated control. Notably, apoptotic cell death induced by the combined treatment is
466 markedly reduced by the addition of AXP3009 or of the antioxidant compound NAC (**Fig. 6B**),
467 further supporting the antiproliferative role of GAPDH nuclear translocation mediated by
468 intracellular oxidant conditions [19, 29]. Moreover, we observed a strong increase of CHOP
469 expression by genipin+everolimus within the first eight hours after cell treatment (**Fig. 6C**), while
470 the expression of the Bcl 2 protein dramatically decreases in the combined setting (**Fig. 6D**),
471 according to the common assumption that the main mechanism of CHOP-induced apoptosis is the
472 suppression of the anti-apoptotic protein Bcl-2 [30]. In addition, the expression of the full length
473 caspase 3 and 9 is significantly reduced by the combined treatment as compared to single
474 treatments, suggesting the involvement of downstream effector caspases in the apoptotic cell death
475 induced by the concomitant inhibition of UCP2 and mTOR complex (Fig. 6D). The regulation of
476 Bcl 2 and of caspase 9, which in turn cleaves the downstream pro-caspase 3 in its truncated active
477 form, suggests that the mitochondrial death pathway is implicated in genipin/everolimus induced
478 apoptosis.

479

480 *3.4 Anti-apoptotic effect of Beclin1-dependent autophagy induced by genipin and everolimus*

481 Since GAPDH nuclear translocation can induce autophagy-related genes [31], we
482 investigated whether the combined treatment stimulates the formation of autophagic vesicles in
483 PDAC cells by using staining with the fluorescent probe monodansylcadaverine (MDC). FACS
484 analysis revealed that PDAC cells treated with the drug combination incorporate a higher amount of
485 MDC probe as compared with single treatments, suggesting an autophagy stimulation (**Fig. 7A**).

These data have been confirmed analyzing MDC incorporation using a microplate fluorescence reader (data not shown). To demonstrate that autophagy stimulation by drug combination results in the fusion of autophagy vesicles with lysosomes, we stained cells with the fluorescent probe acridine orange (AO), which changes its fluorescence emission from green to red upon accumulation into lysosomal acidic compartments revealing the typical pH acidification of lysosomes during autophagic stimulation. Fluorescence microscopy experiments confirmed the presence of wide red areas (acidic lysosomes containing accumulation of AO probe) into the cytoplasm of PDAC cells treated with drug combination (**Fig. 7B**), supporting the statement that the concomitant inhibition of UCP2 and mTOR can contribute to the formation of autophagic vesicles and their fusion with lysosomes in cancer cells.

The investigation of the mechanism involved in the stimulation of autophagy revealed that Beclin 1 (Atg 6), a well-known key regulator of autophagy, is strongly induced by the combined drug setting (**Fig. 7C**). In addition, since heat shock protein 90 (Hsp 90) is a molecular chaperone that regulates the stability of signaling proteins, including the maintenance of Beclin 1 protein stability through an evolutionarily conserved domain [32], we investigated whether genipin and everolimus can affect Beclin1:Hsp90 complex. Intriguingly, we observed by immunoprecipitation assay that everolimus promotes the interaction between Beclin 1 and Hsp 90 and that the formation of this complex is further enhanced by drug combination (**Fig. 7D**), strongly suggesting a role for Hsp 90 in Beclin 1 induction by the combined treatment. To test the functional role of Beclin 1 enhancement in autophagy stimulation, we knocked-down its expression by using a siRNA-Beclin1 (see control experiment in **Suppl. Fig. 5)**. **Figure 7E** indicates that autophagosome vesicle formation by drug combination is completely abolished by siRNA-Beclin1, highlighting the key role of this autophagy mediator protein in the overall process. Furthermore, since the role of autophagy in modulating cell growth is highly dependent on the metabolic context and on the microenvironmental conditions in which the cells lie [33], we investigated the impact of this process on the overall antiproliferative effect induced by drug combination. **Figure 7F** shows that

the percentage of PDAC cell growth is further decreased when a non-toxic concentration of 3-methyladenine (3-MA), a known inhibitor of the autophagosome formation process, is added to increasing concentrations of genipin+everolimus combination. Notably, the apoptotic effect of the drugs is strongly potentiated by 3-MA (**Fig. 7G**), demonstrating that Beclin1-dependent autophagy retains a protective and pro-survival role counteracting apoptotic cell death induced by the drugs.

3.5 Genipin and everolimus strongly inhibit growth of PDAC cells in mice xenografts

The effect of the intraperitoneal delivery of genipin and/or everolimus on growth inhibition of PaCa44 cells subcutaneously xenografted in nude mice was also investigated. **Figure 8A** shows that the volume of tumors in mice treated with the drug combination remains essentially unchanged during the observation time, whereas it strongly increases in the control group and, at a lower extent, in either genipin- or everolimus-treated groups. Tumor masses after mice sacrifice were recorded and shown in **Figure 8B** for control and combined treatment, further pointing out the high efficiency in the reduction of PDAC masses *in vivo*. To confirm this antiproliferative effect by genipin+everolimus treatment and the synergistic outcome observed in PDAC cell cultures, we demonstrated that the number of mitoses dramatically decreases only in tumor masses derived from mice injected with the drug combination (**Fig. 8C**). To investigate whether treatments might determine toxic effects, we analysed mice body weights during all the experiment period and, at the sacrifice of mice, we collected various organs (heart, kidney, liver, lung and pancreas) for haematoxylin and eosin (H&E) staining. **Figure 8D** shows that all the treatments do not change mice body masses during the experiment, suggesting the absence of any apparent toxicity. In addition, H&E histopathologic evaluation of the organs examined revealed the absence of any significant side effects for the animals (**Suppl. Fig. 6**).

4. Discussion

In this study, we demonstrate *in vitro* and in mice xenograft that UCP2 inhibition strongly triggers the oncogenic pathway Akt/mTOR, providing the rationale for the antiproliferative synergistic effect mediated by the UCP2 inhibitor genipin when used in combination with the mTOR inhibitor everolimus. Beyond the Akt/mTOR/P70S6K signaling inhibition, we demonstrate that everolimus strongly potentiates ROS production and PDAC cell death induced by genipin. This anti-proliferative effect by drug combination setting is due to a massive GAPDH nuclear translocation observed both *in vitro* and in mice xenograft. This determines caspase-mediated apoptotic cancer cell death as well as a protective autophagic process mediated by Beclin1 in PDAC cells (**Figure 9**). This latter event can be likely considered as an extreme tentative of cancer cells to survive in drug-induced stressing conditions. Thus, the full anticancer effect by genipin and everolimus combination can be achieved when the autophagic process is blocked.

Beyond glycolysis, several reports have demonstrated that GAPDH has a variety of other functions, including DNA repair [34], transcriptional regulation [35], membrane fusion and transport [36, 37], autophagy [31], and cell death [38, 39]. Indeed, in accord with its multiple activities, the intracellular localization of GAPDH is not restricted to the cytosol for energy production but is detected in the plasma and nuclear membrane, in the endoplasmic reticulum, in the Golgi apparatus, and in the nucleus [28]. GAPDH nuclear translocation is a particularly critical event in the light that, although the enzyme contains a nuclear export signal [40], it does not contain an equivalent nuclear localization signal (NLS). Thus, it is likely that other mechanisms need to be utilized for GAPDH translocation probably by binding with other molecules after post-translational modifications of the enzyme. For instance, upon exposure to oxidative stress, GAPDH nuclear translocation involves S-nitrosyl post-translational modification at its active site Cys152 [29]. Oxidized GAPDH binds to Siah1, an ubiquitin ligase, which contains its own NLS sequence thereby facilitating the intracellular transfer of this protein:protein complex and the subsequent transcriptional induction of apoptotic and cell death-related genes [29, 41]. Many other post-

translational modifications of GAPDH have been described, including phosphorylation, acetylation, glycosylation, poly ADP-ribosylation, and pyruvylation [42]. For these reasons GAPDH has received considerable attention as an appealing drug target for anticancer therapy [43].

Here, we show that the strong increase in GAPDH nuclear translocation and subsequent PDAC cell death by genipin and everolimus combination is due to both: *i)* oxidation of the enzyme by ROS increase, and *ii)* the everolimus-mediated counteraction of the Akt/mTOR pathway stimulated by genipin. Indeed, this oncogenic signaling is described to stabilize GAPDH in the cytosol through phosphorylation in Thr-237 of the enzyme decreasing its nuclear translocation and GAPDH-mediated apoptosis [24, 44]. The functional involvement of GAPDH nuclear translocation has been confirmed by the capability of AXP3009 to counteract PDAC cell death and apoptosis induced by drug combination. AXP3009 is a novel synthetic compound addressed to interact with the *Pf*GAPDH catalytic cysteine [20]. Here, we demonstrate that AXP3009 can prevent the nuclear translocation of GAPDH in PDAC cells, likely through conformational changes observed in recombinant *h*GAPDH that can elude the oxidation of the redox-sensitive catalytic cysteine. Notably, we observe a strong increase in the percentage of GAPDH nuclear positivity in tumor masses in nude mice injected with the drug combination. Concomitantly, tumor volume in mice treated with the two drugs remains essentially unchanged during the observation time without any signs of toxic effects for animals.

The synergistic PDAC cell growth inhibition obtained with everolimus and genipin treatment can allow to markedly reduce the concentrations of the two drug when used in combination. Optimal dosing is a crucial factor in order to achieve a maximum therapeutic efficacy with appropriate drug exposure and to maintain patient quality of life. CalcuSyn software analysis shows that the concentration of everolimus and that of genipin can be strongly reduced to obtain 50% PDAC cell growth inhibition in combined setting as compared to the concentrations needed to obtain the same effect in single treatment (Table 1). Notably, mTOR inhibitors-induced side effects, which can potentially compromise their therapeutic effectiveness, are well characterized and

include epithelial-cutaneous adverse events, pulmonary dysfunctions, metabolic alterations, and fatigue [45]. Although everolimus is a currently approved drug for the treatment of pancreatic cancer, genipin has not been developed for clinical use yet but it represents a valuable tool for the preclinical investigation of UCP2 roles and for the study of the potential clinical usage of next generation UCP2 inhibitors for therapy. In conclusion, our results and the statement that UCP2 overexpression promotes chemoresistance in cancers support the combined inhibition of UCP2 and of Akt/mTOR pathway as a novel therapeutic strategy in the treatment of PDAC.

Acknowledgements

We thank Andrea Mafficini for his technical support. This work was supported by Joint Projects program 2015 from University of Verona to M. Donadelli (n. B12I15002320003) and by Associazione Italiana Ricerca Cancro (AIRC 12182) to A. Scarpa. Ilaria Dando is a fellow of Fondazione Umberto Veronesi. Elisa Dalla Pozza is a fellow of AIRC 5 per mille (grant no. 12182).

Conflict of interest

The authors declare that they have no conflicts of interest.

References

[1] R.L. Siegel, K.D. Miller, A. Jemal, Cancer statistics, 2015, CA: a cancer journal for clinicians 65(1) (2015) 5-29.
[2] A. Vincent, J. Herman, R. Schulick, R.H. Hruban, M. Goggins, Pancreatic cancer, Lancet 378(9791) (2011) 607-20.
[3] N. Silvestris, O. Brunetti, E. Vasile, F. Cellini, I. Cataldo, V. Pusceddu, M. Cattaneo, S. Partelli, M. Scartozzi, G. Aprile, A. Casadei Gardini, A.G. Morganti, V. Valentini, A. Scarpa, M. Falconi, A. Calabrese, V. Lorusso, M. Reni, S. Cascinu, Multimodal treatment of resectable pancreatic ductal adenocarcinoma, Critical reviews in oncology/hematology 111 (2017) 152-165.
[4] N. Silvestris, V. Longo, F. Cellini, M. Reni, A. Bittoni, I. Cataldo, S. Partelli, M. Falconi, A. Scarpa, O. Brunetti, V. Lorusso, D. Santini, A. Morganti, V. Valentini, S. Cascinu, Neoadjuvant multimodal treatment of pancreatic ductal adenocarcinoma, Critical reviews in oncology/hematology 98 (2016) 309-24.
[5] S. Raimondi, P. Maisonneuve, A.B. Lowenfels, Epidemiology of pancreatic cancer: an overview, Nature reviews. Gastroenterology & hepatology 6(12) (2009) 699-708.
[6] N. Le, M. Sund, A. Vinci, G.c.g.o. Pancreas, Prognostic and predictive markers in pancreatic adenocarcinoma, Digestive and liver disease : official journal of the Italian Society of Gastroenterology and the Italian Association for the Study of the Liver 48(3) (2016) 223-30.
[7] L.M. Ballou, R.Z. Lin, Rapamycin and mTOR kinase inhibitors, Journal of chemical biology 1(1-4) (2008) 27-36.
[8] A.S. Strimpakos, E.M. Karapanagiotou, M.W. Saif, K.N. Syrigos, The role of mTOR in the management of solid tumors: an overview, Cancer treatment reviews 35(2) (2009) 148-59.
[9] T. Peng, Q.P. Dou, Everolimus Inhibits Growth of Gemcitabine-Resistant Pancreatic Cancer Cells via Induction of Caspase-Dependent Apoptosis and G2 /M Arrest, Journal of cellular biochemistry (2017).
[10] M. Donadelli, I. Dando, C. Fiorini, M. Palmieri, UCP2, a mitochondrial protein regulated at multiple levels, Cellular and molecular life sciences : CMLS 71(7) (2014) 1171-90.
[11] M.A. Pitt, Overexpression of uncoupling protein-2 in cancer: metabolic and heat changes, inhibition and effects on drug resistance, Inflammopharmacology 23(6) (2015) 365-9.
[12] V. Ayyasamy, K.M. Owens, M.M. Desouki, P. Liang, A. Bakin, K. Thangaraj, D.J. Buchsbaum, A.F. LoBuglio, K.K. Singh, Cellular model of Warburg effect identifies tumor promoting function of UCP2 in breast cancer and its suppression by genipin, PLoS One 6(9) (2011) e24792.
[13] W. Li, K. Nichols, C.A. Nathan, Y. Zhao, Mitochondrial uncoupling protein 2 is up-regulated in human head and neck, skin, pancreatic, and prostate tumors, Cancer biomarkers : section A of Disease markers 13(5) (2013) 377-83.
[14] E. Dalla Pozza, C. Fiorini, I. Dando, M. Menegazzi, A. Sgarbossa, C. Costanzo, M. Palmieri, M. Donadelli, Role of mitochondrial uncoupling protein 2 in cancer cell resistance to gemcitabine, Biochimica et biophysica acta 1823 (2012) 1856-1863.
[15] J. Brandi, D. Cecconi, M. Cordani, M. Torrens-Mas, R. Pacchiana, E.D. Pozza, G. Butera, M. Manfredi, E. Marengo, J. Oliver, P. Roca, I. Dando, M. Donadelli, The antioxidant uncoupling protein 2 stimulates hnRNPA2/B1, GLUT1 and PKM2 expression and sensitizes pancreas cancer cells to glycolysis inhibition, Free radical biology & medicine (2016).
[16] R.J. Mailloux, M.E. Harper, Uncoupling proteins and the control of mitochondrial reactive oxygen species production, Free radical biology & medicine 51(6) (2011) 1106-15.
[17] M.D. Brand, T.C. Esteves, Physiological functions of the mitochondrial uncoupling proteins UCP2 and UCP3, Cell Metab 2(2) (2005) 85-93.
[18] M. Donadelli, I. Dando, E. Dalla Pozza, M. Palmieri, Mitochondrial uncoupling protein 2 and pancreatic cancer: a new potential target therapy, World journal of gastroenterology : WJG 21(11) (2015) 3232-8.
[19] I. Dando, C. Fiorini, E.D. Pozza, C. Padroni, C. Costanzo, M. Palmieri, M. Donadelli, UCP2 inhibition triggers ROS-dependent nuclear translocation of GAPDH and autophagic cell death in pancreatic adenocarcinoma cells, Biochimica et biophysica acta 1833(3) (2013) 672-9.

[20] S. Bruno, A. Pinto, G. Paredi, L. Tamborini, C. De Micheli, V. La Pietra, L. Marinelli, E. Novellino, P. Conti, A. Mozzarelli, Discovery of covalent inhibitors of glyceraldehyde-3-phosphate dehydrogenase, a target for the treatment of malaria, Journal of medicinal chemistry 57(17) (2014) 7465-71.
[21] T.C. Chou, P. Talalay, Quantitative analysis of dose-effect relationships: the combined effects of multiple drugs or enzyme inhibitors, Adv Enzyme Regul 22 (1984) 27-55.
[22] N. Wang, M. Zhu, S.W. Tsao, K. Man, Z. Zhang, Y. Feng, Up-regulation of TIMP-1 by genipin inhibits MMP-2 activities and suppresses the metastatic potential of human hepatocellular carcinoma, PLoS One 7(9) (2012) e46318.
[23] K. Hirashima, Y. Baba, M. Watanabe, R.I. Karashima, N. Sato, Y. Imamura, Y. Nagai, N. Hayashi, K.I. Iyama, H. Baba, Aberrant activation of the mTOR pathway and anti-tumour effect of everolimus on oesophageal squamous cell carcinoma, British journal of cancer 106(5) (2012) 876-82.
[24] Q. Huang, F. Lan, Z. Zheng, F. Xie, J. Han, L. Dong, Y. Xie, F. Zheng, Akt2 kinase suppresses glyceraldehyde-3-phosphate dehydrogenase (GAPDH)-mediated apoptosis in ovarian cancer cells via phosphorylating GAPDH at threonine 237 and decreasing its nuclear translocation, J Biol Chem 286(49) (2011) 42211-20.
[25] Y.I. Henis, A. Levitzki, Mechanism of negative cooperativity in glyceraldehyde-3-phosphate dehydrogenase deduced from ligand competition experiments, Proc Natl Acad Sci U S A 77(9) (1980) 5055-59.
[26] S. Moniot, S. Bruno, C. Vonrhein, C. Didierjean, S. Boschi-Muller, M. Vas, G. Bricogne, G. Branlant, A. Mozzarelli, C. Corbier, Trapping of the thioacylglyceraldehyde-3-phosphate dehydrogenase intermediate from Bacillus stearothermophilus. Direct evidence for a flip-flop mechanism, J Biol Chem 283(31) (2008) 21693-702.
[27] S. Bruno, M. Margiotta, A. Pinto, G. Cullia, P. Conti, C. De Micheli, A. Mozzarelli, Selectivity of 3-bromo-isoxazoline inhibitors between human and Plasmodium falciparum glyceraldehyde-3-phosphate dehydrogenases, Bioorganic & medicinal chemistry 24(12) (2016) 2654-9.
[28] C. Tristan, N. Shahani, T.W. Sedlak, A. Sawa, The diverse functions of GAPDH: views from different subcellular compartments, Cellular signalling 23(2) (2011) 317-23.
[29] M.R. Hara, N. Agrawal, S.F. Kim, M.B. Cascio, M. Fujimuro, Y. Ozeki, M. Takahashi, J.H. Cheah, S.K. Tankou, L.D. Hester, C.D. Ferris, S.D. Hayward, S.H. Snyder, A. Sawa, S-nitrosylated GAPDH initiates apoptotic cell death by nuclear translocation following Siah1 binding, Nature cell biology 7(7) (2005) 665-74.
[30] K.D. McCullough, J.L. Martindale, L.O. Klotz, T.Y. Aw, N.J. Holbrook, Gadd153 sensitizes cells to endoplasmic reticulum stress by down-regulating Bcl2 and perturbing the cellular redox state, Mol Cell Biol 21(4) (2001) 1249-59.
[31] A. Colell, J.E. Ricci, S. Tait, S. Milasta, U. Maurer, L. Bouchier-Hayes, P. Fitzgerald, A. Guio-Carrion, N.J. Waterhouse, C.W. Li, B. Mari, P. Barbry, D.D. Newmeyer, H.M. Beere, D.R. Green, GAPDH and autophagy preserve survival after apoptotic cytochrome c release in the absence of caspase activation, Cell 129(5) (2007) 983-97.
[32] C. Xu, J. Liu, L.C. Hsu, Y. Luo, R. Xiang, T.H. Chuang, Functional interaction of heat shock protein 90 and Beclin 1 modulates Toll-like receptor-mediated autophagy, FASEB journal : official publication of the Federation of American Societies for Experimental Biology 25(8) (2011) 2700-10.
[33] S. Lorin, A. Hamai, M. Mehrpour, P. Codogno, Autophagy regulation and its role in cancer, Seminars in cancer biology 23(5) (2013) 361-79.
[34] K. Meyer-Siegler, D.J. Mauro, G. Seal, J. Wurzer, J.K. deRiel, M.A. Sirover, A human nuclear uracil DNA glycosylase is the 37-kDa subunit of glyceraldehyde-3-phosphate dehydrogenase, Proc Natl Acad Sci U S A 88(19) (1991) 8460-4.
[35] L. Zheng, R.G. Roeder, Y. Luo, S phase activation of the histone H2B promoter by OCA-S, a coactivator complex that contains GAPDH as a key component, Cell 114(2) (2003) 255-66.
[36] E.J. Tisdale, Glyceraldehyde-3-phosphate dehydrogenase is required for vesicular transport in the early secretory pathway, J Biol Chem 276(4) (2001) 2480-6.

[37] E.J. Tisdale, Glyceraldehyde-3-phosphate dehydrogenase is phosphorylated by protein kinase Ciota /lambda and plays a role in microtubule dynamics in the early secretory pathway, J Biol Chem 277(5) (2002) 3334-41.
[38] H. Nakajima, W. Amano, A. Fujita, A. Fukuhara, Y.T. Azuma, F. Hata, T. Inui, T. Takeuchi, The active site cysteine of the proapoptotic protein glyceraldehyde-3-phosphate dehydrogenase is essential in oxidative stress-induced aggregation and cell death, J Biol Chem 282(36) (2007) 26562-74.
[39] H. Nakajima, T. Kubo, H. Ihara, T. Hikida, T. Danjo, M. Nakatsuji, N. Shahani, M. Itakura, Y. Ono, Y.T. Azuma, T. Inui, A. Kamiya, A. Sawa, T. Takeuchi, Nuclear-translocated Glyceraldehyde-3-phosphate Dehydrogenase Promotes Poly(ADP-ribose) Polymerase-1 Activation during Oxidative/Nitrosative Stress in Stroke, J Biol Chem 290(23) (2015) 14493-503.
[40] V.M. Brown, E.Y. Krynetski, N.F. Krynetskaia, D. Grieger, S.T. Mukatira, K.G. Murti, C.A. Slaughter, H.W. Park, W.E. Evans, A novel CRM1-mediated nuclear export signal governs nuclear accumulation of glyceraldehyde-3-phosphate dehydrogenase following genotoxic stress, J Biol Chem 279(7) (2004) 5984-92.
[41] M.R. Hara, S.H. Snyder, Nitric oxide-GAPDH-Siah: a novel cell death cascade, Cellular and molecular neurobiology 26(4-6) (2006) 527-38.
[42] M.A. Sirover, Subcellular dynamics of multifunctional protein regulation: mechanisms of GAPDH intracellular translocation, Journal of cellular biochemistry 113(7) (2012) 2193-200.
[43] S. Ganapathy-Kanniappan, R. Kunjithapatham, J.F. Geschwind, Glyceraldehyde-3-phosphate dehydrogenase: a promising target for molecular therapy in hepatocellular carcinoma, Oncotarget 3(9) (2012) 940-53.
[44] T.M. Leisner, C. Moran, S.P. Holly, L.V. Parise, CIB1 prevents nuclear GAPDH accumulation and non-apoptotic tumor cell death via AKT and ERK signaling, Oncogene 32(34) (2013) 4017-27.
[45] D.A. Yardley, Adverse event management of mTOR inhibitors during treatment of hormone receptor-positive advanced breast cancer: considerations for oncologists, Clinical breast cancer 14(5) (2014) 297-308.

Figure Legends

Figure 1. Akt/mTOR pathway regulation by UCP2 in pancreatic ductal adenocarcinoma cells. (**A**) Qualitative and quantitative analysis of p-Akt expression on PaCa44 derived xenograft tumors (*in vivo*) and on PaCa44 cell line (*in vitro*) untreated/treated with genipin. P-Akt expression representative images are reported for tumors grown in control mice and in mice treated with genipin (for genipin subministration see Materials and Methods) at 20-fold magnification, scale bar 50 μm, and for *in vitro* a representative immunoblot image is reported for p-Akt expression in PaCa44 cells untreated/treated with 200 μM Genpin for 24h. (**B**) Western blot analysis of the total and phosphorylated form of the mTOR target P70S6K in PaCa44 cells transfected with 200 nM siRNA control or siRNA UCP2 for 72 h. (**C**) Analysis of DCF fluorescence intensity, corresponding to the level of ROS production, by a multimode plate reader in PaCa44 cells treated with 200 μM genipin and/or 10 mM NAC for 24 h. (**D**) Western blot analysis of the total and phosphorylated form of Akt or of the mTOR target P70S6K in PaCa44 cells treated with 200 μM genipin and/or 10 mM NAC for 24 h. The value of α-tubulin was used as a normalizing factor and protein fold change is relative to each control. Values are the means (±SD) of three independent experiments. Statistical analysis: (*) $P<0.05$ and (***) $P<0.001$ for treated cells vs each control or genipin vs genipin+NAC. Legend: (ctrl) control and (G) genipin.

Figure 2. The combined treatment genipin/everolimus impairs Akt/mTOR signaling and increases ROS production and anti-proliferative effects. (**A**) Western blot analysis of the total and phosphorylated form of Akt and P70S6K in PaCa44 cells treated with 200 μM genipin and/or 10 μM everolimus for 24 h. (**B**) Analysis of MitoSox fluorescence intensity, corresponding to the level of mitochondrial superoxide production, by a multimode plate reader in PaCa44 cells treated with 140 μM genipin and/or 7 μM everolimus for 24 h. (**C**) Cell growth analysis through the Crystal Violet colorimetric assay of PaCa44 cells treated with 100 μM genipin and/or 5 μM everolimus and/or 10 mM NAC for 48h. Values are the means of three independent experiments each performed in triplicate. Statistical analysis: (*) $P<0.05$, (**) $P<0.01$, and (***) $P<0.001$ for treated cells vs control or genipin+everolimus vs single treatments. Legend: (ctrl) control, (G) genipin, and (E) everolimus.

Figure 3. The combined treatment genipin/everolimus has a synergistic anti-proliferative effect on five PDAC cell lines. (**A**) Cell growth analysis through the Crystal Violet colorimetric

assay of five PDAC cell lines (PaCa44, Panc1, MiaPaCa2, PaCa3, and T3M4) treated with increasing doses of the drugs [genipin from 500 nM to 200 μM; everolimus from 25 nM to 10 μM] maintaining the ratio genipin:everolimus 20:1 for 48 h. Black squares, black rhombus and white circles correspond to genipin, everolimus and the combined treatment, respectively. Values are the means of three independent experiments each performed in triplicate. (**B**) Analysis of the synergistic cell growth inhibition of the five PDAC cell lines (PaCa44, Panc1, MiaPaCa2, PaCa3, and T3M4) treated with increasing doses of the drugs [genipin from 500 nM to 200 μM; everolimus from 25 nM to 10 μM] maintaining the ratio genipin:everolimus 20:1 for 48 h. The values on the x axis correspond to the fraction of growth inhibition (0→1) given by increasing concentrations of drug combinations. The values on the y axis correspond to the measurement of CI (see Materials and Methods).

Figure 4. mTOR inhibition enhances GAPDH nuclear translocation in genipin-treated cells. (**A**) Count of GAPDH positive nuclei in vital neoplastic cells on 20 consecutive HPFs of PaCa44 derived xenograft tumors. Mice have been untreated/treated with genipin and/or everolimus, as reported in Materials and Methods. Representative images are reported for control mice and for mice treated with genipin+everolimus at 40-fold magnification, scale bar 20 μm. (**B**) PaCa44 cells untreated or treated with 200 μM genipin and/or 10 μM everolimus for 24 h. GAPDH positive nuclei have been counted on several different fields for each condition and the amount of positive nuclei has been normalized on cell viability. (**C**) Representative immunofluorescence images of GAPDH (green) translocation into the nuclei (labelled with Hoechst dye) of PaCa44 cells untreated or treated with 200 μM genipin and 10 μM everolimus for 24 h, at 40-fold magnification, scale bar 10 μm. (**D**) Quantitative analysis of GAPDH mRNA though real-time PCR (qPCR) of PaCa44 cells treated with 200 μM genipin and/or 10 μM everolimus for 24 h. Total RNA was extracted from cells and qPCR was performed as described in Materials and Methods. Statistical analysis: (*) $P<0.05$, (**) $P<0.01$, and (***) $P<0.001$ for treated cells vs control or genipin+everolimus vs single treatments. Legend: (ctrl) control, (G) genipin, and (E) everolimus.

Figure 5. AXP3009 alters GAPDH conformation and counteracts cell growth inhibition by genipin/everolimus treatment. (A) Comparison of the circular dichroism spectra of AXP3009-bound (dashed line) and unbound *h*GAPDH (solid line) in the 190-250 nm range. Circular dichroism spectra of GAPDH at 10 μM in a buffered solution containing 10 mM sodium phosphate

799 at pH 7.6 in the 250-345 nm range were collected in the absence of AXP3009 (solid line) and upon
800 overnight incubation with 100 μM AXP3009 (dashed line). (**B**) Thermal denaturation kinetics of
801 AXP3009-bound (open symbols) and unbound *h*GAPDH (closed symbols) from two independent
802 experiments each. The solid lines are the fitting to a sigmoidal equation, indicative of a two-state
803 model. (**C**) Apparent molecular weights of AXP3009-bound and unbound GAPDH on a superdex
804 200 increase 3.2/300 column as estimated by comparison with calibrants in the range 29 -440 kDa.
805 The reported values are the means ± s.e.m. of five independent measurements. (**D**) Western blot
806 analysis and quantification of GAPDH expression into the cytosol and nuclei of PaCa44 cells
807 untreated/treated with 50 μM AXP3009 for 48 h. α-tubulin and Lamin B1 have been used as
808 controls of the quality of the cytoplasmic and nuclear protein fractions, respectively. Amido Black
809 staining was used to confirm equal cytoplasmic and nuclear protein loading in the different lanes.
810 (**E**) Cell growth analysis through the Crystal Violet colorimetric assay of PaCa44 cells treated with
811 50 μM of AXP3009 and/or with 100 μM genipin and/or 5 μM everolimus for 48h. Values are the
812 means (±SD) of three independent experiments. Statistical analysis: (*) $P<0.05$, (**) $P<0.01$, and
813 (***) $P<0.001$ for treated cells vs control or single treatment vs the relative single
814 treatment+AXP3009 or genipin+everolimus vs genipin+everolimus+AXP3009. Legend: (ctrl)
815 control, (G) genipin, (E) everolimus, (C) cytoplasmic fraction, and (N) nuclear fraction.
816

817 **Figure 6. mTOR inhibition increases apoptosis in genipin-treated cells.** Apoptosis analysis
818 through the Annexin V binding assay of PaCa44 cells treated with (**A**) 100 μM genipin and/or 5 μM
819 everolimus for 48 h and/or with (**B**) 1 μM AXP3009 and 10 mM NAC. (**C**) Quantitative analysis of
820 CHOP mRNA though real-time PCR (qPCR) of PaCa44 cells treated with 200 μM genipin and/or
821 10 μM everolimus for 8 h. Total RNA was extracted from cells and qPCR was performed as
822 described in Materials and Methods. (**D**) Western blot analysis of three apoptosis-related proteins
823 (Bcl2, caspase 3 full length, and caspase 9 full length) in PaCa44 cells treated with 100 μM genipin
824 and/or 5 μM everolimus for 48 h. The bands of Western blot analyses were scanned as digital peaks
825 and the areas of the peaks were calculated in arbitrary units. The value of α-tubulin was used as a
826 normalizing factor and protein fold change is relative to control cells. Values are the means (±SD)
827 of three independent experiments. Statistical analysis: (*) $P<0.05$, (**) $P<0.01$, and (***) $P<0.001$
828 for treated cells *vs* control, or single treatments *vs* genipin+everolimus, or genipin+everolimus *vs*
829 genipin+everolimus+AXP3009 or vs genipin+everolimus+NAC. Legend: (ctrl) control, (G)
830 genipin, and (E) everolimus.
831

Figure 7. mTOR inhibition induces autophagy and related-mechanisms in genipin-treated cells. (**A**) Autophagosome formation assay through the analysis of the incorporation of monodansylcadaverine (MDC) probe in PaCa44 cells treated with 100 µM genipin and/or 5 µM everolimus for 48 h though flow cytometry. (**B**) Representative immunofluorescence images of autophagosome formation through acridine orange staining of PaCa44 cells treated with 100 µM genipin and 5 µM everolimus for 24 h, at 40-fold magnification, scale bar 10 µm. (**C**) Western blot analysis of Beclin1 in PaCa44 cells treated with 100 µM genipin and/or 5 µM everolimus for 24 h. Amido black staining was used to confirm equal protein loading in the different lanes. (**D**) Immunoprecipitation analysis and relative quantification of Beclin-1/Hsp90 in PaCa44 cells treated with 200 µM genipin and/or 10 µM everolimus for 24 h. (**E**) Autophagosome formation assay through the incorporation of the MDC probe in PaCa44 cells transfected with 50 nM siRNA Beclin1 for 48 h and/or treated with 200 µM genipin and 10 µM everolimus for 48h. (**F**) Cell growth analysis through the Crystal Violet colorimetric assay of PaCa44 cells pre-treated for 1 h with 5 mM 3-MA and/or treated with increasing doses of the drugs [genipin from 500 nM to 140 µM; everolimus from 25 nM to 7 µM] maintaining the ratio genipin:everolimus 20:1 for 48 h. (**G**) Apoptosis analysis through the Annexin V binding assay of PaCa44 cells pre-treated for 1 h with 5 mM 3-MA and/or treated with 100 µM genipin and 5 µM everolimus for 48 h. Values are the means (±SD) of three independent experiments. Statistical analysis: (*) $P<0.05$, (**) $P<0.01$, and (***) $P<0.001$ for treated cells vs control, or single treatments vs genipin+everolimus, or genipin+everolimus vs genipin+everolimus+3-MA, or genipin+everolimus vs genpin+everolimus+siRNA Beclin1. Legend: (ctrl) control, (G) genipin, and (E) everolimus.

Figure 8. *In vivo* effect of mTOR inhibition in genipin-treated nude mice. PaCa44 cells were subcutaneously injected into female nude mice. After 1 week, i.p. injections with PBS (solution vehicle), genipin, and/or everolimus were administered twice a week for 4 weeks, as described in Materials and Methods. (**A**) Tumor volumes were measured at 3 days after each injection and values are the mean of mice tumor volumes in each group. Statistical analysis is referred to the days at which the tumor volume of the mice treated with genipin+everolimus is significantly lower than the other three groups, such as the control mice and the mice treated with the drugs alone. (*) $P<0.05$. (**B**) Four representative images of tumor masses grown in control mice and in mice treated with genipin+everolimus. (**C**) Count of mitotic figures on 10 consecutive HPFs (high power field, 40-fold magnification, scale bar 20 µm) for each neoplastic sample. Representative images are reported for control mice and for mice treated with genipin+everolimus. Statistical analysis is

865 referred to mice treated with the drug combination genipin+everolimus *vs* control mice. (***)
866 P<0.001. (**D**) Mice body mass was measured at 3 days after each injection and values are the means
867 of mice body in each group. Legend: (ctrl) control, (G) genipin, and (E) everolimus.

868

869 **Figure 9.** Schematic representation of the molecular mechanisms regulated by UCP2 and
870 Akt/mTOR inhibition identified in this study.

871

872 **Supplementary Figure 1.** Quantitative analysis of UCP2 mRNA though real-time PCR (qPCR) of
873 PaCa44 cells transfected with 200 nM siRNA control or siRNA UCP2 for 72 h. Total RNA was
874 extracted from cells and qPCR was performed as described in Materials and Methods.

875 **Supplementary Figure 2.** Western blot analysis of the total and phosphorylated form of the mTOR
876 target P70S6K in three pancreatic ductal cell lines (PaCa3, PaCa44, and Panc1) treated with 400
877 µM genipin for 24 h. Legend: (ctrl) control and (G) genipin.

878 **Supplementary Figure 3.** Isobolograms obtained from the Calcusyn output at 0.5 of fractional
879 effect (IC_{50}) for five PDAC cell lines (PaCa44, Panc1, MiaPaCa2, PaCa3, and T3M4) treated for 48
880 h. IC_{50} of genipin and everolimus alone are reported as cross on the x and y axis, respectively,
881 whereas the black dot represents the IC_{50} of the combined treatment. The combination data point
882 indicates an addictive effect when it is plotted on the diagonal, a synergistic effect when it is on the
883 lower left, and an antagonistic effect when it is on the upper right.

884 **Supplementary Figure 4.** (**A**) Quantitative analysis of GAPDH mRNA though real-time PCR
885 (qPCR) of PaCa44 cells transfected with 200 nM siRNA control or siRNA GAPDH for 72 h. Total
886 RNA was extracted from cells and qPCR was performed as described in Materials and Methods. (**B**)
887 Cell growth analysis through the Crystal Violet colorimetric assay of PaCa44 cells treated with 50
888 µM AXP3009 and/or with GAPDH siRNA for 48h.

889 **Supplementary Figure 5.** Quantitative analysis of Beclin-1 mRNA though real-time PCR (qPCR)
890 of PaCa44 cells transfected with 50 nM siRNA Beclin1 (siBECN1) for 48 h. Total RNA was
891 extracted from cells and qPCR was performed as described in Materials and Methods.

892 **Supplementary Figure 6.** Haematoxylin and eosin (H&E) tissue staining of nude mice injected
893 subcutaneously with PaCa44 cells. Representative images of heart, kidney, liver, lung and pancreas

894 in control mice and in mice treated with the drug combination genipin+everolimus taken at 10-fold
895 magnification, scale bar 100 μm.

UCP2 inhibition induces ROS/Akt/mTOR axis: role of GAPDH nuclear translocation in genipin/everolimus anticancer synergism

Ilaria Dando[1#], Raffaella Pacchiana[1], Elisa Dalla Pozza[1], Ivana Cataldo[2], Stefano Bruno[3], Paola Conti[4], Marco Cordani[5], Anna Grimaldi[6], Giovanna Butera[1], Michele Caraglia[6], Aldo Scarpa[2], Marta Palmieri[1], Massimo Donadelli[1#].

[1]*Department of Neuroscience, Biomedicine and Movement, Biochemistry Section, University of Verona, Verona, Italy;*
[2]*Applied Research on Cancer Centre (ARC-Net) and Department of Diagnostics and Public Health, University of Verona, Verona, Italy;*
[3]*Food and Dug Department, University of Parma, Parma, Italy;*
[4]*Department of Pharmaceutical Sciences, University of Milan, Milan, Italy;*
[5]*Biochemistry Department; Universidad Autónoma de Madrid (UAM), Instituto de Investigaciones Biomédicas "Alberto Sols" (CSIC-UAM), IdiPAZ, Madrid, Spain;*
[6]*Department of Biochemistry, Biophysics and General Pathology, University of Campania "L. Vanvitelli", Naples, Italy.*

[#]Corresponding authors:

Massimo Donadelli, PhD. University of Verona, Strada Le Grazie 8, 37134 Verona, Italy. Phone: +39 045 8027281; fax: +39 045 8027170; e-mail: massimo.donadelli@univr.it;

Ilaria Dando, PhD. University of Verona, Strada Le Grazie 8, 37134 Verona, Italy. Phone: +39 045 8027174; fax: +39 045 8027170; e-mail: ilaria.dando@univr.it

Field Code Changed

Running title: Everolimus and genipin induce anticancer synergism

Keywords: pancreas cancer, uncoupling proteins, UCP2, mTOR, everolimus, GAPDH, cell death.

Abstract

Several studies indicate that mitochondrial uncoupling protein 2 (UCP2) plays a pivotal role in cancer development by decreasing reactive oxygen species (ROS) produced by mitochondrial metabolism and by sustaining chemoresistance to a plethora of anticancer drugs. Here, we demonstrate that inhibition of UCP2 triggers Akt/mTOR pathway in a ROS-dependent mechanism in pancreatic adenocarcinoma cells. This event reduces the antiproliferative outcome of UCP2 inhibition by genipin, creating the conditions for the synergistic counteraction of cancer cell growth with the mTOR inhibitor everolimus. Inhibition of pancreatic adenocarcinoma cell growth and induction of apoptosis by genipin and everolimus treatment are functionally related to nuclear translocation of the cytosolic glycolytic enzyme glyceraldehyde 3-phosphate dehydrogenase (GAPDH). The synthetic compound (S)-benzyl-2-amino-2-(S)-3-bromo-4,5-dihydroisoxazol-5-yl-acetate (AXP3009), which binds GAPDH at its redox-sensitive Cys152, restores cell viability affected by the combined treatment with genipin and everolimus, suggesting a role for ROS production in the nuclear translocation of GAPDH. Caspase-mediated apoptosis by genipin and everolimus is further potentiated by the autophagy inhibitor 3-methyladenine revealing a protective role for Beclin1-mediated autophagy induced by the treatment. Mice xenograft of pancreatic adenocarcinoma further confirmed the antiproliferative outcome of drug combination without toxic effects for animals. Tumor masses from mice injected with UCP2 and mTOR inhibitors revealed a strong reduction in tumor volume and number of mitosis associated with a marked GAPDH nuclear positivity. Altogether, these results reveal novel mechanisms through which UCP2 promotes cancer cell proliferation and support the combined inhibition of UCP2 and of Akt/mTOR pathway as a novel therapeutic strategy in the treatment of pancreatic adenocarcinoma.

1. Introduction

Pancreatic ductal adenocarcinoma (PDAC) is a devastating disease that remains the fourth leading cause of cancer-associated deaths [1, 2]. Despite advances in multimodal therapy [3, 4], PDAC remains extraordinarily lethal, with a 5-year overall survival rate of approximately 5% [1, 5]. Delayed diagnosis, early metastasis, and resistance to almost all the classes of cytotoxic drugs are considered the main reasons for the extremely poor prognosis of pancreas cancer patients [6]. For these reasons, research is now focused on the identification of more efficient therapeutic targets as well as new prognostic and diagnostic biomarkers in order to improve the clinical management of PDAC.

Everolimus, a well-tolerated analogue of rapamycin with improved pharmacokinetic properties and reduced immunosuppressive effects [7], has been approved by the Food and Drug Administration (FDA) in 2012 for the treatment of advanced/metastatic renal cell carcinoma, subependymal giant cell astrocytoma and progressive neuroendocrine tumors of pancreatic origin [8]. Recently, Peng *et al.* demonstrated that everolimus, by inhibiting mTOR complex, can overcome the resistance to gemcitabine-based treatment of PDAC cell lines inducing caspase-dependent apoptosis and cell cycle arrest in the G2 phase [9].

The uncoupling proteins (UCPs) belong to the superfamily of mitochondrial carrier proteins located in the mitochondrial inner membrane [10]. Among them, UCP2 has been found overexpressed in several tumor types triggering both tumorigenesis and cancer progression [11]. An extensive study on Oncomine data sets revealed that UCP2 gene is overexpressed in most of the cancer types examined, i.e. ovarian, bladder, esophageal, testicular, kidney, colorectal, lung, breast, leukemia, prostate, as well as pancreas cancers [12]. Concerning PDAC, some studies have shown that also the protein level of UCP2 is significantly higher in cancer samples than in the adjacent normal tissues, suggesting that UCP2 may sustain pancreatic tumor growth [13]. Along this line of evidence, our research group previously demonstrated that UCP2 is involved in PDAC

chemoresistance to gemcitabine treatment and that this treatment further induces the expression of UCP2 gene [14]. Furthermore, we recently demonstrated that UCP2 promotes the metabolic shift from mitochondrial oxidative phosphorylation (mtOXPHOS) to the glycolytic pathway sustaining the Warburg effect and PDAC cell proliferation [15]. All these properties are mainly ascribable to the diminution of mitochondrial reactive oxygen species (ROS) driven by UCP2, whose antioxidant property is due to the transport of protons from the intermembrane space to the mitochondrial matrix bypassing ATP synthase. This results in a decrease of several consequential events, including mitochondrial inner membrane potential, electron leakage from respiratory electron transport chain and superoxide ion generation into the mitochondrial matrix [16]. Therefore, mild uncoupling of mtOXPHOS may be considered the first line of defense against oxidative stress in cancer cells [17]. Overall, UCP2 overexpression may be considered a strategy adopted by cancer cells to protect themselves from excessive ROS production but can also be a potential target for therapy for different cancers particularly resistant to standard chemotherapies, such as PDAC [18]. We previously demonstrated that UCP2 inhibition triggers PDAC cell death by ROS-dependent nuclear translocation of the glycolytic enzyme glyceraldehyde 3-phosphate dehydrogenase (GAPDH) and stimulation of autophagy in PDAC cells [19]. In the present study, we show for the first time that although UCP2 inhibition determines PDAC cell growth inhibition, it can also stimulate ~~triggers~~ the oncogenic Akt/mTOR pathway in a ROS-dependent manner, *in vitro* and *in vivo*.~~,~~ This is likely due to an extreme attempt of cancer cells to survive in thei~~i~~se stressful conditions and ~~provid~~provides ~~ing~~ the rationale for a combined therapeutic setting with the mTOR inhibitor everolimus in PDAC.

Formatted: Font: Italic

Formatted: Font: Italic

2. Material and Methods

2.1 Drugs and chemicals

Genipin (methyl-2-hydroxy-9-hydroxymethyl-3-oxabicyclonona-4,8-diene-5-carboxylate), everolimus (RAD001), *N*-acetyl-l-cysteine (NAC), and 3-methyladenine (3-MA) were obtained from Sigma-Aldrich. Genipin and everolimus were solubilized in DMSO, NAC was solubilized in bi-distilled sterile water, and 3-MA was freshly prepared and solubilized in cell culture medium. The GAPDH inhibitor (S)-benzyl-2-amino-2-(S)-3-bromo-4,5-dihydroisoxazol-5-yl-acetate (AXP3009) has been designed and synthetized in the laboratory of Dr. Paola Conti at the Department of Pharmaceutical Sciences (University of Milan, Italy) and solubilized in methanol. The chemical structure and the synthesis of the AXP3009 compound have been previously described in Bruno and colleagues [20]. All chemicals were stored at -80°C.

2.2 Cell culture

Pancreatic adenocarcinoma PaCa44, PaCa3, ~~and~~ Panc1, MiaPaCa2, and T3M4 cell lines were grown in RPMI 1640 medium (Gibco, Thermo Fisher), supplemented with 2 mM glutamine, 10% FBS, and 50 µg/ml gentamicin sulfate (BioWhittaker, Lonza), and incubated at 37°C with 5% CO_2.

2.3 Immunoblot analysis

Whole cell lysates. Cells were harvested, washed in PBS, and re-suspended in lysis buffer in the presence of phosphatase and protease inhibitors (50 mM Tris–HCl pH 8, 150 mM NaCl, 1% Igepal CA-630, 0.5% Na-Doc, 0.1% SDS, 1 mM Na_3VO_4, 1 mM NaF, 2.5 mM EDTA, 1 mM PMSF, and 1× protease inhibitor cocktail). After incubation on ice for 30 min, the lysates were centrifuged at 5,000 × g for 10 min at 4 °C and the supernatant fractions were used for Western blot analysis.

123 *Cytoplasmic and nuclear lysates.* Cells were harvested, washed in PBS, and re-suspended in
124 lysis buffer A (10 mM Hepes, 0.1% Igepal CA-630, 1.5 mM $MgCl_2$, 10 mM KCl) in the presence of
125 phosphatase and protease inhibitors (1 mM Na_3VO_4, 1 mM NaF, 0.5 mM DTT, 1 mM PMSF, and
126 1× protease inhibitor cocktail). After incubation on ice for 10 min, the lysates were centrifuged at
127 3,000 × g for 10 min at 4 °C and the supernatant fractions, containing cytoplasmic proteins, were
128 used for Western blot analysis, whereas the pellets, containing nuclei, were re-suspended in lysis
129 buffer C (20 mM Hepes, 25% glycerol, 420 mM NaCl, 1.5 mM $MgCl_2$, 0.2 mM EDTA) in the
130 presence of phosphatase and protease inhibitors. After incubation on ice for 15 min, the lysates
131 were centrifuged at 15,000 × g for 10 min at 4 °C and the supernatant fractions were used for
132 Western blot analysis.

133 Protein concentration was measured by Bradford reagent (Pierce) using bovine serum
134 albumin as a standard. Protein extracts (50 μg/lane for whole cell lysate immunoblots and 6 μg/lane
135 for cytoplasmic and nuclear cell lysate immunoblots) were resolved on a 12% SDS-polyacrylamide
136 gel and electro-blotted onto PVDF membranes (Millipore). Membranes were blocked in 5% low-fat
137 milk in TBST (50 mM Tris pH 7.5, 0.9% NaCl, 0.1% Tween 20) for 1 h at room temperature (RT)
138 and probed overnight at 4 °C with anti-phospho(Ser473)-Akt (1:2,000; Cell Signalling #4060), anti-
139 Akt (1:1,000; Cell Signalling #9272), anti-α-tubulin (1:2,500; Oncogene #CP06-100UG), anti-
140 phospho(Thr389)-P70S6K (1:1,000; Cell Signalling #9206), anti-P70S6K (1:1,000; Cell Signalling
141 #2708), anti-glyceraldehyde 3-phosphate dehydrogenase (GAPDH) (1:1,000; Cell Signaling,
142 #5174S), anti-Lamin B1 (1:1,000; Millipore #05-1531), anti-α-tubulin (1:2,500; Oncogene #CP06-
143 100UG), anti-Bcl2 (1:1,000; Cell Signalling #2872), anti-caspase 3 full length (1:1,000; Cell
144 Signalling #9662), anti-caspase 9 full length (1:1,000; Enzo Life Sciences #ALX-210-815-C100),
145 anti-Beclin1 (1:1,000; Cell Signalling Technology #4122), anti-Hsp90 (1:1,000; Cell Signalling
146 #4874) antibodies. Horseradish peroxidase conjugated anti-mouse (1:10,000; KPL #074-1806) or
147 anti-rabbit IgGs (1:2,000; Cell Signalling #7074) were used as secondary antibodies. The
148 immunocomplexes were visualized by chemiluminescence using the ChemidocMP imaging system

(Bio-Rad Laboratories) and the intensity of the chemiluminescence response was measured by processing the image with NIH Image J software (http://rsb.info.nih.gov/nih-image/). Amido Black staining was used to confirm equal cytoplasmic and nuclear protein loading in different lanes.

2.4 Transient transfection assays

Exponentially growing cells were seeded at $5x10^3$ cells/well in 96-well plates for monodansylcadaverine (MDC) assay and at $2.5x10^5$ cells/plate in 60 mm cell culture plates for protein extractions. UCP2 and Beclin-1 silencing experiments were carried out with specific small interfering RNA (siRNA): siRNA UCP2 (5′-GCUAAAGUCCGGUUACAGATT-3′), siRNA Beclin-1 (5'-ACAGUGAAUUUAAACGACAGCAGCU-3'), siRNA GAPDH (Ambion, #4390850), and a non-targeting siRNA (5'-CAGUCGCGUUUGCGACUGG-3') used as negative control were purchased by Ambion, Thermo Fisher. Cells were transfected with siRNA at a final concentration of 50 nM Lipofectamine 3000 transfection reagent (Thermo Fisher), according to the manufacturer's instructions. Transfection efficiency of cells was about 40% as previously assessed by cytofluorimetric analysis using a pGFP plasmid vector [14].

2.5 Analysis of reactive oxygen species (ROS) and mitochondrial superoxide ion production

ROS production. The non-fluorescent diacetylated 2′,7′-dichlorofluorescein (DCF-DA) probe (Sigma-Aldrich), which becomes highly fluorescent upon oxidation, was used to evaluate intracellular ROS production. Briefly, cells were plated in 96-well plates ($5x10^3$ cells/well) and, the day after, were treated with the various compounds at the indicated concentrations for 24 h. At the end of the various treatments, the cells were incubated in culture medium with 10 μM DCF-DA for 15 min at 37 °C. The cells were washed with Hanks' buffer (20 mM Hepes, pH 7.2, 10 mM glucose, 118 mM NaCl, 4.6 mM KCl, and 1 mM $CaCl_2$) and the DCF fluorescence was measured by using a multimode plate reader ($Ex_{485\ nm}$ and $Em_{535\ nm}$) (GENios Pro, Tecan). The values were normalized on cell proliferation by crystal violet assay.

Mitochondrial superoxide ion production. The nonfluorescent MitoSOX red probe (Molecular Probes) was used to evaluate mitochondrial O_2•− production. The probe is live-cell permeative and is rapidly and selectively targeted to the mitochondria where it becomes fluorescent after oxidation by O_2•−, but not by other ROS or reactive nitrogen species. Briefly, cells were plated in 96-well plates ($5x10^3$ cells/well) and, the day after, were treated with the various compounds at the indicated concentrations for 24 h. At the end of the various treatments, cells were incubated in culture medium with 0.5 µM MitoSOX at 37 °C for 15 min. The cells were then washed with Hanks' buffer and fluorescence was measured by using a multimode plate reader ($Ex_{535\ nm}$ and $Em_{590\ nm}$) (GENios Pro, Tecan). The values were normalized on cell proliferation by crystal violet assay. Three independent experiments were performed for each assay condition.

2.6 Cell proliferation assay

Cells were seeded in 96-well plates ($5x10^3$ cells/well) and the day after were incubated with various compounds at the indicated conditions (see figure legends). At the end of the treatments, cell growth was evaluated by Crystal Violet (Sigma-Aldrich) staining. The dye was solubilized in 1% SDS in PBS and measured photometrically ($A_{595\ nm}$) to determine cell viability (GENios Pro, Tecan). Three independent experiments were performed for each assay condition.

2.7 Drug combination studies

The compounds were added for 48 h at the following concentration ranges: 500 nM–200 µM for genipin and 25 nM–10 µM for everolimus, maintaining the ratio genipin:everolimus 20:1. The CI was calculated by the Chou–Talalay equation, which takes into account both the potency (IC_{50}) and the shape of the dose–effect curve [21] by using the CalcuSyn software. The general equation for the classic isobologram is given by CI=(D)1/(Dx)1+(D)2/(Dx)2+[(D)1*(D)2]/[(Dx)1*(Dx)2], where (Dx)1 and (Dx)2 in the denominators are the doses (or concentrations) for D1 (drug 1) and D2 (drug 2) alone that give x% growth inhibition, whereas (D)1 and (D)2 in the numerators are the

doses of drug 1 and drug 2 in combination that also inhibited x% cell viability (i.e., isoeffective). CI<1 indicates synergism, whereas CI=1 and CI>1 indicates additive effect and antagonism, respectively. CI/effect curve represents the CI versus the fraction (0–1) of cells killed by drug combination. The synergism percentage was obtained analyzing CI/effect curve and measuring the CI values at each 0.05 fraction, that is, 5% growth inhibition, of the antiproliferative effect. Dose reduction index (DRI) represents the measure of how much the dose of each drug in a synergistic combination may be reduced at a given effect level compared with the doses of each drug alone.

2.8 Immunofluorescence analysis of GAPDH nuclear translocation

PaCa44 cells treated or untreated with genipin and everolimus were fixed in 4% paraformaldehyde for 15 min and, after 4 changes (10 min each) of PBS, were permeabilized in 0.1% Triton X–100 for 5 min in PBS. To saturate unspecific binding sites, the cells were incubated for 45 min at RT with a blocking solution containing 5% BSA and 0.05% Triton X-100 in PBS. Samples were then incubated overnight at 4 °C with anti-GAPDH (1:100; Cell Signalling #5174S) primary antibody diluted in blocking solution. After 3 washes with PBS (10 min each), cells were incubated for 1 h at RT in the dark with specific secondary antibodies (1 μg/mL) conjugated with Alexa Fluor-488 (Molecular Probes). The incubation with secondary antibody was followed by 10 min incubation at RT with Hoechst dye (10 μg/ml). Samples were mounted in anti-bleaching medium (Dako Fluorescent Mounting Medium). The negative control procedure omitted the primary antibody. Slices were examined by fluorescence microscope (DM6000B, Leica Microsystem).

2.9 Structural characterization of AXP3009-bound recombinant GAPDH

His-tagged human GAPDH was recombinantly expressed in *E. coli*. Circular dichroism spectra of GAPDH at 10 μM concentration were collected at 25°C with a JASCO J-715 spectropolarimeter in a buffered solution containing 10 mM sodium phosphate at pH 7.6.

Measurements were made either in the 250-345 nm range, using a path length of 1 cm, or in the 190-250 nm range, using a path length of 0.1 cm, in both cases with a 0.5 nm data pitch, a 50 nm/min scanning speed and with 3-5 accumulations per spectrum. GAPDH spectra were collected in the absence of AXP3009 and upon overnight incubation with 30-100 μM AXP3009, to allow for the completion of the time-dependent binding [20]. The thermal stability of AXP3009-bound and unbound GAPDH was monitored with the spectropolarimeter set at 222 nm using a temperature ramp in the 30-80°C range, generated with a JASCO PTC-348 WI temperature controller. Each spectral observation and each denaturation kinetics was confirmed by at least two independent experiments. The elution times of AXP3009-bound and unbound GAPDH were measured on a superdex 200 increase 3.2/300 column (GE Healthcare) mounted on a Prominence HPLC system (Shimadzu) with the detector set at 280 nm. The column was pre-equilibrated and then developed with a solution containing 10 mM sodium phosphate, 50 mM sodium chloride pH 7.6. The flow rate was 0.15 mL/min. The column was calibrated with commercially available gel-filtration standards (Sigma-Aldrich), including carbonic anhydrase (29 kDa), conalbumin (75 kDa), ferritin (440 kDa) and blue dextrane (2000 kDa).

2.10 Apoptosis assay

Cells were seeded in 96-well plates ($5x10^3$ cells/well) and, the day after, treated with the various compounds at the indicated conditions (see figure legends). At the end of the treatment, cells were fixed with 2% paraformaldehyde in PBS at RT for 30 min, then washed twice with PBS and stained with annexinV/FITC (Bender MedSystem) in binding buffer (10 mM HEPES/NaOH pH 7.4, 140 mM NaCl and 2.5 mM $CaCl_2$) for 10 min at RT in the dark. Finally, cells were washed with binding buffer solution and fluorescence was measured by using a multimode plate reader ($Ex_{485\ nm}$ and $Em_{535\ nm}$) (GENios Pro, Tecan). The values were normalized on cell proliferation by Crystal Violet assay. Three independent experiments were performed for each assay condition.

253 *2.11 RNA extraction and qPCR*

254 Total RNA was extracted from 10^6 cells using TRIzol Reagent (Thermo Fisher) and 1 µg of
255 RNA was reverse transcribed using first-strand cDNA synthesis. Real-time quantification was
256 performed in triplicate samples by SYBR Green detection chemistry with Power SYBR Green PCR
257 Master Mix (Applied Biosystems) on a 7900 HT Fast Real-Time PCR System (Thermo Fisher).
258 Normalization was performed analysing the ribosomal protein large P0 (RPLP0) mRNA expression
259 level. The primers used were: CHOP For, 5'-GCAGCCCATGAAGGAGAAAG-3'; CHOP Rev, 5'-
260 CGGTCGATTTCCTGCTTGAG-3'; UCP2 For, 5'-CTCCTGAAAGCCAACCTCAT-3'; UCP2
261 Rev, 5'-CCCAAAGGCAGAAGTGAAGT-3'; GAPDH For, 5'-ATCAGCAATGCCTCCTGCAC-
262 3'; GAPDH Rev, 5'-TGGTCATGAGTCCTTCCACG-3'; Beclin1 For, 5'-
263 GTAGACCGGACTTGGGTGAC-3'; Beclin1 Rev, 5'-CTGCATGGTGCTGTTGTTG-3'; RPLP0
264 For, 5'-ACATGTTGCTGGCCAATAAGGT-3' and RPLP0 Rev, 5'-
265 CCTAAAGCCTGGAAAAAGGAGG-3'. The thermal cycle reaction was performed as follows: 95
266 °C for 10 minutes followed by 40 cycles at 95 °C for 15 seconds and 60°C for 1 minute. The
267 average of cycle threshold of each triplicate was analyzed according to the $2^{(-\Delta\Delta Ct)}$ method. Three
268 independent experiments were performed for each assay condition.

269

270 *2.12 Autophagosome formation assay*

271 To quantify the induction of autophagy, cells were treated with the various compounds (see
272 figure legends) and then were incubated with the fluorescent probe monodansylcadaverine (MDC;
273 Sigma-Aldrich). MDC is a selective marker for acidic vesicular organelles, such as autophagic
274 vacuoles and especially autolysosomes.

275 *Flow cytometry*: briefly, following the treatments, cells were incubated with 50 µM MDC in
276 PBS at 37 °C for 15 min. After incubation, cells were washed with PBS, trypsinized, and
277 immediately analyzed by flow cytometry. All fluorescences were analyzed with a FACScalibur
278 flow cytometer (Becton Dickinson). The fluorescent emissions were collected through a 530 nm

band pass filter (FL-1 channel). At least 10,000 events were acquired in log mode. For the quantitative evaluation of MDC, CellQuest software (Becton Dickinson) was used to calculate mean fluorescence intensities (MFIs) by the formula MFI-treated/MFI-control, where MFI-treated is the fluorescence intensity of cells treated with the various compounds and MFI-control is the fluorescence intensity of cells untreated. Figures show the means of fluorescence intensity ± SD from three independent experiments.

Multimode plate reader: briefly, cells were seeded in 96-well plates ($5x10^3$ cells/well) and treated with the various compounds at the indicated conditions (see figure legends). At the end of the treatments, cells were incubated in culture medium with 50 μM MDC at 37 °C for 15 min. After incubation, cells were washed with Hanks' buffer and fluorescence was measured by using a multimode plate reader ($Ex_{340\ nm}$ and $Em_{535\ nm}$) (GENios Pro, Tecan). The values were normalized on cell proliferation by Crystal Violet assay. Three independent experiments were performed for each assay condition.

2.13 Detection of acidic vesicular organelles with acridine orange

In acridine orange (AO) stained cells, the cytoplasm and nucleus are bright green and dim red, whereas acidic compartments are bright red. The intensity of the red fluorescence is proportional to the degree of acidity. Following the treatments (see figure legend), cells were incubated with AO solution (1 μg/ml) at 37 °C for 15 min, then were washed with PBS, and observed with a fluorescence microscope (Nikon Eclipse TE300 Inverted microscope - Nikon Instruments).

2.14 Immunoprecipitation assay

Following the treatments (see figure legend), cells were washed twice with ice-cold PBS/BSA, and lysed for 30 min at 4 °C in lysis buffer (50 mM Tris, pH 7.4, 150 mM sodium chloride, 1% Nonidet P-40, 1 mM EDTA, 1 mM sodium orthovanate, 1 mM sodium fluoride, 1

305 µg/ml leupeptin, 1 µg/ml aprotinin, 1 µg/ml pepstatin A, 1 mM PMSF). Lysates were centrifuged at
306 10,000 x g for 10 min and supernatants were collected. Protein concentration was determined by
307 Lowry method using bovine serum albumin for the standard curve. Protein lysates (120 µg) were
308 incubated with anti-Beclin1 (Cell Signalling Technology #4122) and anti-Hsp90 (Cell Signalling
309 #4874) primary antibodies overnight at 4°C. Immune complexes were collected with 50 µl of
310 protein A-agarose and incubated for 16 h at 4°C. The protein A-agarose/ immune complex was
311 washed twice with cold PBS, resuspended in 20 µl of SDS-loading buffer, heated to 95°C for 5 min
312 and used for protein gel blotting analysis. Proteins were separated by 12.5% polyacrylamide gel
313 SDS-PAGE (Mini-PROTEAN® TGX Stain-Free™ Precast Gels, BIORAD). After electrophoretic
314 separation the proteins were transferred on nitrocellulose filter (Trans-Blot Turbo Mini, BIORAD)
315 by Western Blotting, using Trans-Blot Turbo®Transfer System (BIORAD) and the filter was
316 reacted using either anti-Beclin1 or anti-Hsp90 antibodies. After incubation with secondary
317 antibodies, the signal was detected using enhanced chemiluminescence detection reagents Clarity™
318 Western ECL Blotting Substrate (BIORAD). The bands derived from western blotting were
319 analyzed and quantified by Image Lab 5.2.1 software obtained by ChemiDocTMXRS^{+} (BIORAD)
320 and the expression of total protein was used for normalization. The error bars shown in the
321 histograms represent the standard deviation from the mean of different densitometric scanning in at
322 least 3 different experiments.
323
324 *2.15 In vivo studies*
325 All procedures involving mice were performed in compliance with our institutional animal
326 care guidelines and following national and international directives (D.L. 4 March 2014, no. 26;
327 directive 2010/63/EU of the European parliament and of the council). PaCa44 cells (1x10^{6}
328 cells/mice) were s.c. injected into the dorsal flank of six nude female mice for each condition (5
329 weeks of age; Charles River Laboratories, Inc.). For the control groups, mice received 200 µl
330 injections of 1X PBS. One week after cell inoculation, experimental group received 30 mg/kg

331 genipin based on previous published data [22], or/and 4.5 mg/m^2 everolimus based on its clinical
332 use following US Food and Drug Administration directives, and vehicle solution (PBS) for control
333 group, by intraperitoneal injection biweekly for 4 weeks. Body mass was recorded weekly for each
334 animal. Tumor size was monitored weekly in two perpendicular dimensions parallel to the surface
335 of the mouse using a caliper. Tumor volume was calculated using the formula of V = π/6 x [(w x
336 L)^(3/2)]. Animals were sacrificed at the volume of 2 cm^3. After euthanizing the mice, the
337 neoplasms along with the visceral organs (heart, kidney, liver, lung, and pancreas) were retrieved
338 for each mouse. All the samples were formalin fixed [in 10% (v/v) neutral-buffered formalin for 24-
339 48 h] and paraffin embedded for further evaluations. Serial histological sections (4-6 μm thick)
340 were obtained from each paraffin block and stained for histology assessment.

341 *Hematoxylin and eosin (H&E) stain*: One 4μm H&E slide was obtained for each sample
342 (neoplasm and normal tissue) for each mouse to perform histopathological evaluation, including
343 mitotic rate, grade of tumour necrosis and presence of lympho-granulocytic infiltrate in parenchyma
344 of visceral organs and skin as sign of potential drug-related cytotoxicity. Mitotic count was assessed
345 as absolute number of mitosis on 10 consecutive HPFs (high power field, 400X magnification) for
346 each neoplastic sample.

347 *Immunohistochemistry*: 4 μm slides were obtained for each sample for
348 immunohistochemical evaluation for anti-GAPDH (clone D16H11; 1:900; Cell Signalling) and
349 phospho-Akt (clone EP2109Y; 1:100; Abcam). Human breast carcinoma was considered as positive
350 control for GAPDH, while prostatic carcinoma for p-Akt. All the samples were analysed by a
351 pathologist, blind for the treatment and control groups distribution. GAPDH-positivity was defined
352 by the identification of a more intense nuclear stain compared to cytoplasmic and/or background
353 stain. A count of viable GAPDH-positive neoplastic cells was assessed on 20 consecutive HPFs,
354 away from necrotic area, in order to avoid potential artefacts due to necrosis. The apoptotic cells
355 were excluded from the count because it was not always possible to discriminate between nuclear
356 and cytoplasmic positivity due to the alterations occurring in the late apoptotic phases (nuclear

shrinkage and blebbing). Qualitative and quantitative p-Akt cytoplasmic and membranous expression was evaluated on neoplastic viable cells on 20 consecutive HPFs, away from necrotic area, in all the samples analysed. The quantitative analysis was performed through an evaluation of the percentage of p-Akt positive cells on each slide.

2.16 Statistical analysis

ANOVA (post hoc Bonferroni) analysis was performed by GraphPad Prism 5 (GraphPad Software, Inc., La Jolla, CA, USA). P-values < 0.05, 0.01, or 0.001 were indicated as *, **, or ***, respectively.

3. Results

3.1 UCP2 inhibition stimulates Akt/mTOR signaling pathway in a ROS-dependent manner

Previously, we demonstrated that ROS production by UCP2 inhibition triggers PDAC cell death [19]. Here, we show that this production concurrently induces the oncogenic Akt/mTOR pathway. **Figure 1A** shows that the activated form of Akt (phospho-Ser473Akt) is significantly increased after treatment with the UCP2 inhibitor genipin both in tumor masses derived from PDAC xenografts and in PDAC PaCa44 cells. Following the knockdown of UCP2 expression, the observed increase of the Thr389-phosphorylated level of P70S6K, a direct target of mTOR kinase complex, indicates that the Akt/mTOR pathway is functionally stimulated by UCP2 inhibition and also provides a valuable control of UCP2 inhibition (**Fig. 1B**). Accordingly, **Supplementary Figure 1** demonstrates the effective knockdown of UCP2 gene expression by siRNA-UCP2 as compared with a scramble siRNA used as negative control. In addition, the increase of Thr389-phosphorylation of P70S6K is revealed in three PDAC cell lines treated with genipin, thus indicating that Akt/mTOR induction is a common event in PDAC cells after UCP2 blockage (**Suppl. Fig. 2**). **Figure 1C** shows that genipin strongly induces ROS production and the radical scavenger *N*-acetyl-L-cysteine (NAC) counteracts this event. To investigate whether Akt/mTOR pathway regulation is functionally related to the antioxidant effect of UCP2, we analyzed Akt and P70S6K phosphorylation levels in genipin-treated PDAC cells after NAC pre-treatment. **Figure 1D** shows that Akt and P70S6K phosphorylation induced by genipin is at least partially rescued by NAC demonstrating the involvement of ROS production in this signaling regulation driven by UCP2 blockage.

3.2 Genipin and everolimus synergistically inhibit PDAC cell proliferation through GAPDH nuclear translocation

Since stimulation of Akt/mTOR pathway has an established role in cancer proliferation and everolimus, an oral anticancer mTOR inhibitor used in clinics, has shown particularly promising

results in cancer patients by inhibiting tumour growth and displaying anti-angiogenic effects also in combined therapies [23], we investigated whether genipin and everolimus combination might determine an enhanced antiproliferative effect in PDAC cells. First, we demonstrated that the addition of everolimus counteracts both Akt and P70S6K phosphorylation induced by genipin (**Fig. 2A**), establishing the rational basis for the combined therapeutic strategy. In addition, drug combination strongly enhances ROS production as compared with single drugs (**Fig. 2B**) and the ROS-mediated antiproliferative effect in PDAC cells (**Fig. 2C)**. By a therapeutic point of view, the addition of everolimus in the combined setting can assure the blockage of the Akt/mTOR pathway, avoiding a further ROS-mediated Akt/mTOR signaling stimulation even in the presence of enhanced ROS production.

In order to evaluate whether the antiproliferative effect of genipin+everolimus treatment was synergistic, we analyzed cell growth inhibition curves by using the dedicated software CalcuSyn (see Material and Methods). Dose-dependent analyses performed with increasing concentrations of genipin and/or everolimus showed that the combined setting induces a strong antiproliferative synergism in all five PDAC cell lines tested~~PaCa44 cells~~, as revealed by the curve of the combination index (CI) values ± sd *versus* the fraction (0 → 1) of cells killed by drug combination (**Fig. 3A~~2D~~**). CI values lying below 1 are widely distributed in the x axis, indicating a synergistic effect occurring at both low and high drug concentrations in all PDAC cell lines tested (**Fig. 3B**). In particular, CI_{50} values of all PDAC cell lines are markedly below 1 indicating a strong synergism, and the ~~is 0.129 and the~~ reduction folds (dose reduction index; DRI) of drug concentration to obtain 50% cell growth inhibition in combination setting as compared to each drug administered alone (DRI_{50}) ~~is 24.16 for everolimus and 11.39 for genipin~~are reported in **Table 1** ~~(**Table 1**)~~. Moreover, isobolograms at the IC_{50} of each drug for each PDAC cell line are reported in **Supplementary Figure 3**, further supporting the synergistic effect observed in these conditions. Taken together, these data demonstrate that the addition of everolimus to genipin treatment produces a synergistic PDAC cell growth inhibition which is likely due to both enhanced ROS production in combined

Formatted: Font: Bold

Formatted: Font: Bold

Formatted: Subscript

Formatted: Font: Bold

setting and to the counteraction of genipin-induced Akt/mTOR oncogenic signaling by everolimus. DRI_{50} values obtained *in vitro* suggest that this synergism might allow decreasing the concentrations of the two compounds reducing eventual side effects.

Since we previously demonstrated that UCP2 inhibition determines a ROS-dependent nuclear translocation of GAPDH [19] and since GAPDH nuclear translocation is counteracted by Akt/mTOR pathway through direct phosphorylation of the enzyme [24], we explored if nuclear GAPDH positivity is further enhanced by the drug combination treatment. Importantly, we proved that tumor masses derived from mice treated with the combined therapy show a considerable increase in the number of GAPDH-positive nuclei (**Fig. 4~~3~~A**). Also *in vitro*, we observed that the combined treatment strongly increases the amount of GAPDH positive nuclei, as compared to genipin-treated PDAC cells (**Fig. 4~~3~~B**). Representative images of nuclear GAPDH positivity after PDAC cell treatment with the drug combination are reported in **Figure 4~~3~~C**. The total amount of GAPDH mRNA remains unchanged after treatments (**Fig. 4~~3~~D**), indicating that genipin and everolimus regulate the subcellular distribution of the enzyme rather than its expression level. To investigate the functional role of GAPDH nuclear translocation in cell growth inhibition by drug combination, we used the 3-bromo-isoxazoline derivative (S)-benzyl-2-amino-2-(S)-3-bromo-4,5-dihydroisoxazol-5-yl-acetate (AXP3009) (see Material and Methods), previously reported to alkylate the catalytic cysteine residue of tetrameric *Plasmodium falciparum* GAPDH (*Pf*GAPDH) without affecting other solvent-exposed cysteine residues [20]. In consideration of the negative cooperativity of NAD^+ binding [25] and structural observations [26], it was concluded that the alkylation of one subunit of the GAPDH tetramer produces a conformational rearrangement that severely limits the accessibility of the remaining active sites [20]. Since 3-bromo-isoxazoline derivatives were also shown to bind to the redox sensitive catalytic cysteine of *human* GAPDH (*h*GAPDH) [27], we hypothesized that AXP3009 can alter *h*GAPDH conformation, prevent intracellular GAPDH oxidation by ROS produced after cell treatment with genipin and everolimus, and counteract GAPDH nuclear translocation. To test this hypothesis, we first investigated

Formatted: English (United Kingdom)

AXP3009-induced conformational rearrangements of recombinant *h*GAPDH. Circular dichroism spectra of *h*GAPDH pre-incubated with AXP3009 show significant differences in the 250-345 nm range, suggesting significant tertiary alterations in comparison to the control sample (**Figure 54A**). The melting temperature, as determined by the fitting of the thermic denaturation kinetics, is 2.2°C lower when *h*GAPDH is pre-incubated with AXP3009 (61.4±0.1 *versus* 63.6±0.1), suggesting a difference in stability of the two forms (**Figure 54B)**. Finally, gel filtration experiments of AXP3009-bound and unbound *h*GAPDH show a small but significant difference in the apparent molecular weight (**Figure 54C)**. Both forms fall within the range of the tetramer (expected weight 148000 Da), but with a 12% difference that might reflect a difference in shape or a different stability of the quaternary structure. Furthermore, we tested the specificity of AXP3009 on GAPDH interaction by knocking-down intracellular GAPDH expression with siRNA-GAPDH (**Suppl. Fig. 43A**), revealing that after target deprivation the compound loses its cytotoxic effect on PDAC cells (**Suppl. Fig. 43B**). Importantly, **Figure 54D** shows that AXP3009 stabilizes the cytosolic localization of the GAPDH enzyme by diminishing its nuclear transport, thus providing a valuable tool to investigate the role of nuclear GAPDH in cell death induced by genipin and everolimus treatment. According to the cell death-related role assumed by nuclear GAPDH translocation [28], we observed that AXP3009 is able to completely restore PDAC cell proliferation affected by genipin alone, or by genipin and everolimus combined treatment ~~in a concentration dependent manner~~ (**Fig. 54E**).

3.3 Genipin and everolimus strongly induce apoptosis in PDAC cells

We further investigated whether apoptosis is involved in PDAC cell growth inhibition by drug combination. As shown in **Figure 65A**, annexin V assay revealed that PDAC cells treated with the drug combination expose a strongly higher amount of phosphatidylserine as compared to single treatments or untreated control. Notably, apoptotic cell death induced by the combined treatment is markedly reduced by the addition of AXP3009 or of the antioxidant compound NAC (**Fig. 65B**),

479 further supporting the antiproliferative role of GAPDH nuclear translocation mediated by
480 intracellular oxidant conditions [19, 29]. Moreover, we observed a strong increase of CHOP
481 expression by genipin+everolimus within the first eight hours after cell treatment (**Fig. 6~~5~~C**), while
482 the expression of the Bcl 2 protein dramatically decreases in the combined setting (**Fig. 6~~5~~D**),
483 according to the common assumption that the main mechanism of CHOP-induced apoptosis is the
484 suppression of the anti-apoptotic protein Bcl-2 [30]. In addition, the expression of the full length
485 caspase 3 and 9 is significantly reduced by the combined treatment as compared to single
486 treatments, suggesting the involvement of downstream effector caspases in the apoptotic cell death
487 induced by the concomitant inhibition of UCP2 and mTOR complex (Fig. 6~~5~~D). The regulation of
488 Bcl 2 and of caspase 9, which in turn cleaves the downstream pro-caspase 3 in its truncated active
489 form, suggests that the mitochondrial death pathway is implicated in genipin/everolimus induced
490 apoptosis.
491
492 *3.4 Anti-apoptotic effect of Beclin1-dependent autophagy induced by genipin and everolimus*
493 Since GAPDH nuclear translocation can induce autophagy-related genes [31], we
494 investigated whether the combined treatment stimulates the formation of autophagic vesicles in
495 PDAC cells by using staining with the fluorescent probe monodansylcadaverine (MDC). FACS
496 analysis revealed that PDAC cells treated with the drug combination incorporate a higher amount of
497 MDC probe as compared with single treatments, suggesting an autophagy stimulation (**Fig. 7~~6~~A**).
498 These data have been confirmed analyzing MDC incorporation using a microplate fluorescence
499 reader (data not shown). To demonstrate that autophagy stimulation by drug combination results in
500 the fusion of autophagy vesicles with lysosomes, we stained cells with the fluorescent probe
501 acridine orange (AO), which changes its fluorescence emission from green to red upon
502 accumulation into lysosomal acidic compartments revealing the typical pH acidification of
503 lysosomes during autophagic stimulation. Fluorescence microscopy experiments confirmed the
504 presence of wide red areas (acidic lysosomes containing accumulation of AO probe) into the

cytoplasm of PDAC cells treated with drug combination (**Fig. 7~~6~~B**), supporting the statement that the concomitant inhibition of UCP2 and mTOR can contribute to the formation of autophagic vesicles and their fusion with lysosomes in cancer cells.

The investigation of the mechanism involved in the stimulation of autophagy revealed that Beclin 1 (Atg 6), a well-known key regulator of autophagy, is strongly induced by the combined drug setting (**Fig. 7~~6~~C**). In addition, since heat shock protein 90 (Hsp 90) is a molecular chaperone that regulates the stability of signaling proteins, including the maintenance of Beclin 1 protein stability through an evolutionarily conserved domain [32], we investigated whether genipin and everolimus can affect Beclin1:Hsp90 complex. Intriguingly, we observed by immunoprecipitation assay that everolimus promotes the interaction between Beclin 1 and Hsp 90 and that the formation of this complex is further enhanced by drug combination (**Fig. 7~~6~~D**), strongly suggesting a role for Hsp 90 in Beclin 1 induction by the combined treatment. To test the functional role of Beclin 1 enhancement in autophagy stimulation, we knocked-down its expression by using a siRNA-Beclin1 (see control experiment in **Suppl. Fig. 5~~4~~)**. **Figure 7~~6~~E** indicates that autophagosome vesicle formation by drug combination is completely abolished by siRNA-Beclin1, highlighting the key role of this autophagy mediator protein in the overall process. Furthermore, since the role of autophagy in modulating cell growth is highly dependent on the metabolic context and on the microenvironmental conditions in which the cells lie [33], we investigated the impact of this process on the overall antiproliferative effect induced by drug combination. **Figure 7~~6~~F** shows that the percentage of PDAC cell growth is further decreased when a non-toxic concentration of 3-methyladenine (3-MA), a known inhibitor of the autophagosome formation process, is added to increasing concentrations of genipin+everolimus combination. Notably, the apoptotic effect of the drugs is strongly potentiated by 3-MA (**Fig. 7~~6~~G**), demonstrating that Beclin1-dependent autophagy retains a protective and pro-survival role counteracting apoptotic cell death induced by the drugs.

3.5 Genipin and everolimus strongly inhibit growth of PDAC cells in mice xenografts

The effect of the intraperitoneal delivery of genipin and/or everolimus on growth inhibition of PaCa44 cells subcutaneously xenografted in nude mice was also investigated. **Figure 8~~7~~A** shows that the volume of tumors in mice treated with the drug combination remains essentially unchanged during the observation time, whereas it strongly increases in the control group and, at a lower extent, in either genipin- or everolimus-treated groups. Tumor masses after mice sacrifice were recorded and shown in **Figure 8~~7~~B** for control and combined treatment, further pointing out the high efficiency in the reduction of PDAC masses *in vivo*. To confirm this antiproliferative effect by genipin+everolimus treatment and the synergistic outcome observed in PDAC cell cultures, we demonstrated that the number of mitoses dramatically decreases only in tumor masses derived from mice injected with the drug combination (**Fig. 8~~7~~C**). To investigate whether treatments might determine toxic effects, we analysed mice body weights during all the experiment period and, at the sacrifice of mice, we collected various organs (heart, kidney, liver, lung and pancreas) for haematoxylin and eosin (H&E) staining. **Figure 8~~7~~D** shows that all the treatments do not change mice body masses during the experiment, suggesting the absence of any apparent toxicity. In addition, H&E histopathologic evaluation of the organs examined revealed the absence of any significant side effects for the animals (**Suppl. Fig. 6~~5~~**).

4. Discussion

~~UCP2 over expression is a general phenomenon correlated with the progression of human cancers, including PDAC, and can be thus considered a valuable potential target for therapy [12, 18]. UCP2 has been reported to promote chemoresistance [34], metabolic aberrant alterations in cancer cells [15, 35], and to overcome oxidant stressful stimuli of various origins [36] enhancing the development of the neoplastic disease.~~

In this study, we demonstrate *in vitro* and in mice xenograft that UCP2 inhibition strongly triggers the oncogenic pathway Akt/mTOR, providing the rationale for the antiproliferative synergistic effect mediated by the UCP2 inhibitor genipin when used in combination with the mTOR inhibitor everolimus. Beyond the Akt/mTOR/P70S6K signaling inhibition, we demonstrate that everolimus strongly potentiates ROS production and PDAC cell death induced by genipin. This anti-proliferative effect by drug combination setting is due to a massive GAPDH nuclear translocation observed both *in vitro* and in mice xenograft. This determines caspase-mediated apoptotic cancer cell death as well as a protective autophagic process mediated by Beclin1 in PDAC cells (**Figure 9~~8~~**). This latter event can be likely considered as an extreme tentative of cancer cells to survive in drug-induced stressing conditions. Thus, the full anticancer effect by genipin and everolimus combination can be achieved when the autophagic process is blocked.

Beyond glycolysis, several reports have demonstrated that GAPDH has a variety of other functions, including DNA repair [37], transcriptional regulation [38], membrane fusion and transport [39, 40], autophagy [31], and cell death [41, 42]. Indeed, in accord with its multiple activities, the intracellular localization of GAPDH is not restricted to the cytosol for energy production but is detected in the plasma and nuclear membrane, in the endoplasmic reticulum, in the Golgi apparatus, and in the nucleus [28]. GAPDH nuclear translocation is a particularly critical event in the light that, although the enzyme contains a nuclear export signal [43], it does not contain an equivalent nuclear localization signal (NLS). Thus, it is likely that other mechanisms need to be utilized for GAPDH translocation probably by binding with other molecules after post-translational

575 modifications of the enzyme. For instance, upon exposure to oxidative stress, GAPDH nuclear
576 translocation involves S-nitrosyl post-translational modification at its active site Cys152 [29].
577 Oxidized GAPDH binds to Siah1, an ubiquitin ligase, which contains its own NLS sequence
578 thereby facilitating the intracellular transfer of this protein:protein complex and the subsequent
579 transcriptional induction of apoptotic and cell death-related genes [29, 44]. Many other post-
580 translational modifications of GAPDH have been described, including phosphorylation, acetylation,
581 glycosylation, poly ADP-ribosylation, and pyruvylation [45]. For these reasons GAPDH has
582 received considerable attention as an appealing drug target for anticancer therapy [46].

583 Here, we show that the strong increase in GAPDH nuclear translocation and subsequent
584 PDAC cell death by genipin and everolimus combination is due to both: *i)* oxidation of the enzyme
585 by ROS increase, and *ii)* the everolimus-mediated counteraction of the Akt/mTOR pathway
586 stimulated by genipin. Indeed, this oncogenic signaling is described to stabilize GAPDH in the
587 cytosol through phosphorylation in Thr-237 of the enzyme decreasing its nuclear translocation and
588 GAPDH-mediated apoptosis [24, 47]. The functional involvement of GAPDH nuclear translocation
589 has been confirmed by the capability of AXP3009 to counteract PDAC cell death and apoptosis
590 induced by drug combination. AXP3009 is a novel synthetic compound addressed to interact with
591 the *Pf*GAPDH catalytic cysteine [20]. Here, we demonstrate that AXP3009 can prevent the nuclear
592 translocation of GAPDH in PDAC cells, likely through conformational changes observed in
593 recombinant *h*GAPDH that can elude the oxidation of the redox-sensitive catalytic cysteine.
594 Notably, we observe a strong increase in the percentage of GAPDH nuclear positivity in tumor
595 masses in nude mice injected with the drug combination. Concomitantly, tumor volume in mice
596 treated with the two drugs remains essentially unchanged during the observation time without any
597 signs of toxic effects for animals.

598 The synergistic PDAC cell growth inhibition obtained with everolimus and genipin
599 treatment can allow to markedly reduce the concentrations of the two drug when used in
600 combination. Optimal dosing is a crucial factor in order to achieve a maximum therapeutic efficacy

with appropriate drug exposure and to maintain patient quality of life. CalcuSyn software analysis shows that the concentration of everolimus ~~can be reduced of about 24 folds~~ and that of genipin ~~of about 11 folds~~can be strongly reduced to obtain 50% PDAC cell growth inhibition in combined setting as compared to the concentrations needed to obtain the same effect in single treatment (Table 1). Notably, mTOR inhibitors-induced side effects, which can potentially compromise their therapeutic effectiveness, are well characterized and include epithelial-cutaneous adverse events, pulmonary dysfunctions, metabolic alterations, and fatigue [48]. Although everolimus is a currently approved drug for the treatment of pancreatic cancer, genipin has not been developed for clinical use yet but it represents a valuable tool for the preclinical investigation of UCP2 roles and for the study of the potential clinical usage of next generation UCP2 inhibitors for therapy. ~~Overall~~In conclusion, our results and the statement that UCP2 overexpression promotes chemoresistance in cancers support the combined inhibition of UCP2 and of Akt/mTOR pathway as a novel therapeutic strategy in the treatment of PDAC.

Acknowledgements

We thank Andrea Mafficini for his technical support. This work was supported by Joint Projects program 2015 from University of Verona to M. Donadelli (n. B12I15002320003) and by Associazione Italiana Ricerca Cancro (AIRC 12182) to A. Scarpa. Ilaria Dando is a fellow of Fondazione Umberto Veronesi. Elisa Dalla Pozza is a fellow of AIRC 5 per mille (grant no. 12182).

Conflict of interest

The authors declare that they have no conflicts of interest.

References

[1] R.L. Siegel, K.D. Miller, A. Jemal, Cancer statistics, 2015, CA: a cancer journal for clinicians 65(1) (2015) 5-29.

[2] A. Vincent, J. Herman, R. Schulick, R.H. Hruban, M. Goggins, Pancreatic cancer, Lancet 378(9791) (2011) 607-20.

[3] N. Silvestris, O. Brunetti, E. Vasile, F. Cellini, I. Cataldo, V. Pusceddu, M. Cattaneo, S. Partelli, M. Scartozzi, G. Aprile, A. Casadei Gardini, A.G. Morganti, V. Valentini, A. Scarpa, M. Falconi, A. Calabrese, V. Lorusso, M. Reni, S. Cascinu, Multimodal treatment of resectable pancreatic ductal adenocarcinoma, Critical reviews in oncology/hematology 111 (2017) 152-165.

[4] N. Silvestris, V. Longo, F. Cellini, M. Reni, A. Bittoni, I. Cataldo, S. Partelli, M. Falconi, A. Scarpa, O. Brunetti, V. Lorusso, D. Santini, A. Morganti, V. Valentini, S. Cascinu, Neoadjuvant multimodal treatment of pancreatic ductal adenocarcinoma, Critical reviews in oncology/hematology 98 (2016) 309-24.

[5] S. Raimondi, P. Maisonneuve, A.B. Lowenfels, Epidemiology of pancreatic cancer: an overview, Nature reviews. Gastroenterology & hepatology 6(12) (2009) 699-708.

[6] N. Le, M. Sund, A. Vinci, G.c.g.o. Pancreas, Prognostic and predictive markers in pancreatic adenocarcinoma, Digestive and liver disease : official journal of the Italian Society of Gastroenterology and the Italian Association for the Study of the Liver 48(3) (2016) 223-30.

[7] L.M. Ballou, R.Z. Lin, Rapamycin and mTOR kinase inhibitors, Journal of chemical biology 1(1-4) (2008) 27-36.

[8] A.S. Strimpakos, E.M. Karapanagiotou, M.W. Saif, K.N. Syrigos, The role of mTOR in the management of solid tumors: an overview, Cancer treatment reviews 35(2) (2009) 148-59.

[9] T. Peng, Q.P. Dou, Everolimus Inhibits Growth of Gemcitabine-Resistant Pancreatic Cancer Cells via Induction of Caspase-Dependent Apoptosis and G2 /M Arrest, Journal of cellular biochemistry (2017).

[10] M. Donadelli, I. Dando, C. Fiorini, M. Palmieri, UCP2, a mitochondrial protein regulated at multiple levels, Cellular and molecular life sciences : CMLS 71(7) (2014) 1171-90.

[11] M.A. Pitt, Overexpression of uncoupling protein-2 in cancer: metabolic and heat changes, inhibition and effects on drug resistance, Inflammopharmacology 23(6) (2015) 365-9.

[12] V. Ayyasamy, K.M. Owens, M.M. Desouki, P. Liang, A. Bakin, K. Thangaraj, D.J. Buchsbaum, A.F. LoBuglio, K.K. Singh, Cellular model of Warburg effect identifies tumor promoting function of UCP2 in breast cancer and its suppression by genipin, PLoS One 6(9) (2011) e24792.

[13] W. Li, K. Nichols, C.A. Nathan, Y. Zhao, Mitochondrial uncoupling protein 2 is up-regulated in human head and neck, skin, pancreatic, and prostate tumors, Cancer biomarkers : section A of Disease markers 13(5) (2013) 377-83.

[14] E. Dalla Pozza, C. Fiorini, I. Dando, M. Menegazzi, A. Sgarbossa, C. Costanzo, M. Palmieri, M. Donadelli, Role of mitochondrial uncoupling protein 2 in cancer cell resistance to gemcitabine, Biochimica et biophysica acta 1823 (2012) 1856-1863.

[15] J. Brandi, D. Cecconi, M. Cordani, M. Torrens-Mas, R. Pacchiana, E.D. Pozza, G. Butera, M. Manfredi, E. Marengo, J. Oliver, P. Roca, I. Dando, M. Donadelli, The antioxidant uncoupling protein 2 stimulates hnRNPA2/B1, GLUT1 and PKM2 expression and sensitizes pancreas cancer cells to glycolysis inhibition, Free radical biology & medicine (2016).

[16] R.J. Mailloux, M.E. Harper, Uncoupling proteins and the control of mitochondrial reactive oxygen species production, Free radical biology & medicine 51(6) (2011) 1106-15.

[17] M.D. Brand, T.C. Esteves, Physiological functions of the mitochondrial uncoupling proteins UCP2 and UCP3, Cell Metab 2(2) (2005) 85-93.

[18] M. Donadelli, I. Dando, E. Dalla Pozza, M. Palmieri, Mitochondrial uncoupling protein 2 and pancreatic cancer: a new potential target therapy, World journal of gastroenterology : WJG 21(11) (2015) 3232-8.

[19] I. Dando, C. Fiorini, E.D. Pozza, C. Padroni, C. Costanzo, M. Palmieri, M. Donadelli, UCP2 inhibition triggers ROS-dependent nuclear translocation of GAPDH and autophagic cell death in pancreatic adenocarcinoma cells, Biochimica et biophysica acta 1833(3) (2013) 672-9.

Formatted: Italian (Italy)

Formatted: Italian (Italy)

677 [20] S. Bruno, A. Pinto, G. Paredi, L. Tamborini, C. De Micheli, V. La Pietra, L. Marinelli, E. Novellino, P. Conti,
678 A. Mozzarelli, Discovery of covalent inhibitors of glyceraldehyde-3-phosphate dehydrogenase, a target for
679 the treatment of malaria, Journal of medicinal chemistry 57(17) (2014) 7465-71.
680 [21] T.C. Chou, P. Talalay, Quantitative analysis of dose-effect relationships: the combined effects of
681 multiple drugs or enzyme inhibitors, Adv Enzyme Regul 22 (1984) 27-55.
682 [22] N. Wang, M. Zhu, S.W. Tsao, K. Man, Z. Zhang, Y. Feng, Up-regulation of TIMP-1 by genipin inhibits
683 MMP-2 activities and suppresses the metastatic potential of human hepatocellular carcinoma, PLoS One
684 7(9) (2012) e46318.
685 [23] K. Hirashima, Y. Baba, M. Watanabe, R.I. Karashima, N. Sato, Y. Imamura, Y. Nagai, N. Hayashi, K.I.
686 Iyama, H. Baba, Aberrant activation of the mTOR pathway and anti-tumour effect of everolimus on
687 oesophageal squamous cell carcinoma, British journal of cancer 106(5) (2012) 876-82.
688 [24] Q. Huang, F. Lan, Z. Zheng, F. Xie, J. Han, L. Dong, Y. Xie, F. Zheng, Akt2 kinase suppresses
689 glyceraldehyde-3-phosphate dehydrogenase (GAPDH)-mediated apoptosis in ovarian cancer cells via
690 phosphorylating GAPDH at threonine 237 and decreasing its nuclear translocation, J Biol Chem 286(49)
691 (2011) 42211-20.
692 [25] Y.I. Henis, A. Levitzki, Mechanism of negative cooperativity in glyceraldehyde-3-phosphate
693 dehydrogenase deduced from ligand competition experiments, Proc Natl Acad Sci U S A 77(9) (1980) 5055-
694 59.
695 [26] S. Moniot, S. Bruno, C. Vonrhein, C. Didierjean, S. Boschi-Muller, M. Vas, G. Bricogne, G. Branlant, A.
696 Mozzarelli, C. Corbier, Trapping of the thioacylglyceraldehyde-3-phosphate dehydrogenase intermediate
697 from Bacillus stearothermophilus. Direct evidence for a flip-flop mechanism, J Biol Chem 283(31) (2008)
698 21693-702.
699 [27] S. Bruno, M. Margiotta, A. Pinto, G. Cullia, P. Conti, C. De Micheli, A. Mozzarelli, Selectivity of 3-bromo-
700 isoxazoline inhibitors between human and Plasmodium falciparum glyceraldehyde-3-phosphate
701 dehydrogenases, Bioorganic & medicinal chemistry 24(12) (2016) 2654-9.
702 [28] C. Tristan, N. Shahani, T.W. Sedlak, A. Sawa, The diverse functions of GAPDH: views from different
703 subcellular compartments, Cellular signalling 23(2) (2011) 317-23.
704 [29] M.R. Hara, N. Agrawal, S.F. Kim, M.B. Cascio, M. Fujimuro, Y. Ozeki, M. Takahashi, J.H. Cheah, S.K.
705 Tankou, L.D. Hester, C.D. Ferris, S.D. Hayward, S.H. Snyder, A. Sawa, S-nitrosylated GAPDH initiates
706 apoptotic cell death by nuclear translocation following Siah1 binding, Nature cell biology 7(7) (2005) 665-
707 74.
708 [30] K.D. McCullough, J.L. Martindale, L.O. Klotz, T.Y. Aw, N.J. Holbrook, Gadd153 sensitizes cells to
709 endoplasmic reticulum stress by down-regulating Bcl2 and perturbing the cellular redox state, Mol Cell Biol
710 21(4) (2001) 1249-59.
711 [31] A. Colell, J.E. Ricci, S. Tait, S. Milasta, U. Maurer, L. Bouchier-Hayes, P. Fitzgerald, A. Guio-Carrion, N.J.
712 Waterhouse, C.W. Li, B. Mari, P. Barbry, D.D. Newmeyer, H.M. Beere, D.R. Green, GAPDH and autophagy
713 preserve survival after apoptotic cytochrome c release in the absence of caspase activation, Cell 129(5)
714 (2007) 983-97.
715 [32] C. Xu, J. Liu, L.C. Hsu, Y. Luo, R. Xiang, T.H. Chuang, Functional interaction of heat shock protein 90 and
716 Beclin 1 modulates Toll-like receptor-mediated autophagy, FASEB journal : official publication of the
717 Federation of American Societies for Experimental Biology 25(8) (2011) 2700-10.
718 [33] S. Lorin, A. Hamai, M. Mehrpour, P. Codogno, Autophagy regulation and its role in cancer, Seminars in
719 cancer biology 23(5) (2013) 361-79.
720 [34] Z. Derdak, N.M. Mark, G. Beldi, S.C. Robson, J.R. Wands, G. Baffy, The mitochondrial uncoupling
721 protein-2 promotes chemoresistance in cancer cells, Cancer research 68(8) (2008) 2813-9.
722 [35] A. Vozza, G. Parisi, F. De Leonardis, F.M. Lasorsa, A. Castegna, D. Amorese, R. Marmo, V.M. Calcagnile,
723 L. Palmieri, D. Ricquier, E. Paradies, P. Scarcia, F. Palmieri, F. Bouillaud, G. Fiermonte, UCP2 transports C4
724 metabolites out of mitochondria, regulating glucose and glutamine oxidation, Proc Natl Acad Sci U S A
725 111(3) (2014) 960-5.
726 [36] D.G. Pons, M. Nadal-Serrano, M. Torrens-Mas, A. Valle, J. Oliver, P. Roca, UCP2 inhibition sensitizes
727 breast cancer cells to therapeutic agents by increasing oxidative stress, Free radical biology & medicine 86
728 (2015) 67-77.

729 [37] K. Meyer-Siegler, D.J. Mauro, G. Seal, J. Wurzer, J.K. deRiel, M.A. Sirover, A human nuclear uracil DNA
730 glycosylase is the 37-kDa subunit of glyceraldehyde-3-phosphate dehydrogenase, Proc Natl Acad Sci U S A
731 88(19) (1991) 8460-4.
732 [38] L. Zheng, R.G. Roeder, Y. Luo, S phase activation of the histone H2B promoter by OCA-S, a coactivator
733 complex that contains GAPDH as a key component, Cell 114(2) (2003) 255-66.
734 [39] E.J. Tisdale, Glyceraldehyde-3-phosphate dehydrogenase is required for vesicular transport in the early
735 secretory pathway, J Biol Chem 276(4) (2001) 2480-6.
736 [40] E.J. Tisdale, Glyceraldehyde-3-phosphate dehydrogenase is phosphorylated by protein kinase Ciota
737 /lambda and plays a role in microtubule dynamics in the early secretory pathway, J Biol Chem 277(5) (2002)
738 3334-41.
739 [41] H. Nakajima, W. Amano, A. Fujita, A. Fukuhara, Y.T. Azuma, F. Hata, T. Inui, T. Takeuchi, The active site
740 cysteine of the proapoptotic protein glyceraldehyde-3-phosphate dehydrogenase is essential in oxidative
741 stress-induced aggregation and cell death, J Biol Chem 282(36) (2007) 26562-74.
742 [42] H. Nakajima, T. Kubo, H. Ihara, T. Hikida, T. Danjo, M. Nakatsuji, N. Shahani, M. Itakura, Y. Ono, Y.T.
743 Azuma, T. Inui, A. Kamiya, A. Sawa, T. Takeuchi, Nuclear-translocated Glyceraldehyde-3-phosphate
744 Dehydrogenase Promotes Poly(ADP-ribose) Polymerase-1 Activation during Oxidative/Nitrosative Stress in
745 Stroke, J Biol Chem 290(23) (2015) 14493-503.
746 [43] V.M. Brown, E.Y. Krynetski, N.F. Krynetskaia, D. Grieger, S.T. Mukatira, K.G. Murti, C.A. Slaughter, H.W.
747 Park, W.E. Evans, A novel CRM1-mediated nuclear export signal governs nuclear accumulation of
748 glyceraldehyde-3-phosphate dehydrogenase following genotoxic stress, J Biol Chem 279(7) (2004) 5984-92.
749 [44] M.R. Hara, S.H. Snyder, Nitric oxide-GAPDH-Siah: a novel cell death cascade, Cellular and molecular
750 neurobiology 26(4-6) (2006) 527-38.
751 [45] M.A. Sirover, Subcellular dynamics of multifunctional protein regulation: mechanisms of GAPDH
752 intracellular translocation, Journal of cellular biochemistry 113(7) (2012) 2193-200.
753 [46] S. Ganapathy-Kanniappan, R. Kunjithapatham, J.F. Geschwind, Glyceraldehyde-3-phosphate
754 dehydrogenase: a promising target for molecular therapy in hepatocellular carcinoma, Oncotarget 3(9)
755 (2012) 940-53.
756 [47] T.M. Leisner, C. Moran, S.P. Holly, L.V. Parise, CIB1 prevents nuclear GAPDH accumulation and non-
757 apoptotic tumor cell death via AKT and ERK signaling, Oncogene 32(34) (2013) 4017-27.
758 [48] D.A. Yardley, Adverse event management of mTOR inhibitors during treatment of hormone receptor-
759 positive advanced breast cancer: considerations for oncologists, Clinical breast cancer 14(5) (2014) 297-
760 308.

761

762

Figure Legends

Figure 1. Akt/mTOR pathway regulation by UCP2 in pancreatic ductal adenocarcinoma cells. (**A**) Qualitative and quantitative analysis of p-Akt expression on PaCa44 derived xenograft tumors (*in vivo*) and on PaCa44 cell line (*in vitro*) untreated/treated with genipin. P-Akt expression representative images are reported for tumors grown in control mice and in mice treated with genipin (for genipin subministration see Materials and Methods) at 20-fold magnification, scale bar 50 μm, and for *in vitro* a representative immunoblot image is reported for p-Akt expression in PaCa44 cells untreated/treated with 200 μM Genpin for 24h. (**B**) Western blot analysis of the total and phosphorylated form of the mTOR target P70S6K in PaCa44 cells transfected with 200 nM siRNA control or siRNA UCP2 for 72 h. (**C**) Analysis of DCF fluorescence intensity, corresponding to the level of ROS production, by a multimode plate reader in PaCa44 cells treated with 200 μM genipin and/or 10 mM NAC for 24 h. (**D**) Western blot analysis of the total and phosphorylated form of Akt or of the mTOR target P70S6K in PaCa44 cells treated with 200 μM genipin and/or 10 mM NAC for 24 h. The value of α-tubulin was used as a normalizing factor and protein fold change is relative to each control. Values are the means (±SD) of three independent experiments. Statistical analysis: (*) $P<0.05$ and (***) $P<0.001$ for treated cells vs each control or genipin vs genipin+NAC. Legend: (ctrl) control and (G) genipin.

Figure 2. The combined treatment genipin/everolimus impairs Akt/mTOR signaling and increases ROS production and anti-proliferative effects. (**A**) Western blot analysis of the total and phosphorylated form of Akt and P70S6K in PaCa44 cells treated with 200 μM genipin and/or 10 μM everolimus for 24 h. (**B**) Analysis of MitoSox fluorescence intensity, corresponding to the level of mitochondrial superoxide production, by a multimode plate reader in PaCa44 cells treated with 140 μM genipin and/or 7 μM everolimus for 24 h. (**C**) Cell growth analysis through the Crystal Violet colorimetric assay of PaCa44 cells treated with 100 μM genipin and/or 5 μM everolimus and/or 10 mM NAC for 48h. Values are the means of three independent experiments each performed in triplicate. Statistical analysis: (*) $P<0.05$, (**) $P<0.01$, and (***) $P<0.001$ for treated cells vs control or genipin+everolimus vs single treatments. Legend: (ctrl) control, (G) genipin, and (E) everolimus.

Figure 3. The combined treatment genipin/everolimus has a synergistic anti-proliferative effect on five PDAC cell lines. (**A**) Cell growth analysis through the Crystal Violet colorimetric

assay of five PDAC cell lines (PaCa44, Panc1, MiaPaCa2, PaCa3, and T3M4) treated with increasing doses of the drugs [genipin from 500 nM to 200 µM; everolimus from 25 nM to 10 µM] maintaining the ratio genipin:everolimus 20:1 for 48 h. Black squares, black rhombus and white circles correspond to genipin, everolimus and the combined treatment, respectively. Values are the means of three independent experiments each performed in triplicate. (**B**) Analysis of the synergistic cell growth inhibition of the five PDAC cell lines (PaCa44, Panc1, MiaPaCa2, PaCa3, and T3M4) treated with increasing doses of the drugs [genipin from 500 nM to 200 µM; everolimus from 25 nM to 10 µM] maintaining the ratio genipin:everolimus 20:1 for 48 h. The values on the x axis correspond to the fraction of growth inhibition (0→1) given by increasing concentrations of drug combinations. The values on the y axis correspond to the measurement of CI (see Materials and Methods).

Figure 4. mTOR inhibition enhances GAPDH nuclear translocation in genipin-treated cells. (**A**) Count of GAPDH positive nuclei in vital neoplastic cells on 20 consecutive HPFs of PaCa44 derived xenograft tumors. Mice have been untreated/treated with genipin and/or everolimus, as reported in Materials and Methods. Representative images are reported for control mice and for mice treated with genipin+everolimus at 40-fold magnification, scale bar 20 µm. (**B**) PaCa44 cells untreated or treated with 200 µM genipin and/or 10 µM everolimus for 24 h. GAPDH positive nuclei have been counted on several different fields for each condition and the amount of positive nuclei has been normalized on cell viability. (**C**) Representative immunofluorescence images of GAPDH (green) translocation into the nuclei (labelled with Hoechst dye) of PaCa44 cells untreated or treated with 200 µM genipin and 10 µM everolimus for 24 h, at 40-fold magnification, scale bar 10 µm. (**D**) Quantitative analysis of GAPDH mRNA though real-time PCR (qPCR) of PaCa44 cells treated with 200 µM genipin and/or 10 µM everolimus for 24 h. Total RNA was extracted from cells and qPCR was performed as described in Materials and Methods. Statistical analysis: (*) $P<0.05$, (**) $P<0.01$, and (***) $P<0.001$ for treated cells vs control or genipin+everolimus vs single treatments. Legend: (ctrl) control, (G) genipin, and (E) everolimus.

Figure 5. AXP3009 alters GAPDH conformation and counteracts cell growth inhibition by genipin/everolimus treatment. (A) Comparison of the circular dichroism spectra of AXP3009-bound (dashed line) and unbound *h*GAPDH (solid line) in the 190-250 nm range. Circular dichroism spectra of GAPDH at 10 µM in a buffered solution containing 10 mM sodium phosphate

827 at pH 7.6 in the 250-345 nm range were collected in the absence of AXP3009 (solid line) and upon
828 overnight incubation with 100 µM AXP3009 (dashed line). (**B**) Thermal denaturation kinetics of
829 AXP3009-bound (open symbols) and unbound *h*GAPDH (closed symbols) from two independent
830 experiments each. The solid lines are the fitting to a sigmoidal equation, indicative of a two-state
831 model. (**C**) Apparent molecular weights of AXP3009-bound and unbound GAPDH on a superdex
832 200 increase 3.2/300 column as estimated by comparison with calibrants in the range 29 -440 kDa.
833 The reported values are the means ± s.e.m. of five independent measurements. (**D**) Western blot
834 analysis and quantification of GAPDH expression into the cytosol and nuclei of PaCa44 cells
835 untreated/treated with 50 µM AXP3009 for 48 h. α-tubulin and Lamin B1 have been used as
836 controls of the quality of the cytoplasmic and nuclear protein fractions, respectively. Amido Black
837 staining was used to confirm equal cytoplasmic and nuclear protein loading in the different lanes.
838 (**E**) Cell growth analysis through the Crystal Violet colorimetric assay of PaCa44 cells treated with
839 50 µM of AXP3009 and/or with 100 µM genipin and/or 5 µM everolimus for 48h. Values are the
840 means (±SD) of three independent experiments. Statistical analysis: (*) P<0.05, (**) P<0.01, and
841 (***) P<0.001 for treated cells vs control or single treatment vs the relative single
842 treatment+AXP3009 or genipin+everolimus vs genipin+everolimus+AXP3009. Legend: (ctrl)
843 control, (G) genipin, (E) everolimus, (C) cytoplasmic fraction, and (N) nuclear fraction.
844

845 **Figure 6. mTOR inhibition increases apoptosis in genipin-treated cells.** Apoptosis analysis
846 through the Annexin V binding assay of PaCa44 cells treated with (**A**) 100 µM genipin and/or 5 µM
847 everolimus for 48 h and/or with (**B**) 1 µM AXP3009 and 10 mM NAC. (**C**) Quantitative analysis of
848 CHOP mRNA though real-time PCR (qPCR) of PaCa44 cells treated with 200 µM genipin and/or
849 10 µM everolimus for 8 h. Total RNA was extracted from cells and qPCR was performed as
850 described in Materials and Methods. (**D**) Western blot analysis of three apoptosis-related proteins
851 (Bcl2, caspase 3 full length, and caspase 9 full length) in PaCa44 cells treated with 100 µM genipin
852 and/or 5 µM everolimus for 48 h. The bands of Western blot analyses were scanned as digital peaks
853 and the areas of the peaks were calculated in arbitrary units. The value of α-tubulin was used as a
854 normalizing factor and protein fold change is relative to control cells. Values are the means (±SD)
855 of three independent experiments. Statistical analysis: (*) P<0.05, (**) P<0.01, and (***) P<0.001
856 for treated cells *vs* control, or single treatments *vs* genipin+everolimus, or genipin+everolimus *vs*
857 genipin+everolimus+AXP3009 or vs genipin+everolimus+NAC. Legend: (ctrl) control, (G)
858 genipin, and (E) everolimus.
859

Figure 7. mTOR inhibition induces autophagy and related-mechanisms in genipin-treated cells. (**A**) Autophagosome formation assay through the analysis of the incorporation of monodansylcadaverine (MDC) probe in PaCa44 cells treated with 100 µM genipin and/or 5 µM everolimus for 48 h though flow cytometry. (**B**) Representative immunofluorescence images of autophagosome formation through acridine orange staining of PaCa44 cells treated with 100 µM genipin and 5 µM everolimus for 24 h, at 40-fold magnification, scale bar 10 µm. (**C**) Western blot analysis of Beclin1 in PaCa44 cells treated with 100 µM genipin and/or 5 µM everolimus for 24 h. Amido black staining was used to confirm equal protein loading in the different lanes. (**D**) Immunoprecipitation analysis and relative quantification of Beclin-1/Hsp90 in PaCa44 cells treated with 200 µM genipin and/or 10 µM everolimus for 24 h. (**E**) Autophagosome formation assay through the incorporation of the MDC probe in PaCa44 cells transfected with 50 nM siRNA Beclin1 for 48 h and/or treated with 200 µM genipin and 10 µM everolimus for 48h. (**F**) Cell growth analysis through the Crystal Violet colorimetric assay of PaCa44 cells pre-treated for 1 h with 5 mM 3-MA and/or treated with increasing doses of the drugs [genipin from 500 nM to 140 µM; everolimus from 25 nM to 7 µM] maintaining the ratio genipin:everolimus 20:1 for 48 h. (**G**) Apoptosis analysis through the Annexin V binding assay of PaCa44 cells pre-treated for 1 h with 5 mM 3-MA and/or treated with 100 µM genipin and 5 µM everolimus for 48 h. Values are the means (±SD) of three independent experiments. Statistical analysis: (*) $P<0.05$, (**) $P<0.01$, and (***) $P<0.001$ for treated cells vs control, or single treatments vs genipin+everolimus, or genipin+everolimus vs genipin+everolimus+3-MA, or genipin+everolimus vs genpin+everolimus+siRNA Beclin1. Legend: (ctrl) control, (G) genipin, and (E) everolimus.

Figure 8. *In vivo* effect of mTOR inhibition in genipin-treated nude mice. PaCa44 cells were subcutaneously injected into female nude mice. After 1 week, i.p. injections with PBS (solution vehicle), genipin, and/or everolimus were administered twice a week for 4 weeks, as described in Materials and Methods. (**A**) Tumor volumes were measured at 3 days after each injection and values are the mean of mice tumor volumes in each group. Statistical analysis is referred to the days at which the tumor volume of the mice treated with genipin+everolimus is significantly lower than the other three groups, such as the control mice and the mice treated with the drugs alone. (*) $P<0.05$. (**B**) Four representative images of tumor masses grown in control mice and in mice treated with genipin+everolimus. (**C**) Count of mitotic figures on 10 consecutive HPFs (high power field, 40-fold magnification, scale bar 20 µm) for each neoplastic sample. Representative images are reported for control mice and for mice treated with genipin+everolimus. Statistical analysis is

referred to mice treated with the drug combination genipin+everolimus *vs* control mice. (***) P<0.001. (**D**) Mice body mass was measured at 3 days after each injection and values are the means of mice body in each group. Legend: (ctrl) control, (G) genipin, and (E) everolimus.

Figure 9. Schematic representation of the molecular mechanisms regulated by UCP2 and Akt/mTOR inhibition identified in this study.

Supplementary Figure 1. Quantitative analysis of UCP2 mRNA though real-time PCR (qPCR) of PaCa44 cells transfected with 200 nM siRNA control or siRNA UCP2 for 72 h. Total RNA was extracted from cells and qPCR was performed as described in Materials and Methods.

Supplementary Figure 2. Western blot analysis of the total and phosphorylated form of the mTOR target P70S6K in three pancreatic ductal cell lines (PaCa3, PaCa44, and Panc1) treated with 400 µM genipin for 24 h. Legend: (ctrl) control and (G) genipin.

Supplementary Figure 3. Isobolograms obtained from the Calcusyn output at 0.5 of fractional effect (IC_{50}) for five PDAC cell lines (PaCa44, Panc1, MiaPaCa2, PaCa3, and T3M4) treated for 48 h. IC_{50} of genipin and everolimus alone are reported as cross on the x and y axis, respectively, whereas the black dot represents the IC_{50} of the combined treatment. The combination data point indicates an addictive effect when it is plotted on the diagonal, a synergistic effect when it is on the lower left, and an antagonistic effect when it is on the upper right.

Supplementary Figure 4. (**A**) Quantitative analysis of GAPDH mRNA though real-time PCR (qPCR) of PaCa44 cells transfected with 200 nM siRNA control or siRNA GAPDH for 72 h. Total RNA was extracted from cells and qPCR was performed as described in Materials and Methods. (**B**) Cell growth analysis through the Crystal Violet colorimetric assay of PaCa44 cells treated with 50 µM AXP3009 and/or with GAPDH siRNA for 48h.

Supplementary Figure 5. Quantitative analysis of Beclin-1 mRNA though real-time PCR (qPCR) of PaCa44 cells transfected with 50 nM siRNA Beclin1 (siBECN1) for 48 h. Total RNA was extracted from cells and qPCR was performed as described in Materials and Methods.

Supplementary Figure 6. Haematoxylin and eosin (H&E) tissue staining of nude mice injected subcutaneously with PaCa44 cells. Representative images of heart, kidney, liver, lung and pancreas

922 in control mice and in mice treated with the drug combination genipin+everolimus taken at 10-fold
923 magnification, scale bar 100 μm.

Table 1. Combination Index (CI) and Dose Reduction Index (DRI) values for genipin (G) and everolimus (E) combination.

Cell lines	CI_{50}	CI_{75}	CI<1	DRI_{50}	*r*
PaCa44	0.129	0.561	75%	E: 24.16 G: 11.39	0.84
Panc1	0.085	0.823	100%	E: 88.6 G: 13.6	0.91
MiaPaCa2	0.112	1.37	100%	E: 5929.7 G: 8.9	0.88
PaCa3	7.1×10^{-5}	6.9×10^{-5}	90%	E: 5×10^{14} G: 1.4×10^{4}	0.88
T3M4	0.09	1.45	80%	E: 548.9 G: 11.2	0.90

CI_{50} was calculated for 50% cell growth inhibition in the combined treatment by isobologram analyses performed with the CalcuSyn software. CI value < 1 indicates the percentage of experimental conditions with increasing drug concentrations determining a synergistic effect. DRI_{50} represents the folds of dose reduction to obtain 50% cell growth inhibition in combination setting as compared to each drug alone.

Figure 1

Click here to download high resolution image

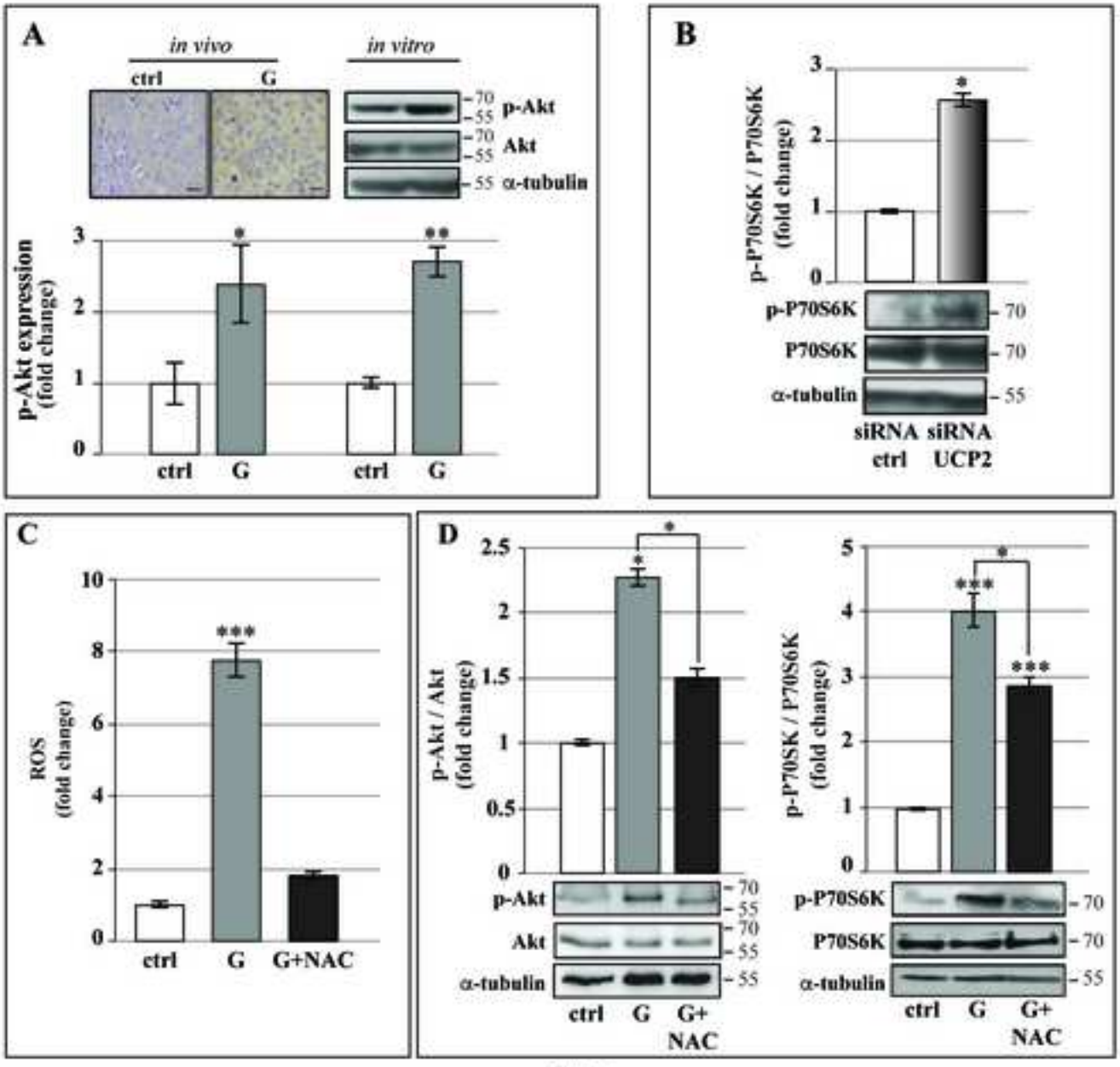

Fig.1

Figure 2

Click here to download high resolution image

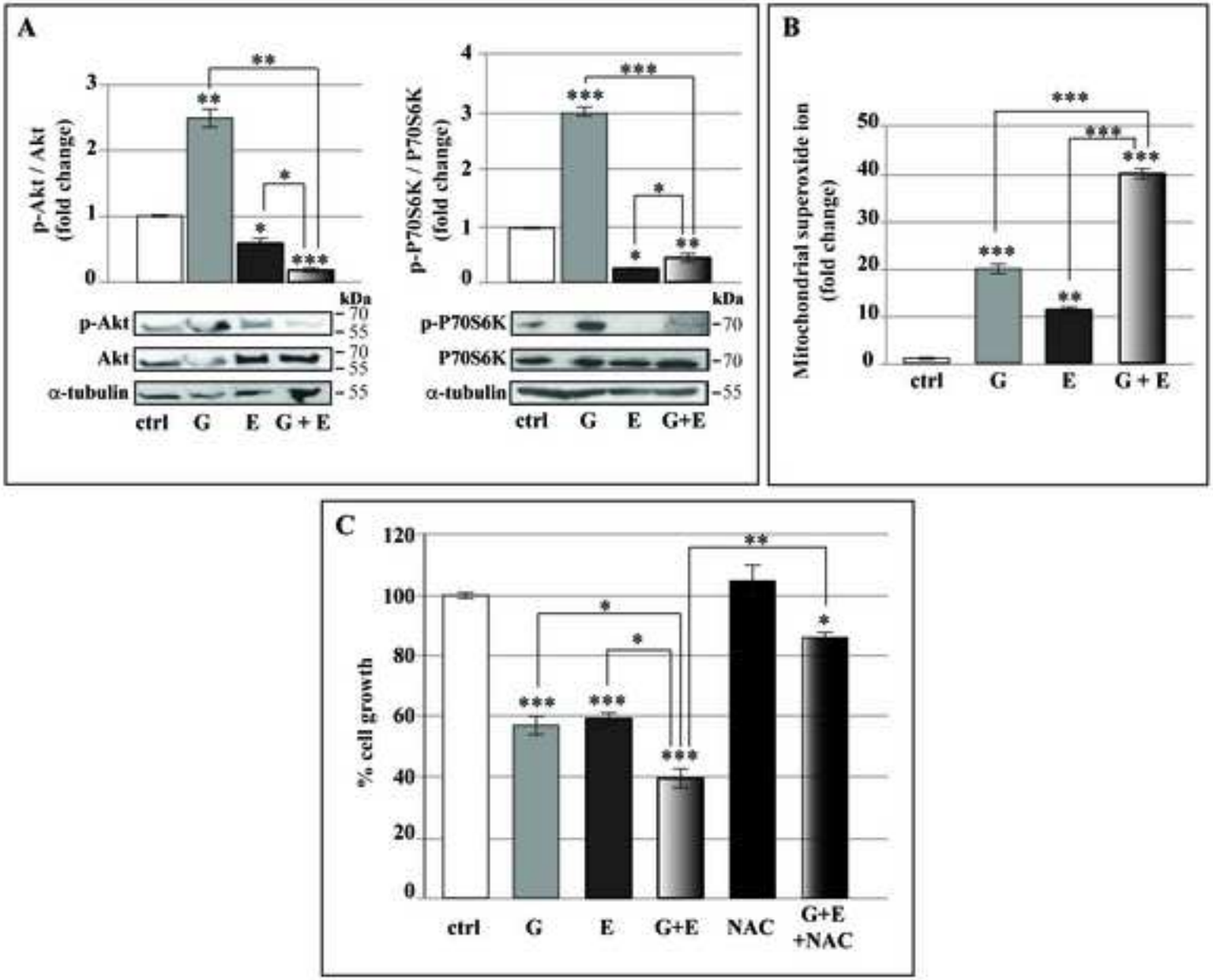

Fig. 2

Figure 3

Click here to download high resolution image

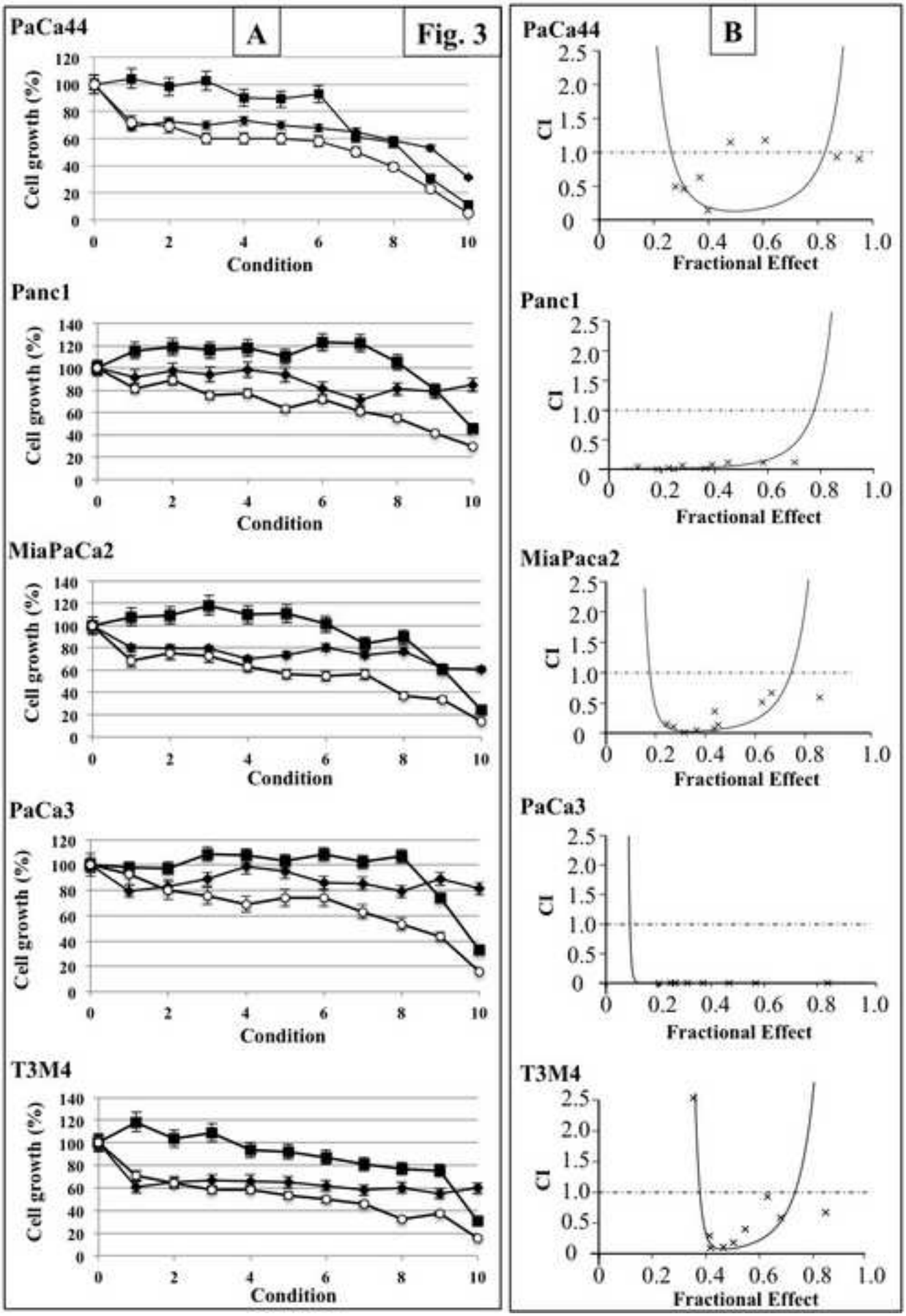

Figure 4

Click here to download high resolution image

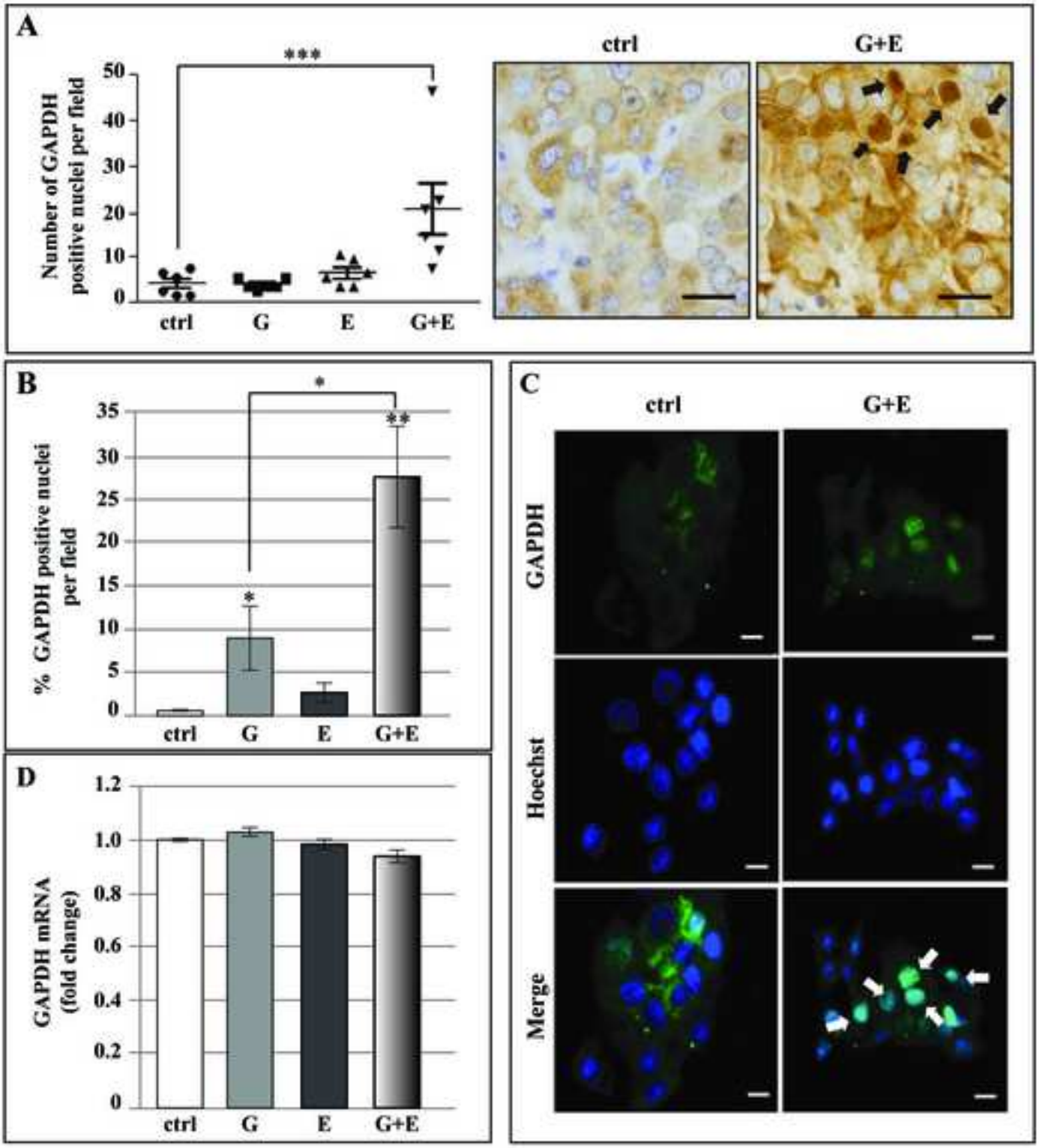

Fig. 4

Figure 5

Click here to download high resolution image

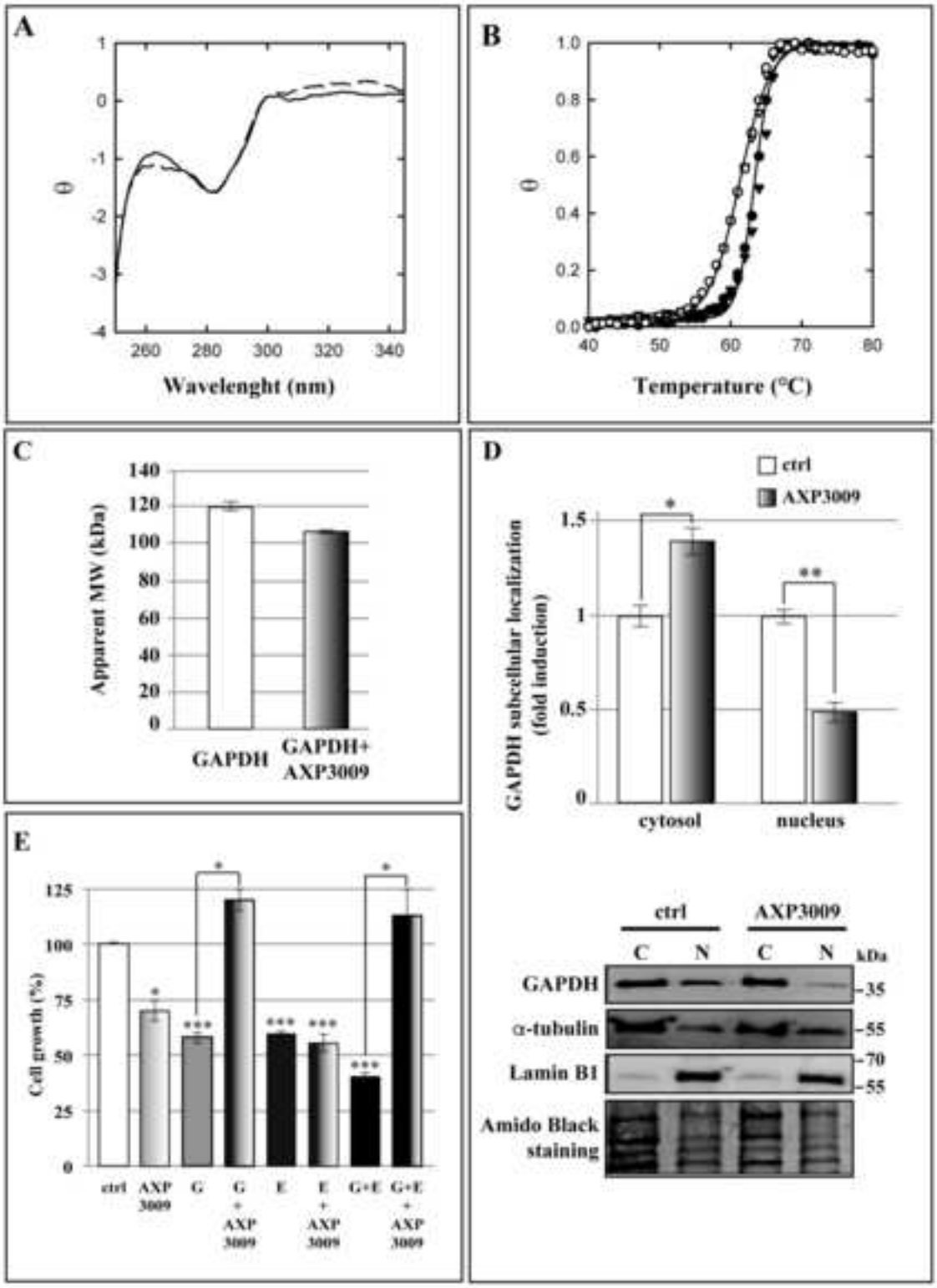

Fig. 5

Figure 6

Click here to download high resolution image

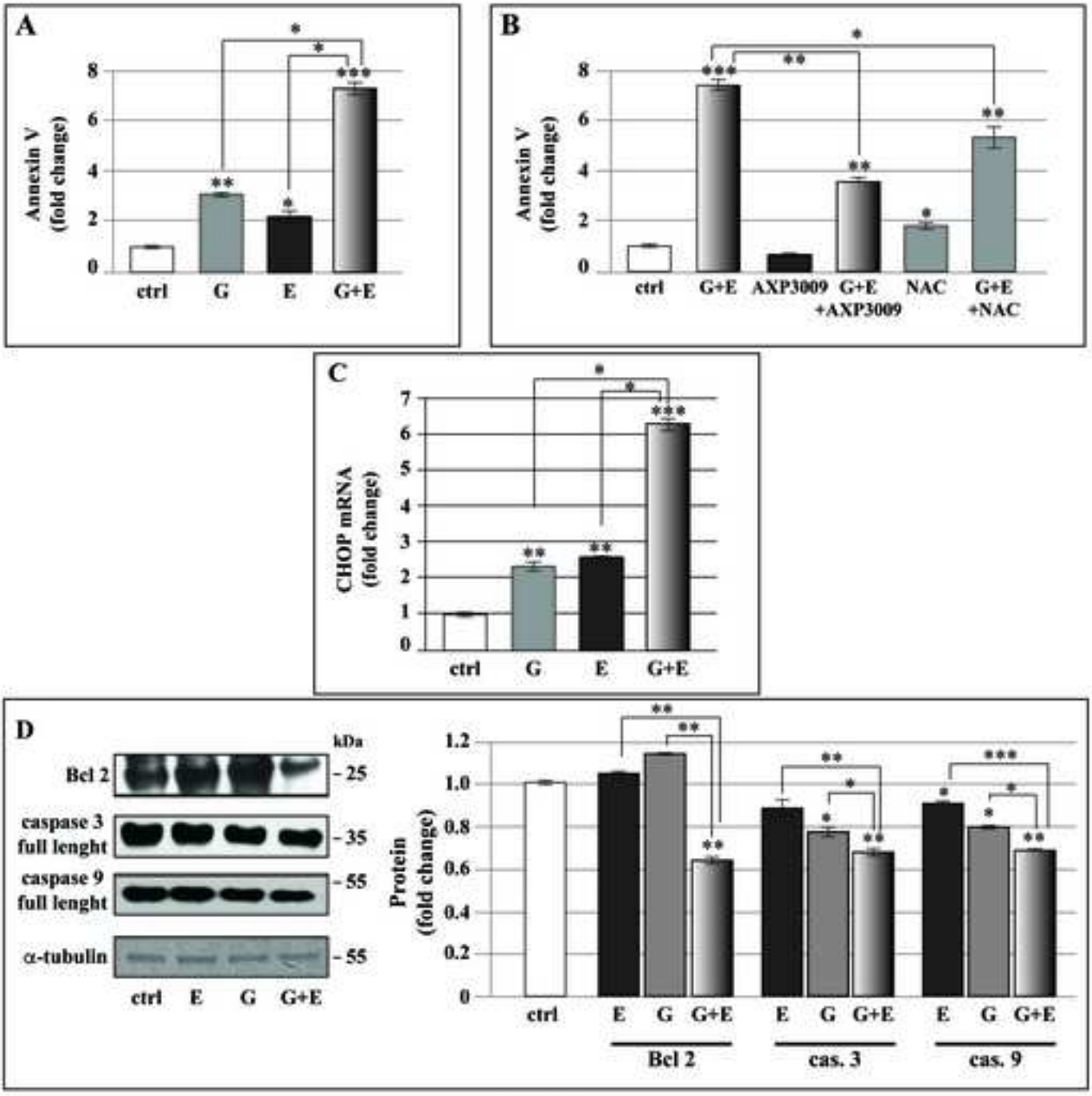

Fig. 6

Figure 7
Click here to download high resolution image

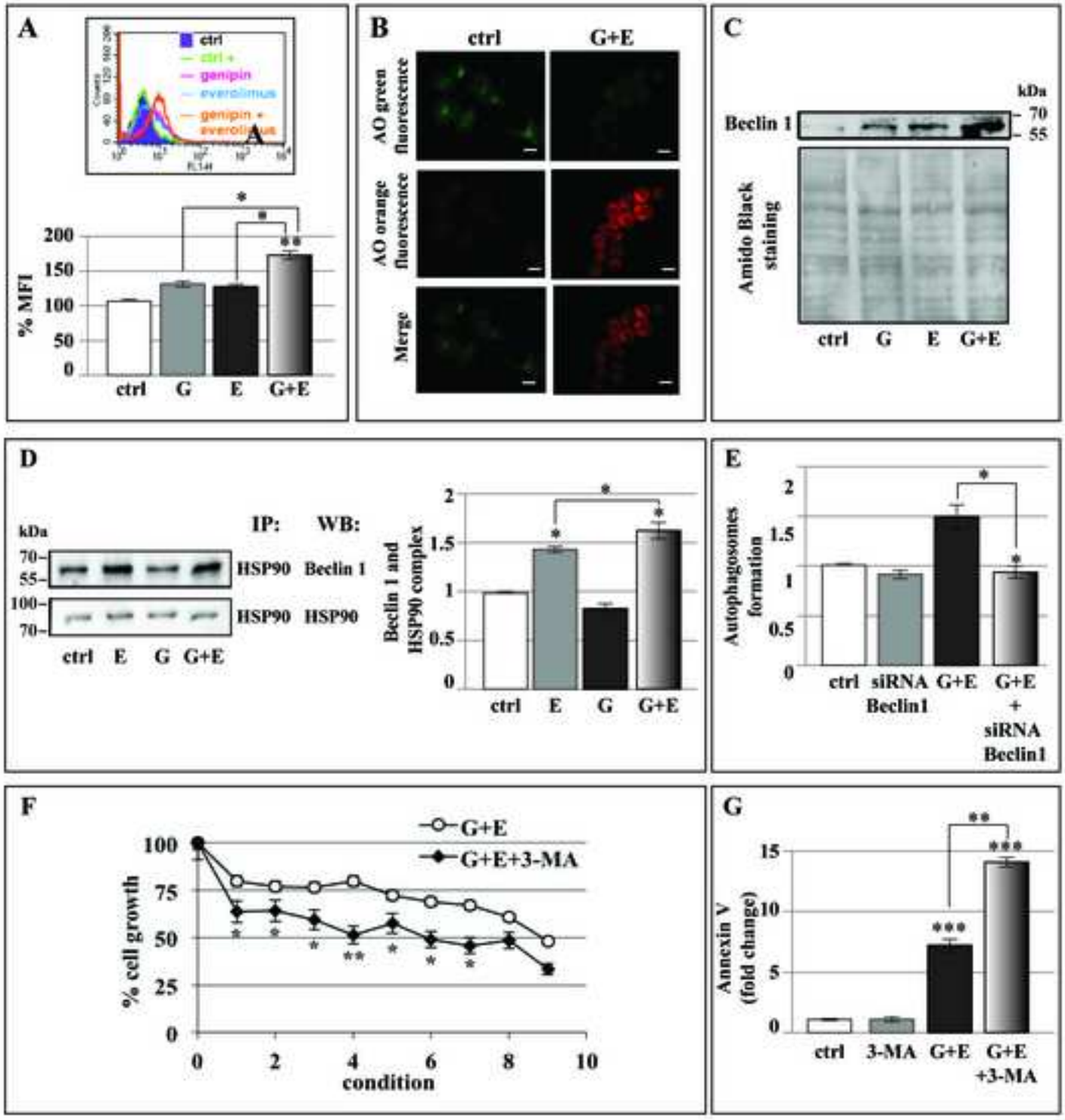

Fig.7

Figure 8

Click here to download high resolution image

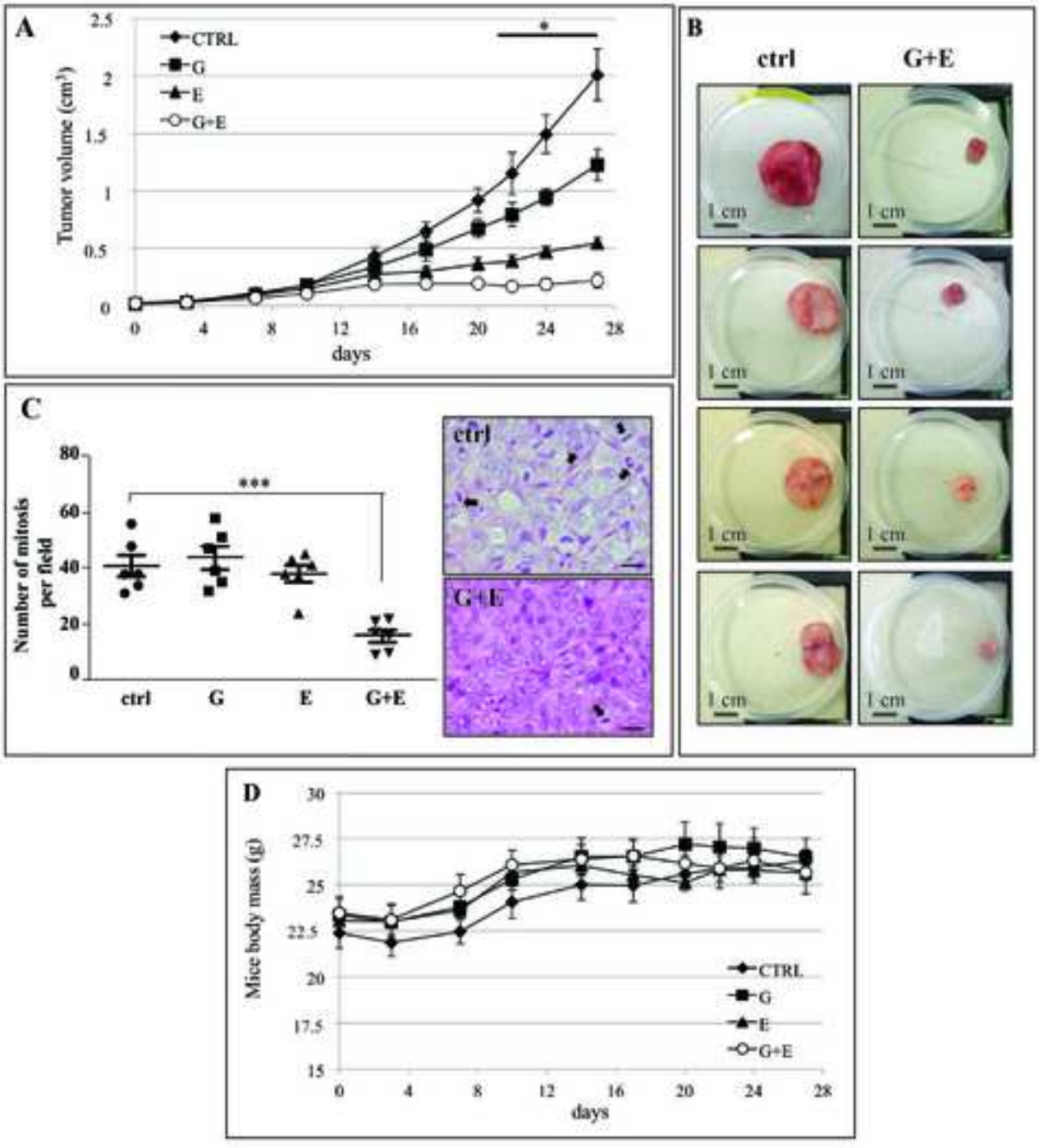

Fig.8

Figure 9
Click here to download high resolution image

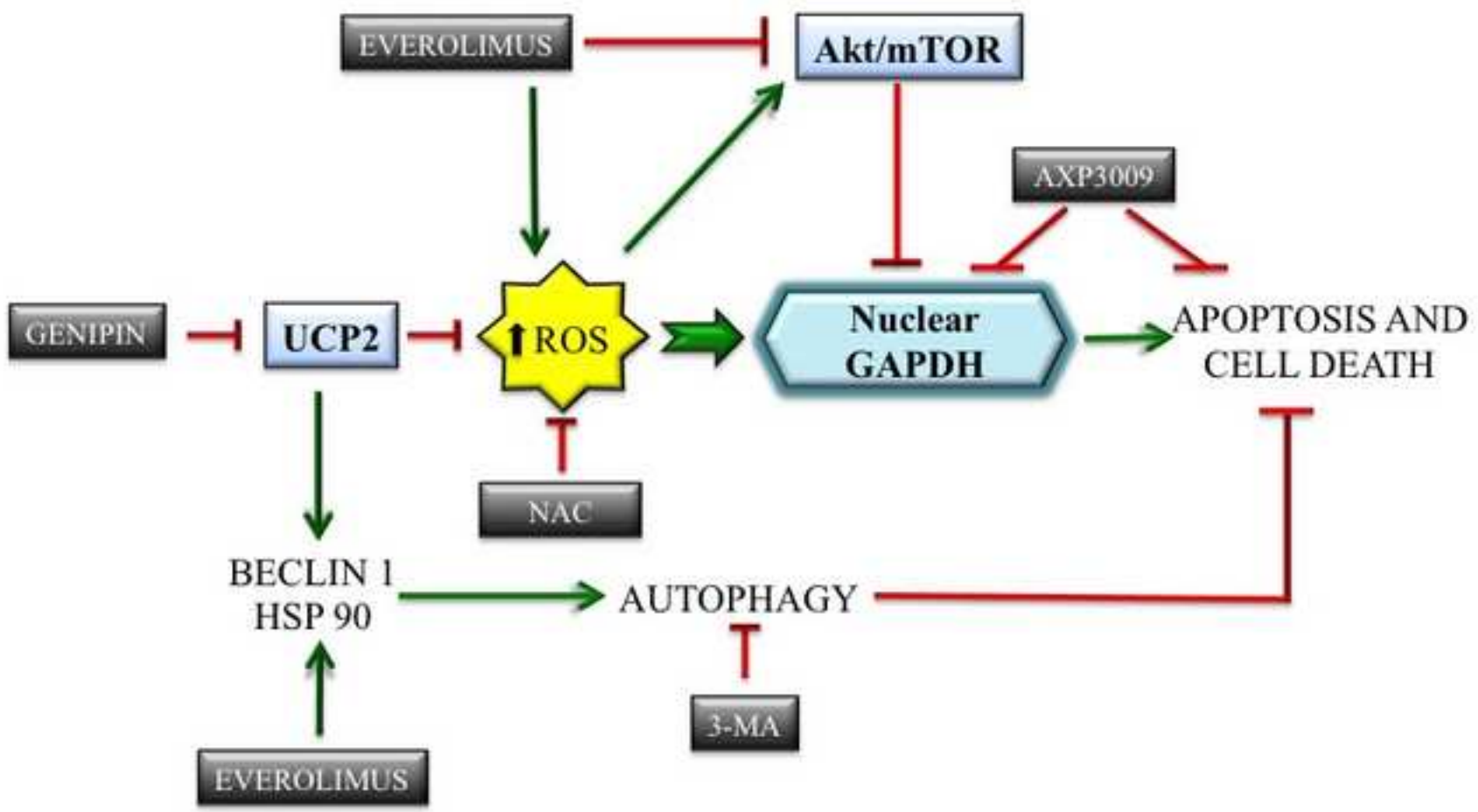

Fig. 9

Supplementary Figure 1

Click here to download Supplementary Material: Suppl. Fig. 1.jpg

Supplementary Figure 2

Click here to download Supplementary Material: Suppl. Fig. 2.jpg

Supplementary Figure 3

Click here to download Supplementary Material: Suppl. Fig. 3.jpg

Supplementary Figure 4

Click here to download Supplementary Material: Suppl. Fig. 4.jpg

Supplementary Figure 5

Click here to download Supplementary Material: Suppl. Fig. 5.jpg

Supplementary Figure 6

Click here to download Supplementary Material: Suppl. Fig. 6.jpg